POLITECNICO DI TORINO

COLLEGIO DI INGEGNERIA ENERGETICA

CORSO DI LAUREA MAGISTRALE IN INGEGNERIA ENERGETICA E NUCLEARE

MASTER THESIS

Energy analysis of the integration of a molten carbonate fuel cell for high efficiency carbon capture from internal combustion engines

Relatore:
Prof. Marta Gandiglio
Co-Relatore:
Prof. Armando Portoraro

Candidato:
Luca Arneodo

Anno accademico 2019/2020

Abstract

Carbon dioxide emissions from fossil fuel power plants are considered among the main reasons for the greenhouse effect. Various technologies have been developed to capture CO_2 from power plants, but they require a considerable consumption of energy, penalizing the plant.

Molten Carbonate Fuel Cell (MCFC) technology can play an important role in CO_2 capture, thanks to the operating principle based on the electrochemical reaction, through the carbonate ions CO_3^{2-}, in which electricity is generated. The production of energy makes this capture system "active" thus avoiding the energy consumption typical of passive systems.

The MCFC has two advantages in carbon capture: the cell removes CO_2 fed at the cathode to promote carbonate ion transport across the electrolyte and any dilution of the oxidized products is avoided.

In this work a MCFC is retrofitted to an internal combustion engine (ICE) for CHP application achieving a reduction of 75% of CO_2 emissions. The MCFC is modeled using Aspen Plus software with the implementation of an electrochemical model found in the literature.

The new system does not introduce important penalties to the plant, as for passive systems, managing to maintain energy efficiencies similar to the original system.

Two options for CO_2 purification in the CCS unit are investigated. The first uses a membrane to remove hydrogen due to the excess of chemical reactants in the fuel cell. This component does not consume energy but reach a CO_2 purity of 91.6% due to the presence of other impurities.

This option can increase the power of the plant of 244 kW and the thermal recovery of 164 kW.

The second case uses an oxy combustor which burns all the excesses of the cell, thus recovering the chemical energy not used in the cell, obtaining a high CO_2 purity of 97.9%. However, this system requires the use of an Air Separation Unit (ASU), which consumes electricity to produce the necessary oxygen, reducing the power output of the MCFC module to 232 kW but the presence of a post combustion increase the plant thermal power of 527 kW.

An energy analysis is carried out for the two cases analyzed and they are compared with other possible options, which can be adopted in the context of cogeneration, showing positive results with the achievement of high-efficiency cogeneration status. The first case achieves a primary energy saving of 27.2% and an energy utilization factor of 82.9% while the oxy-combustion case achieves a primary energy saving of 26.8% and an energy utilization factor of 82.6%.

The CCS drastically reduce the CO_2 emissions of the plant, the analysis shows that the membrane case has an emission factor of 37.1 $\frac{g_{CO_2}}{kWh}$ with a SPECCA of 1.26 $\frac{MJ}{kg_{CO_2}}$ while the oxy combustion achieve 37.3 $\frac{g_{CO_2}}{kWh}$ with a SPECCA of 1.49 $\frac{MJ}{kg_{CO_2}}$.

Contents

List of figures

List of tables

Nomenclature

$\%O_2$	Oxygen content
A	Area
AC	Alternate Current
AFC	Alkaline Fuel Cell
AGR	Acid Gas Removal
ASU	Air Separation Unit
AU	Air Utilization factor
c	Specific heat
C	Cumulate
CCR	Carbon Capture Ratio
CCS	Carbon Capture and Sequestration
C_f	Correction Factor
CHP	Combined Heat and Power
DC	Direct Current
e	Emission
E	Energy
$ECBM$	Enhanced Carbon-bed Methane Recovery
EGR	Enhanced Gas Recovery
ELP	ELectric Penalty
EOR	Enhanced Oil Recovery
EUF	Energy Utilization Factor
$\dot{F}$	Introduced fuel power
FU	Fuel Utilization factor
GHG	Greenhouse Gases
GT	Gas Turbine
h	Mass enthalpy
h_{work}	Work hours per year
HEC	High Efficiency Cogeneration
$HRSG$	Heat Recovery Steam Generator
I	Current
$IGCC$	Integrated Gasification Combined Cycle
$IPCC$	Intergovernmental Panel on Climate Change
i	Current Density
ICE	Internal Combustion Engine
LHV	Lower Heating Value
LV	Low Voltage
M	Mass
MEA	Mono Ethanol Amine
$MCFC$	Molten Carbonate Fuel Cell
MW	Molar Weight
n	Air index
n°	Number of
$\dot{n}$	Molar flow
NG	Natural Gas
$NGCC$	Natural Gas Combined Cycle
OCV	Open Circuit Voltage

$OEUF$	Overall Energy Utilization Factor	T	Temperature
$OPES$	Overall Primary Energy Savings	U	Internal Energy
p	Partial pressure	U_{CO_2}	CO_2 Utilization factor
$PAFC$	Phosphoric Acid Fuel Cell	U_{O_2}	O_2 Utilization Factor
$PEMFC$	Proton Exchange Membrane Fuel Cell	V	Voltage
PES	Primary Energy Savings	$\dot{V}$	Volumetric flow
$q_{f,net}$	Specific net consumption	v_{mol}	Molar volume
R	Resistance	W	Power
RES	Renewable Energy Source	WGS	Water Gas Shift reaction
S/C	Steam to Carbon ratio	y_i	Molar fraction of i-th specie
$SOFC$	Solid Oxide Fuel Cell	z_i	Charge number of i-th specie
$SPECCA$	Specific Primary Energy Consumption for CO_2 Avoided		

Greek symbols

α	Dosage	$\Delta\tilde{h}$	Molar enthalpy variation
β	Pressure ratio	η	Efficiency
ΔG	Gibbs free energy variation	λ	Cogeneration ratio
ΔH	Enthalpy variation	ϕ	Heat flux
$\Delta H^0_{298\,K}$	Standard enthalpy of formation at 298 K and 1 atm		

Subscripts

@	at
AC	Alternate Current
act	Activation
an	Anode
c	Isentropic
$C.V.$	Control Volume
cat	Cathode
$COND$	Condenser
$cool$	Cooler
ct	Compression Train
DC	Direct Current
el	Electric
em	Emitted
exh	Exhaust
ext	External
f	Fuel
FC	Fuel Cell
g	Global
hc	Hydrocarbons
in	Inlet
int	Internal
inv	Inverter
m	Mechanical
max	Maximum
min	Minimum
$N.c.$	Normal conditions
ohm	Ohmic
out	Outlet
p	Primary
pl	Plant
pp	Pinch Point
$react$	Reaction
REC	Recovery
rec	Recovered
ref	Reference
s	Separated Production
seq	Sequestrated
st	Stoichiometric
t	Technical
th	Thermal
tot	Total

Apex

$*$	Corrected value

Constants

F	Faraday constant
R	Gas constant

1 Introduction

In the Fifth Assessment Report of IPCC [1] is reported that there is a strong evidence on human emissions of greenhouse gases (GHG), by the means of fossil fuel, and a primary driver on climate change. The most compelling issue is the projected rise in the Earth's surface temperature that could lead to catastrophic scenarios. Since the industrial revolution the average Earth temperature is rise of 1.1 °C leading to ecological, physical and health impacts affecting life and ecosystems.

The Paris Agreement's central aim is to strengthen the global response to the threat of climate change by keeping a global temperature rise this century "well below 2 °C" above pre-industrial levels and to pursue efforts to limit the temperature increase even further to 1.5 °C. The main anthropogenic GHG is carbon dioxide, its concentration in atmosphere is over 400 ppm. The problem is not only the level but also the rate of change. Natural changing of CO_2 concentration happened in the Earth history but with rates of centuries or even thousands of years.

Reaching the 2°C target allow us to emit at maximum only about 720 $GtCO_2$ between 2018 and 2100 into the atmosphere while the 1.5 °C target impose a limit of 580 $GtCO_2$ [2].

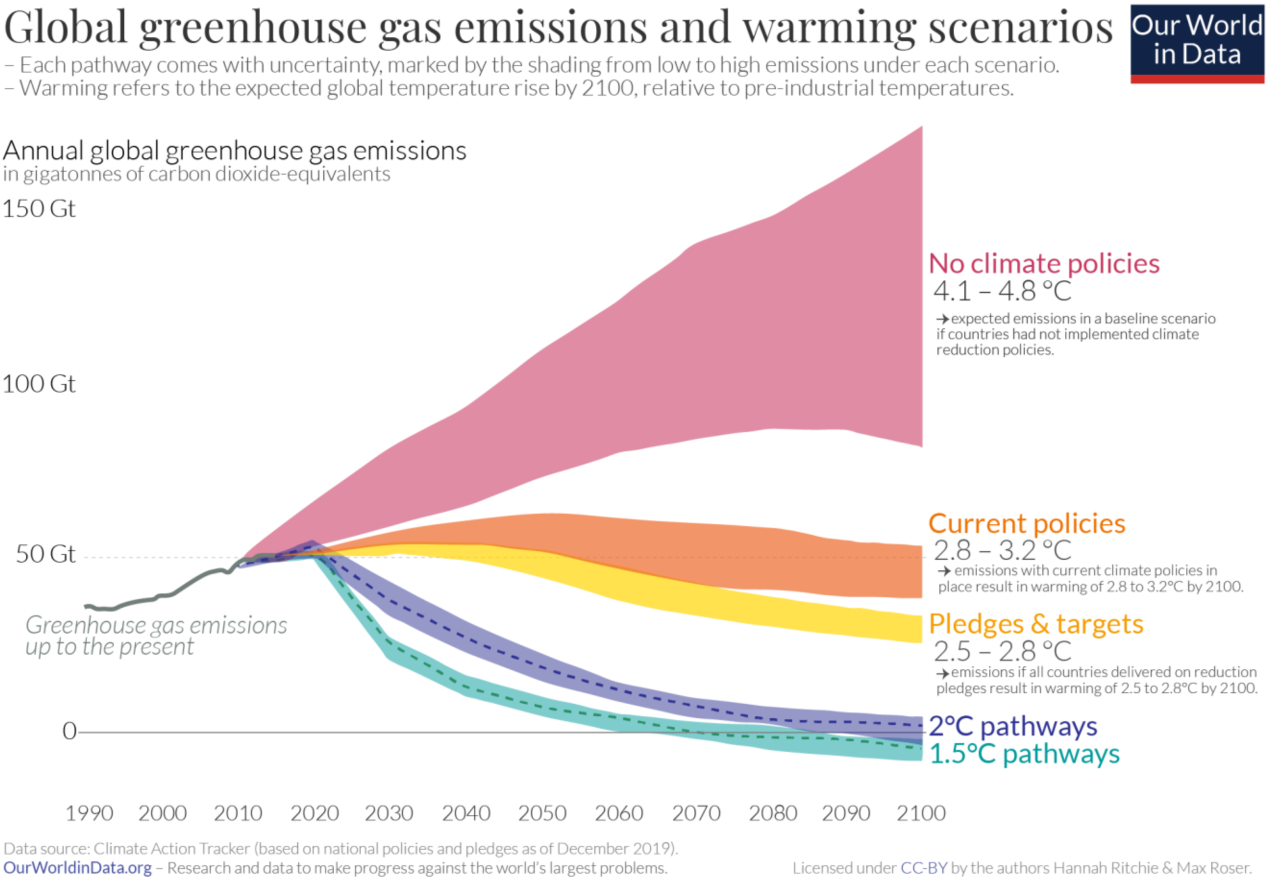

Figure 1 – Global Warming scenarios. Source: [3]

Climate change and the growing demand for energy are among the most important challenges of this century, as they are deeply related. In 2019, the world energy mix is mainly composed by fossil fuels. In the last decades, the role of Renewable Energy Sources (RESs) gain more and more importance as a possible solution for a low-carbon energy system. Nowadays, RESs are still not enough mature to completely substitute the fossil fuels, but at the same time actions to reducing greenhouse gases must be taken.

In power plants the main GHG emitted is carbon dioxide, due the combustion of fossil fuel.

The role of Carbon Capture and Sequestration (CCS) is to act as a solution to stabilize GHG emissions while still using fossil fuel power plants. The future of the energy sector should be decarbonized. However, there is a large (and even growing) fossil fuel infrastructure already in place. So, the only way to mitigate a trend towards increasing CO_2 emissions is to apply CCS to both existing and future fossil power plants.

Different CCS technologies have been developed, the majority of these are "passive" because they treat fuel or flue gas, penalizing the plant because these processes consume some of the energy produced, introducing a penalty of power up to 30% [4]. Among CCS technologies, very interesting is the application of high temperature fuel cell technology. The advantages of fuels cells are high efficiencies and low impacts on the environment. Between the high temperature fuel cells, Molten Carbonate Fuel Cells (MCFCs) exploit the carbon dioxide inside flue gases to perform an electrochemical reaction through carbonate ions $CO_3^{=}$. This gives a unique advantage to this technology: power production while concentrating carbon dioxide, making MCFCs an "active" CCS technology very suitable for retrofitting exiting power plants. In Figure 2 is illustrated the application of MCFCs as CCS.

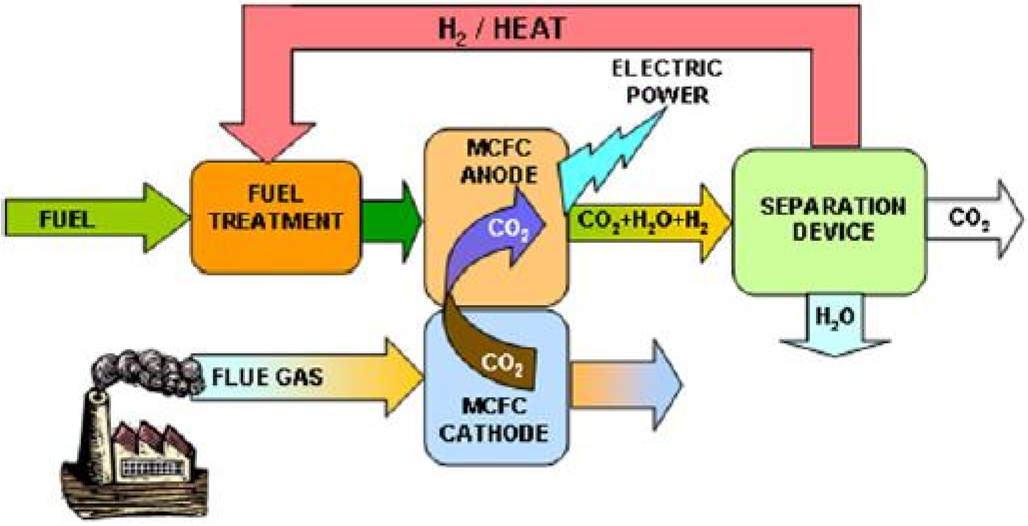

Figure 2 – MCFC applied as CCS. Source: [4]

Thanks to these advantages, the MCFCs are deeply studied as retrofitting CCS for large power plants.

Wang et al. [5] explore the state of art of fuel cells applied for CCS, discuss the performances and opportunities for future development of this technology.

In Duan et al. works [6]–[8] integration of MCFCs are studied for coal-fired, IGCC (Integrated Gasification Combined Cycle) and gas-steam combined cycle power plants to perform CCS without efficiencies penalties and superior thermal performance compared to other passive CCS techniques. Campanari et al. [9], [10] studied the integration of MCFC in natural gas combined cycle plants (NGCC) as a retrofitting CCS and developed an experimental model to describe the

electrochemical behavior. Spinelli et co. [11], [12] compare the application of MCFC as retrofit CCS in a coal-fired combined cycle and NGCC and propose suitable plant layouts.
Recently, Sartori da Silva [13] proposed a novel combined MCFC – Steam turbine system with CCS from the steam generator.
Less investigated are the applications of MCFCs for CCS in small combined heat and power (CHP) plants, typical of industrial scenarios.
Desideri et al. [14] studied the retrofitting of a small CHP for district heating with a MCFC for CCS. Rinaldi et al. [15] investigated the performance of MCFC-CCS in a tri-generation plant with an internal combustion engine. In Badami at al. work [16] is investigated the energetic and exergetic performance of MCFCs compared to MEA (Mono Ethanol Amine) technology when retrofit an internal combustion engine.

The presented work wants to investigate the application and performance of CCS through MCFC to a typical industrial CHP system based on an internal combustion engine.
In the next chapter are described the technologies to give the reader a brief overview on the covered topics. Then in chapter 3 is addressed the modelling of each component of the system with the software Aspen Plus. The cell performances are evaluated using an electrochemical model present in literature. Two options for CO_2 purification in the CCS unit were investigated. The first uses a membrane to remove hydrogen due to the excess of chemical reactants in the fuel cell. While the second one uses an oxy combustor which burns all the excesses of the cell, thus recovering the chemical energy not used in the cell. Also, a pinch analysis methodology is applied to perform a heat recovery inside the plant. This chapter is concluded with the evaluation of the overall performance of the plant.
Then an energy analysis is carried out in chapter 4, the two cases analyzed are compared with other possible options, which can be adopted in the context of cogeneration. Various energy indexes are used to evaluate the energetic performance and the emission of each scenario, such as the Primary Energy Savings (PES), the Energy Utilization Factor (EUF) and the specific CO_2 emission per energy unit. Also, for the two CCS scenarios are evaluated the efficiency penalty due to the carbon capture and the Specific Primary Energy Consumption for CO_2 Avoided (SPECCA).

2 Technologies overview

In this chapter are described the technologies treated in this work to give the reader an overview of the touched topics.

2.1 Carbon Capture and Sequestration technologies

The role of Carbon Capture and Sequestration (CCS) is to act as a solution to stabilize GHG emissions while still using fossil fuel power plants during the decarbonization of the energy sector.

These technologies aim to capture carbon dioxide from stationary industrial sources, its transportation, and its removal from atmosphere in a permanent storage isolated from the environment. The three main steps in the CCS chain: capture, transport and storage, are reported in Figure 3.

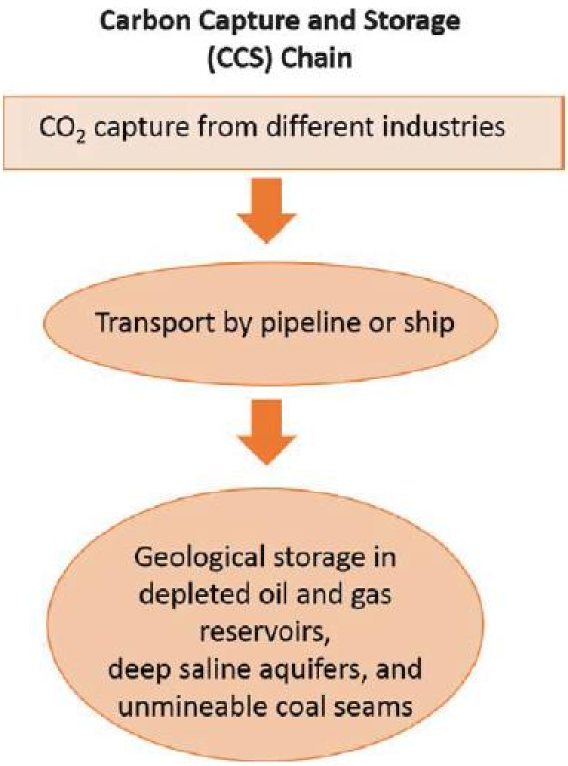

Figure 3 – CCS chain. Source: [17]

CO_2 capture technologies can be categorized [18] as:

a. Carbon capture from concentrated point sources or from mobile/distributed point or non-point sources.
b. Techniques involving physical/chemical or biological processes.

In category a. the CO_2 is removed or separated from the other gases produced when fossil fuels are burnt. Three different way are used: "oxy-fuel combustion", "pre-combustion" and "post-combustion"

In "oxy-fuel combustion" systems, pure oxygen (produced with an air separation unit) is used in the combustion process instead of air, the combustion is almost in stoichiometric conditions. The resulting flue gas is N_2-free made only by H_2O and CO_2. The capture and purification of

CO_2 is easier because involves only the condensation of water in the exhaust gases. The energy intensive step for CO_2 separation from the flue gas is avoided, however the burden is now on the air separation process to extract pure oxygen from atmospheric air.

In "pre-combustion capture" systems, fuel in any form is converted to a syngas by a gasification process and a mixture of H_2 and CO_2 is obtained with a Water Gas Shift (WGS) reaction, then followed by a CO_2 separation process. Carbon dioxide is removed from the shifted syngas in an Acid Gas Removal (AGR) unit through an absorption process with a physical solvent (such as methanol). The most popular, successful and commercialized AGR process is the Rectisol® one [19]. The purified hydrogen can be used as a fuel for power production or mobility with zero emissions (decarbonized fuel) while the CO_2 can go to a geological sequestration site or can be used for Enhanced Oil Recovery (EOR) or other destination use.

"Post-combustion capture" systems, implies the capture of CO_2 from the flue gas of a combustion process. Different methods for CO_2 separation have been developed such as absorption – desorption processes, cryogenic separation and high-pressure membrane filtration. Between these methods, the most established method is absorption. There are two types: physical absorption (physical organic solvent-based process) and chemical absorption (chemical wash). The chemical absorption is based on solvent scrubbing with amine solvents to capture CO_2 from flue gases, then solvent and CO_2 are separated in a stripper reactor. This type of capture introduces an efficiency penalty on the plant due to the energy consumption of the CCS system.

In Figure 4 are resumed the carbon capture methods of category a.

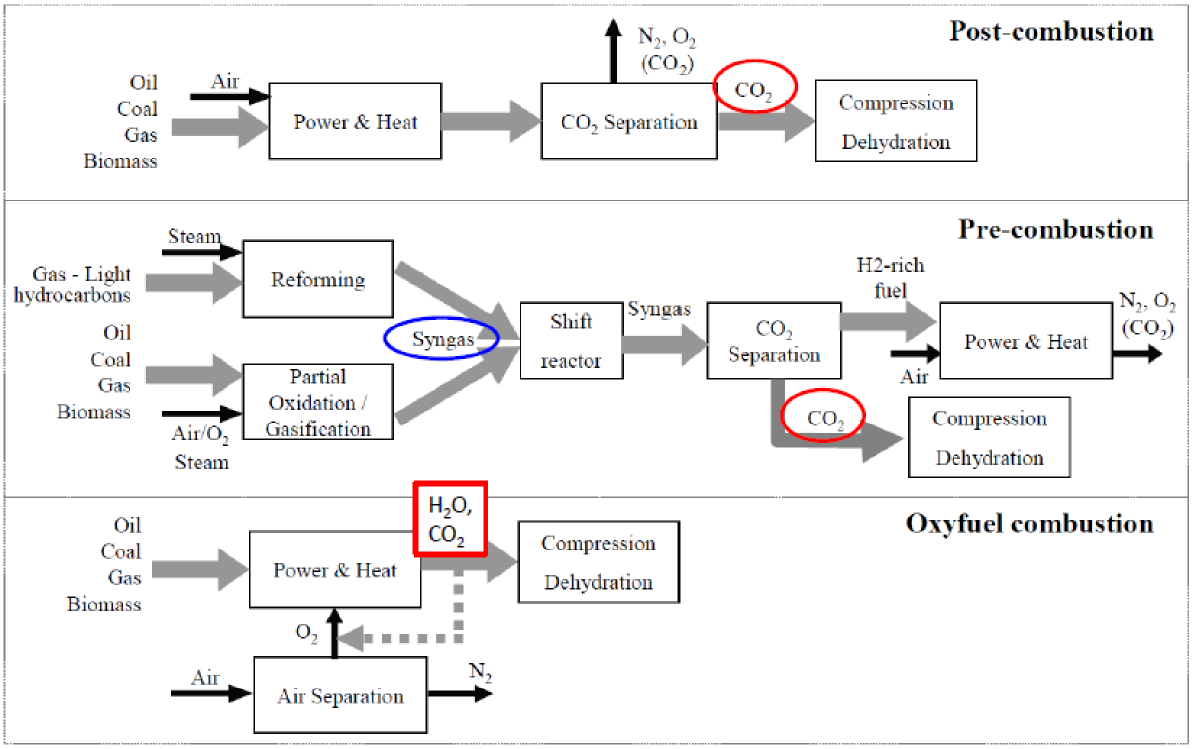

Figure 4 – CCS processes. Source: [19]

Other than the three technologies described before, sorption and membranes technologies are the two major options between category b. Alternative biological carbon capture technologies can be used for point or non-point such as trees, organism and ocean flora or biomass fueled power plant, biofuels and biochar.

After capturing, the CO_2 needs to be transported to a suitable site for final disposal. The means used for transportation can be pipelines, trucks, trains or ships. With pipelines is possible to move high quantity of CO_2 through a network. When the distance is short and the quantities are small, land transportation (rail or tankers) is adopted. In case of offshore disposal of CO_2, shipping can be a suitable solution when the distance between emission point and seaport is adequate.

The last step of the CCS chain is the final disposal, various options are available such as depleted or declining gas and oil reservoir, deep saline reservoir or Enhanced Hydrocarbon Recovery. Enhanced Hydrocarbon Recovery includes Enhanced Oil Recovery (EOR), Enhanced Gas Recovery (EGR) and Enhanced Coal-bed Methane Recovery (ECBM). Enhanced techniques are the injection of CO_2 inside a depleted oil or gas reservoir, the CO_2 increase the internal pressure making easier the extraction and, at the same time, performing sequestration. Between all the options, the geological storage is the most realistic ones because the storage in ocean depths is currently experiencing public opposition due to insufficient knowledge of the effects on marine ecosystems. Also, the mineralization option requires a high amount of energy and materials resources, discouraging this option.

Today, only large-scale point sources with a production of 50% of CO_2 are considered for CCS applications. The considered sources are power plants, cement plants, coal-to-liquid plants, steel mills and refineries. The technical maturity of CCS components varies significantly, as reported in Figure 6, the components technologies are quite mature but they are not fully integrated resulting in an overall CCS maturity that is not the same level as its components. Actually, 37 CCS large scale project are under study, 17 are in operation, 4 in construction and the remining into development [20]. Most of this project is in U.S. and China as showed in Figure 5.
In CCS projects there are barriers that need to be overcome such as high capital investment, policy options, uncertainties in regulations and technical performance, public safety and environmental risks.

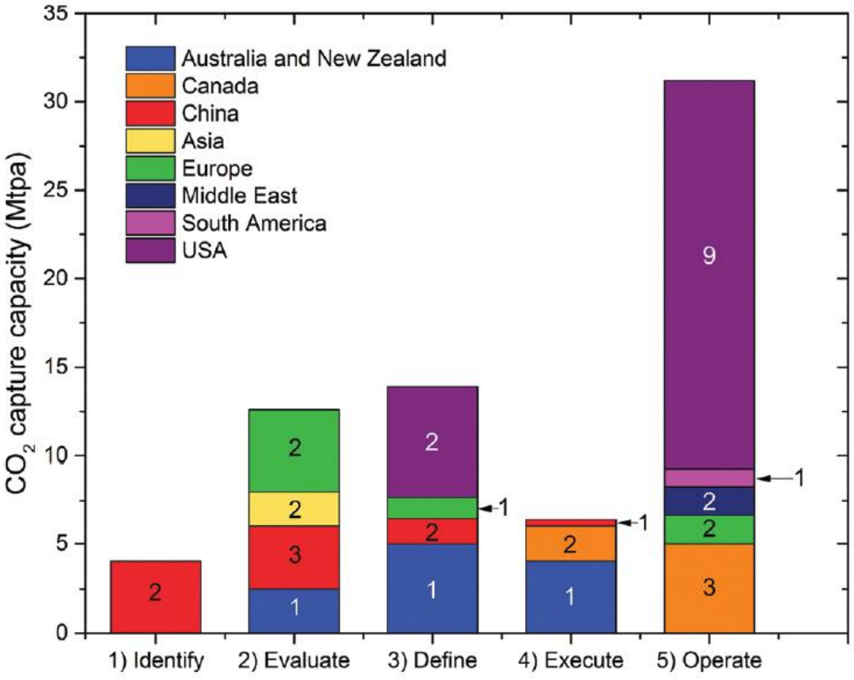

Figure 5 – CCS projects. Source: [20]

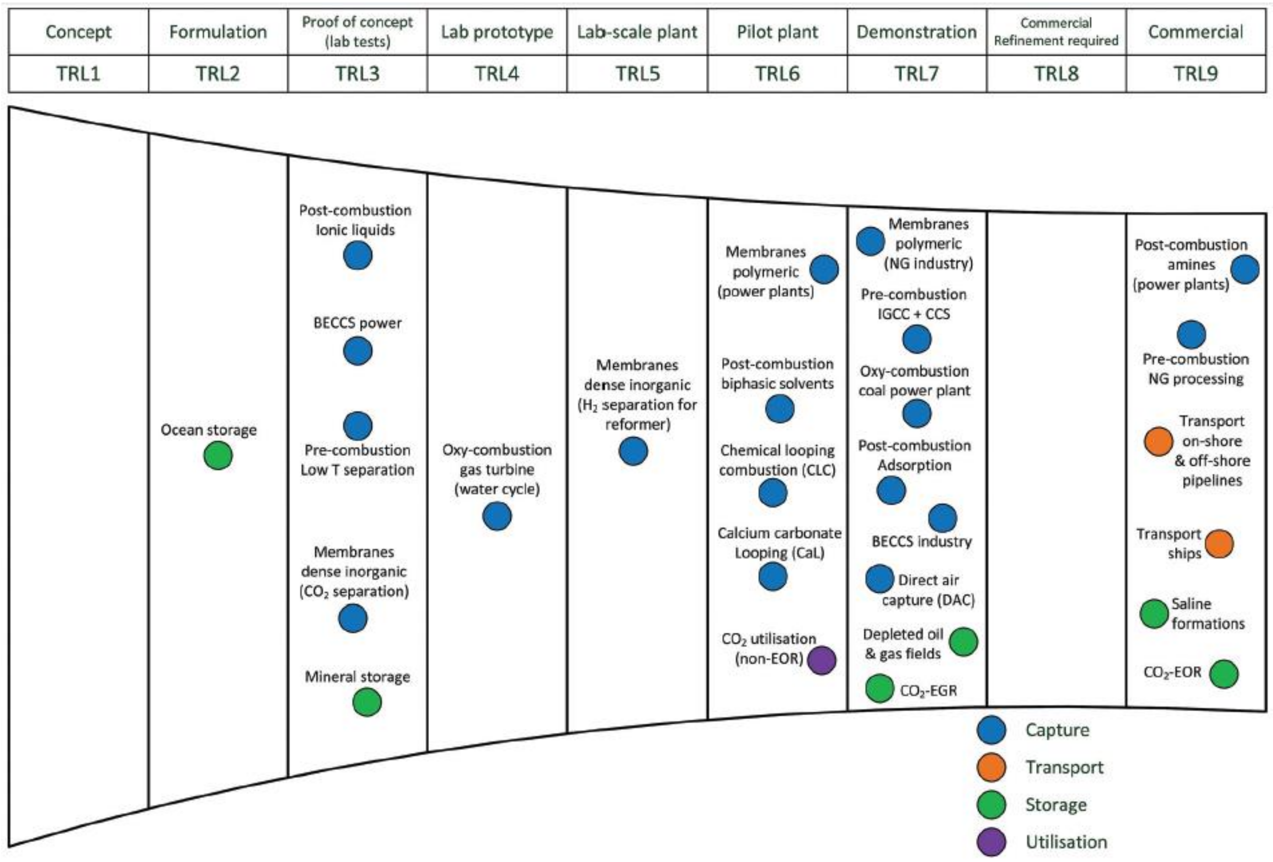

Figure 6 – CCS components maturity. Source: [20]

2.2 Molten Carbonate Fuel Cell technology

In this work a Molten Carbonate Fuel Cell is used, this section gives a brief overview on the structure of the cell and materials involved in this technology.

Fuel cells are open thermodynamic system exploiting the electrochemical reaction between hydrogen and oxygen to form water, generating electricity and heat. The main difference between fuel cells is the chemical characteristics of the electrolyte.

Fuel cells are classified based on the choice of fuel and electrolyte into 5 major groups (ordered by operating temperature):

1. Proton Exchange Membrane Fuel Cell (PEMFC): use a Nafion membrane as electrolyte.
2. Alkaline Fuel Cell (AFC): the electrolyte is potassium hydroxide in water solution.
3. Phosphoric Acid Fuel Cell (PAFC): use carbon paper electrodes and liquid phosphoric acid electrolyte.
4. Molten Carbonate Fuel Cell (MCFC): molten carbonate salt mixture as electrolyte.
5. Solid Oxide Fuel Cell (SOFC): metallic oxide solid ceramic electrolyte.

MCFC is a high temperature fuel cell operating between 600-700 °C [21], the main reaction involved at anode (1) and cathode (2) are:

$$\begin{gathered} H_2 + CO_3^{2-} \rightarrow H_2O + CO_2 + 2e^- \\ CO + CO_3^{2-} \rightarrow 2CO_2 + 2e^- \end{gathered} \tag{1}$$

$$\frac{1}{2}O_2 + CO_2 + 2e^- \rightarrow CO_3^{2-} \tag{2}$$

At the anode, the feed gas (usually methane or natural gas) and water H_2O are converted to hydrogen H_2, carbon monoxide CO and carbon dioxide CO_2 through a steam reforming and water gas shift reactions that are favored by the high operating temperature.

The fuel feed to the anode (mainly H_2) reacts with carbonate ions to form water and carbon dioxide.

At the cathode occurs the reduction reaction between oxygen and carbon dioxide which produce carbonate ions. A particular feature of this fuel cell is the possibility of recirculating the anode exhaust to the cathode inlet, leaving in theory only water at the anode outlet, as showed in Figure 7.

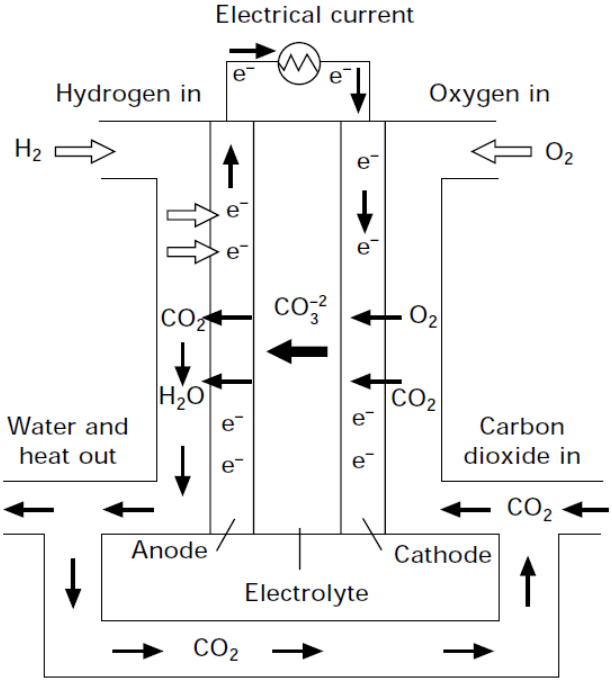

Figure 7 – MCFC reactions. Source: [22]

Thanks to the high temperature, reactions kinetics are facilitated, and the catalytic activity of the electrodes need not to be exceptional, this avoid the necessity for noble metals.

The material needs to have a high electrocatalytic activity but, at the same time, need to be resistant to hydrogen embrittlement, Sulphur poisoning, low solubility in the liquid electrolyte and good wettability.

The porosity is very important to guarantee the diffusion of gases and have enough capillary force to draw the liquid electrolyte to the catalyst surface, this determines two different levels of porosity: small pores are filled with electrolyte and are responsible for the transport of ions, while larger pores provide access for the gaseous species. A stable electrolyte/gas interface in the electrodes is established exclusively due to a balance in capillary forces.

Also, the electrodes need to be thermo-mechanically stable to achieve resistance to fracture, sintering, creep and thermal dilatation due the high temperature.

The most used material for the anode is Nickel alloyed with Chromium and/or Aluminum while for the cathode there is a difficulty in satisfying all the requirements to the desired level simultaneously so, the material adopted is a lithiated Nickel oxide. On the anode side can be also applied a reforming layer for steam reforming and water gas shift of natural gas. The cathode can also be coated with lithium cobaltite to decrease the NiO dissolution in the electrolyte.

The electrolyte transport carbonate ions and dissolved reactants. Also, must provide a physical barrier to separate the fuel and oxidant and provide the gas sealing between separator plates. The liquid electrolyte is a mixture of Li/Na or Li/K with additives.

The liquid electrolyte cannot be implemented without a support structure that contains it. This ceramic support is called matrix and need to satisfy a combination of requirements: a porosity that guarantee to be impregnated by the liquid, providing mechanical stability and be resistance to the corrosive environment. The ceramic material is α- or γ-$LiAlO_2$ with fiber or particulate reinforcement.

In Figure 8 is showed the distribution of the electrolyte in the three cell components which is a critical factor for the performance and endurance of the cell. The three-phase region is a specific site where the electrochemical reaction (charge transfer) happens.

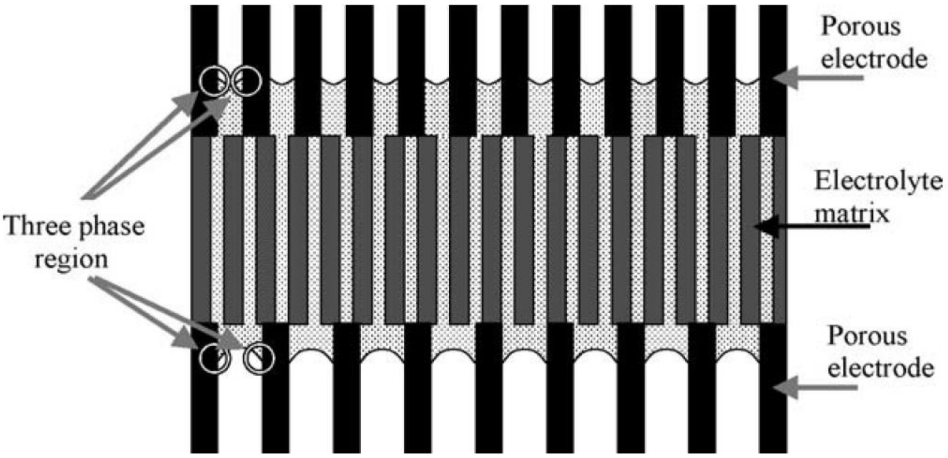

Figure 8 – Distribution of electrolyte in porous electrodes of MCFC. Source: [23]

These three active components of the cell are manufactured with a tape casting process. The metal powder is mixed with a solvent, dispersant and binder to make a slurry, then is cast into a tape of polyethylene carrier sheet under a moving doctor blade that impose the thickness. The obtained green tape is dewaxed and sintered in a furnace.

For the anode we use a powder composed of Nickel with alloying additives.

For the cathode there are 3 different way to prepare the lithiated NiO:

1) Ni electrode is prepared and oxidated, then lithiated inside the cell.
2) In the Ni powder is added the lithium carbonate and the powder is oxidated at high temperature with air.
3) Pre lithiated Ni tape casted and after is oxidated and sintered.

For the matrix, a tape-casting is used but with modification of the base powder, solvent and binder because $LiAlO_2$ is reactive with water. The matrix tape cast is composed by several thin layers cross-laid on top of each other, to increase structure control and its ultimate mechanical strength.

To assemble a single cell, the active components are jointed with a metallic component, called “bipolar plate”, forming the single repeating unit. This is the most critical non-active component because is placed between the reducing environment of the fuel (anode) and the oxidizing environment of air (cathode) in the presence of liquid salt (electrolyte). The bipolar plate is usually made of stainless-steel alloys.
The main functions of this component are:

1) Separate fuel and oxidant streams between adjacent cells, while providing electrical contact.
2) Create flow channels to guide the gases from the manifolds to the electrodes.
3) Provide a leak-tight gas flange around the electrodes (wet seal).

The wet seal is accomplished extending the electrolyte tile to the plate edges where it is sandwiched between two juxtaposing plate, the area of the seal is relatively small.

In Figure 9 is reassumed the schematic of a single repeating unit, to form a stack, multiple single repeating unit are placed in series.

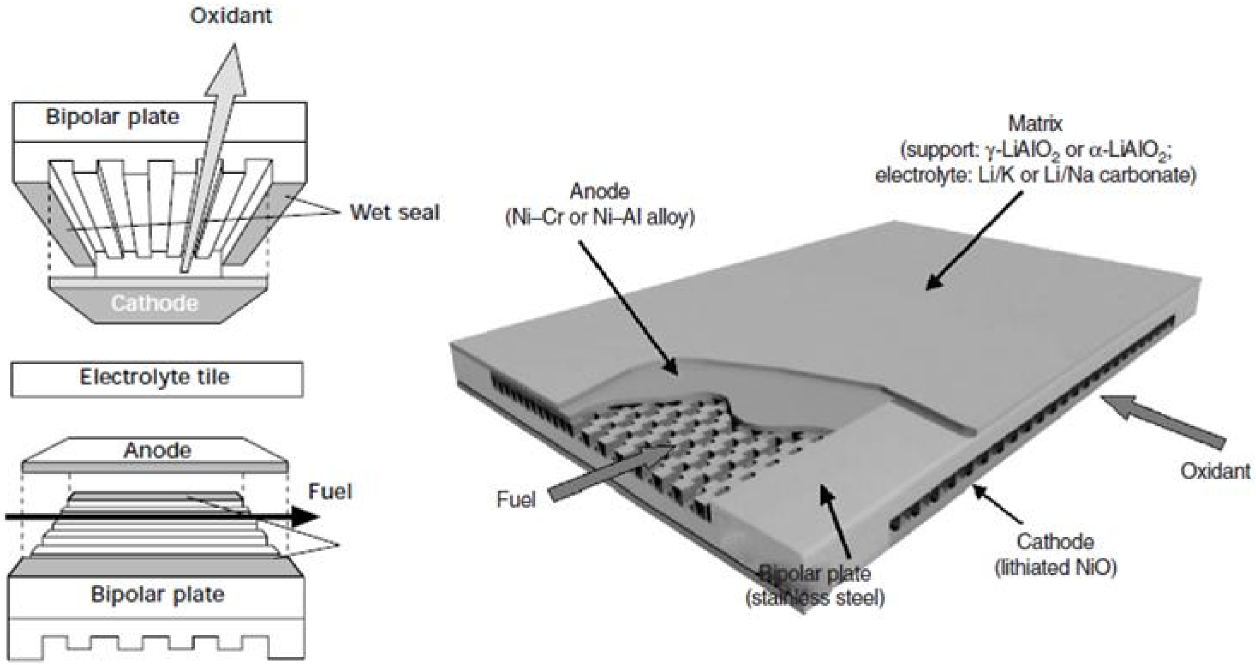

Figure 9 – Single cell unit. Source: [22], [24]

MCFCs can achieve high efficiencies, up to 60% in some cases [25], but the liquid electrolyte introduces some problems causing the reduction of lifespan and efficiency of the cell.
The first is the loss of liquid electrolyte during cell operation, due to reaction with the electrode materials or vaporization or corrosion. Another issue is the gas cross over phenomena: the migration of gas species from one electrode to the other through the electrolyte.
The electrolyte and matrix need to avoid as much as possible this phenomenon. It is caused by two reason: changes in the characteristic of the matrix due to the sintering and depleting of the liquid electrolyte.

The MCFC is one of the thickest among the fuel cells (1.2 – 4 mm) [23], a thick electrolyte is needed to neutralize the phenomenon of NiO dissolution. This phenomenon lead to formation of Ni dendrites and cause short circuit between electrodes.

2.3 Cogeneration

Cogeneration or combined heat and power (CHP) is the production of electricity and useful heat at the same time.

CHP technology is an energy efficient technology that uses the heat produced for electricity generation, that would be wasted, to provide useful thermal energy. This also permits to reduce the consumptions of fuels needed to provide the same thermal energy as showed in Figure 10.

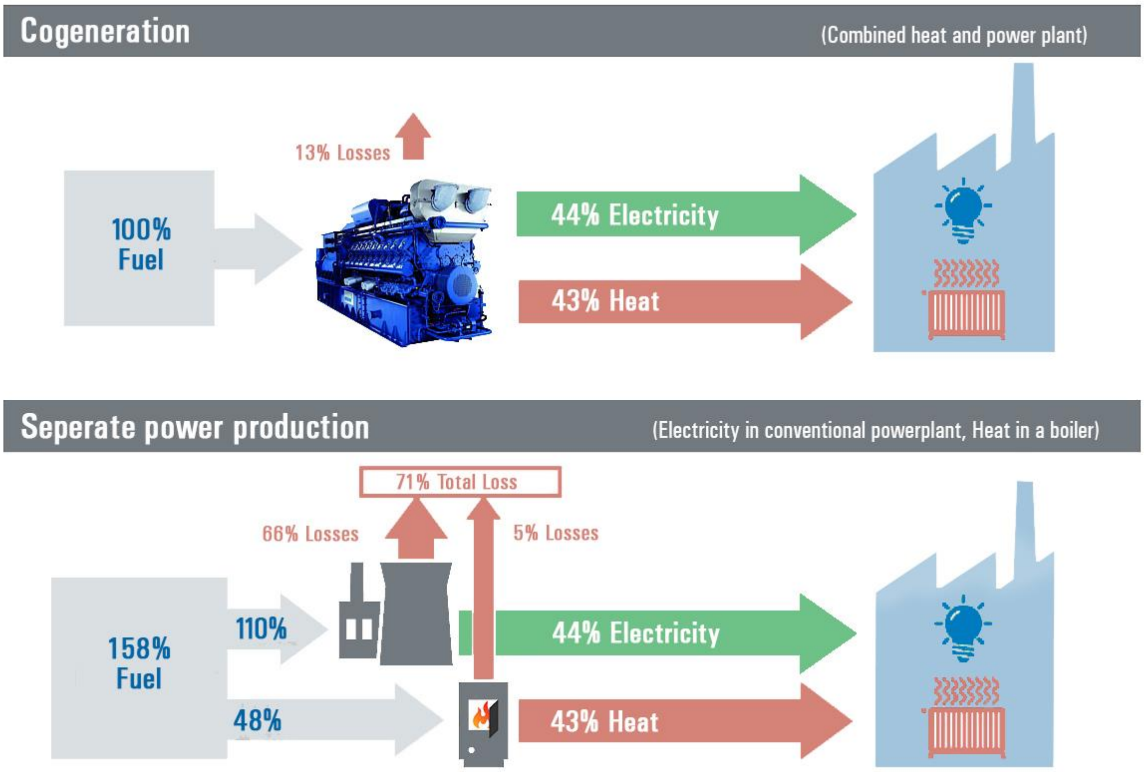

Figure 10 – Power plants, traditional vs. CHP. (Example values) Source: MWM site [26]

Usually, the recovered heat is used for hot water or steam production which is used for low temperature applications such as district heating, domestic hot water production and industrial processes.

Common CHP plants are:

- Gas Turbine: electricity is produced with a Bryton-Joule cycle performed by the GT and the high temperature exhausts are used to produce heat in a heat recovery unit (HRSG). In this type of plants can be also performed a post-combustion of exhausts to increase the heat recovered in the HRSG. Microturbines are small regenerative GT system used for small CHP application (kW).
- Steam Turbine: electricity is produced with a Rankine-Hirn cycle, the heat is produced by steam condensation. There are two type of plants: non-condensing (back-pressure)

turbine and extraction turbine. In back-pressure turbine the entire flow of steam is sent to the user, usually at ambient pressure. In extraction turbine a portion of the steam is extracted at medium pressure and used for CHP purposes.

- Internal Combustion Engine: electricity is produced with a Diesel or Otto cycle performed by a reciprocating engine. The heat is produced as a combination of a heat recovery from the ICE cooling system (jacket water, lube oil and air intercooler heat exchangers) and from the gas exhausts heat exchanger.
- Fuel Cell: electricity is produced with high temperature fuel cell, such as molten carbonate fuel cell (MCFC) or solid oxide fuel cell (SOFC), while the high temperature exhausts are used for heat recovery.
- Hybrid configuration: the most common is the combined cycle which is a combination of gas turbine and steam turbine technologies. The GT is the top cycle, the exhausts are used to produce steam in a HRSG for the bottom cycle (Rankine-Hirn cycle), the residual heat recovered is used for thermal applications (such as district heating). There are other combinations, less popular because not yet mature, such as GT-SOFC systems.

Different fuels can be used in a CHP system, in Figure 11 are reported the ones that are used.

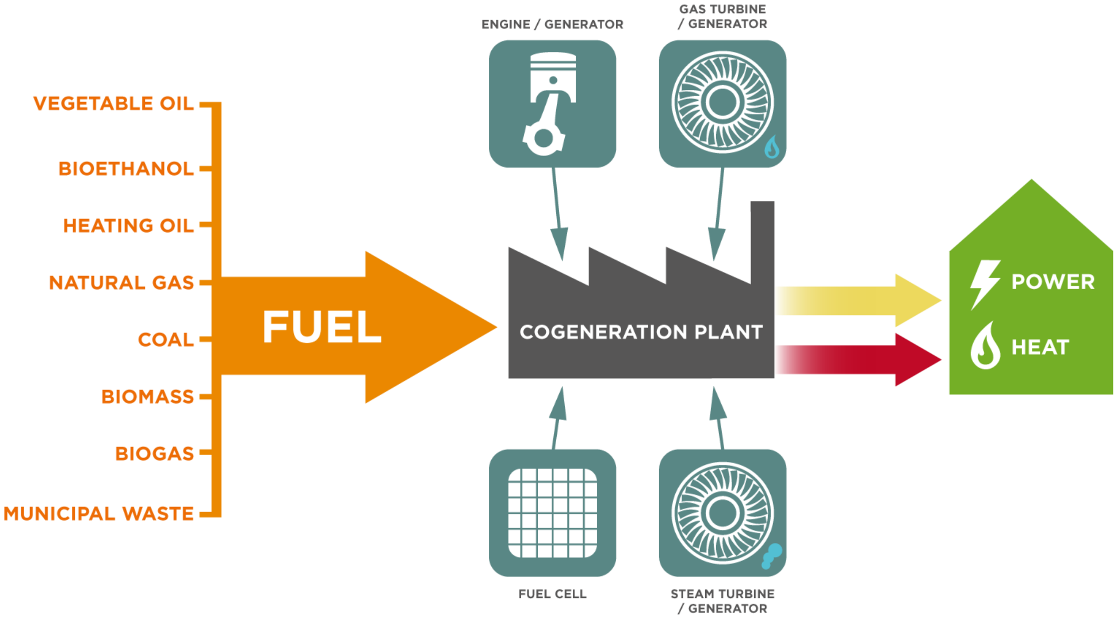

Figure 11 – CHP systems fuels. Source: [27]

The CHP technology has several key advantages such as:

- Financial benefits: energy costs are reduced thanks to electrical generation on site that remove the need of electrical procurement from a 3rd party and reduced fuel costs thanks to the combined production.
- Efficiency benefits: fuel choice benefits, a CHP system can operate with several fuels, and increase of energy security because the system can operate entirely in off-grid mode.
- Environmental benefits: reduced emissions of CO_2 and other pollutants and reduced electric energy transmission losses from the grid compared to traditional (separated) power production.

- Legislative benefits: CHP systems are subject to economic benefits that encourage their use compared to traditional power generation.

There are also some disadvantages of CHP because is not suitable for all sites and can be financially intensive due to a high initial cost.

3 Plant model

This section discusses the modeling approach and the assumptions adopted to simulate the Molten Carbonate Fuel Cell using the software Aspen Plus.

3.1 Plant layout

The MCFC is installed as downstream process of a cogeneration (CHP) engine (model JMS 420 G8 B02). Figure 12 shows a concept of the system which has been simulated in Aspen Plus. The ICE is not included in the modelling since it considered an existing process within the generic analyzed plant. The modeling is focused on the MCFC system using the exhaust from the engine to produce electricity and heat, and on the CO_2 capture line.

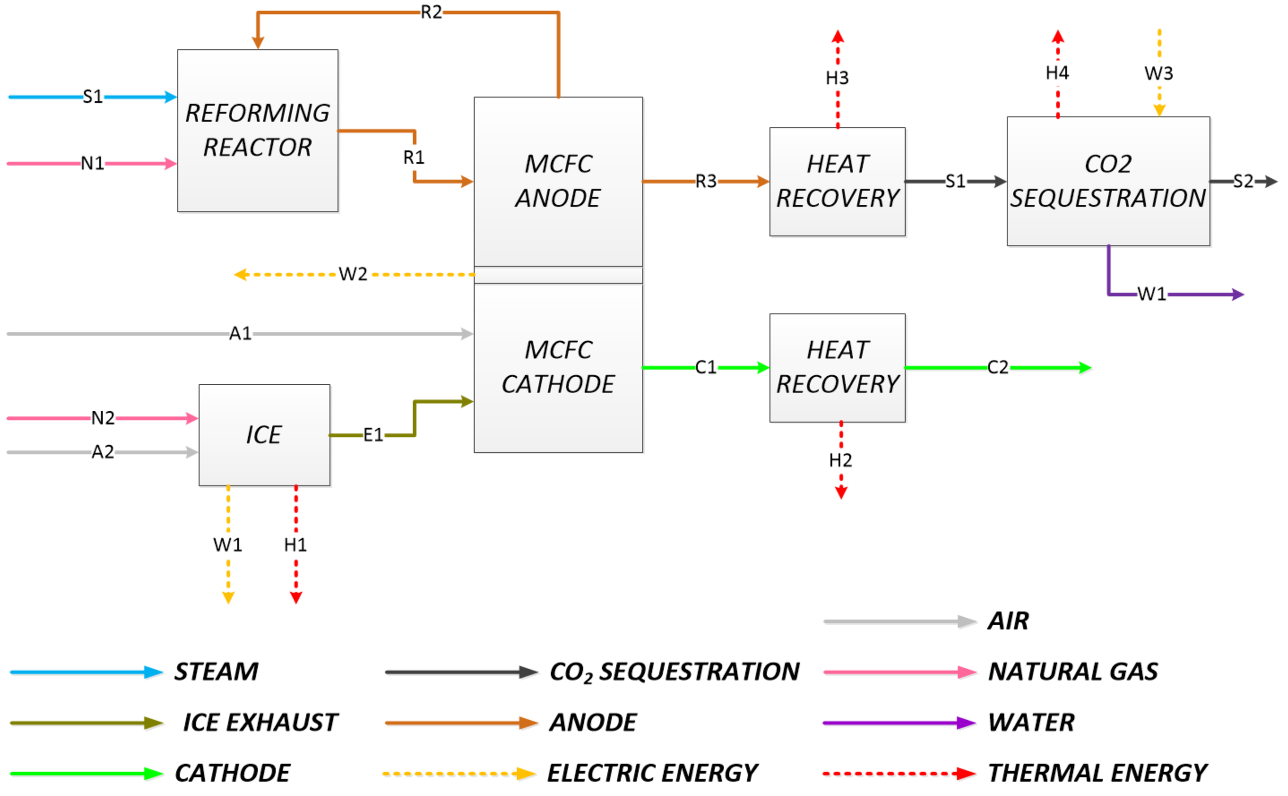

Figure 12 – Plant concept layout

The ICE exhausts (E1) are mixed with ambient air (A1), heated up until 628 °C and sent to the cathode of the MCFC. The anode side is fed with steam (S1), produced onsite, and natural gas (N1), which are mixed, heated up to 640 °C before being sent to the reformer (working at 640 °C), which will convert methane and other heavy hydrocarbons contained into the NG stream into hydrogen and carbon monoxide. The reforming agent used for this conversion is the steam, partially provided by the external and partially recirculated from the anode exhaust (R2)

Inside the cell cathode the carbon dioxide and oxygen contained in the exhaust are converted in carbonate ions and electrons through an electrochemical reaction. The ions migrate towards the anode passing through the liquid electrolyte while the electrons using an external electric circuit, generating electricity (W2).

Once the carbonate ions and electrons reach the anode, a second electrochemical reaction occurs where hydrogen, carbonate ions and electrons are converted in carbon dioxide and water.

Once the reactions inside the cells occur, at the cathode the ICE exhausts (C1) are released but with most of the CO_2 removed. Before release the stream in atmosphere, a cathodic heat recovery is performed.

On the anode outlet (R3) CO_2, water, and unreacted fuel are available. A part (10%) of the anode exhaust is recirculated to the reformer to provide a fraction of the required steam.

In traditional MCFC systems where carbon capture is not performed, anode and cathode exhausts are burnt together to convert the remaining chemical energy contained in the unreacted fuel into thermal energy, then heat recovery is performed before venting the flow to the atmosphere. In case of carbon capture, the anode stream is not mixed with the cathode one, to avoid nitrogen dilution of the stream, which will make the carbon capture process more difficult.

In this model different solutions have been analyzed for what concerning the carbon capture process:

- In the first layout the anode stream is cooled until water condensation temperature while performing heat recovery, then unreacted hydrogen is removed by means of membranes and the CO_2 compressed [28]–[31]. This system allows to produce a pure hydrogen stream but lead to a lower quality CO_2 output, because some CO is trapped inside.
- The second layout includes an oxy-combustor to convert unreacted H_2 and CO by means of pure oxygen (produced onsite with a dedicated ASU). In this way chemical energy is converted into thermal energy avoiding nitrogen dilution, leading to a higher purity CO_2 outlet stream.

In Figure 12 only the common streams of the two solutions are considered to make more understandable the plant concept. In both cases the captured stream needs to be cooled down to remove water by condensation (W1), an anodic heat recovery can be performed before reaching the condensation temperature. After the water is removed the CO_2 need to be further cooled down to 40 °C before being compressed to 150 bar.

The compression stage uses an intercooled compression train to reduce the mechanical work.

When compressed, the CO_2 (S2) can be injected in a CO_2 pipeline (if satisfy the quality requirements) or used on site in other applications.

3.2 Properties

In order to build the model a correct definition of units set and chemical components is needed. Firstly, a set based on default International System of Units (SI), inside the software, is implemented with some modifications: bar is chosen for pressure and Celsius degree for temperature. The chemical components defined are reported in Table 1, the state equation solving method adopted is Peng-Rob method.

Table 1 – Chemical components

Component ID	**Component name**
CH_4	Methane
CO_2	Carbon dioxide
H_2	Hydrogen
CO	Carbon monoxide
H_2O	Water
N_2	Nitrogen
O_2	Oxygen
C_2H_6	Ethane
C_3H_8	Propane
NO	Nitric oxide
NO_2	Nitrogen dioxide

3.3 Aspen Plus tools

In Aspen Plus a fuel cell cannot be modeled as single component because there is no library for fuel cell components so anode and cathode should be modeled separately by using other components available in the library. Each part with the related streams and components is now described in detail.

In the development of the model two tools are used that may be unknown for readers not used to the Aspen Plus software.

The first is the Calculator tool, this utility permits to perform calculations involving data, that can be evaluated by the software, using Fortran or a Microsoft Excel spreadsheet.

The second one is Design Specification; this tool sets the value of a variable that the software would otherwise calculate. In a design specification, is needed to identify the variables or other simulation inputs to be manipulated to meet the specification imposed.

3.4 Cathode and anode inlet streams

The anode inlet streams are natural gas and steam needed for reforming the fuel.

A composition of natural gas is supposed [16] and its reported in Table 2.

Table 2 – Natural gas composition

Component	**Molar fraction**	**Molecular weight [g/mol]**	**Mass [g]**	**LHV [MJ/kg]**
CH_4	0.912	16.04	14.629	50
N_2	0.043	14	0.602	0
C_2H_6	0.044	30.08	1.324	47.8
C_3H_8	0.001	44.11	0.0441	46.4

On the cathode side, the inlet streams are air, needed to provide oxygen to the MCFC and for the stack cooling, and the ICE exhaust. The air composition used is 21% oxygen and 79% nitrogen.

Not having data on the composition of the exhaust of the engine, a calculation of the combustion reaction is made, using the data present in Appendix I: JMS 420 G8 B02 datasheet [32].
Full load values are used for this calculation, as it is assumed that the ICE works most of the time at full load; those values are reported in Table 3.

Table 3 – JMS 420 full load data from datasheet

Parameter	Value	Unit
$\dot{V}_{fuel,CHP,ref}$	360	[Nm³/h]
LHV_{ref}	9.5	[kWh/Nm³]
$\dot{F}$	3417	[kW]
$G_{air,CHP,ref}$	7819	[kg/h]
$G_{exh,wet,CHP,ref}$	8064	[kg/h]
T_{exh}	378	[°C]

The LHV of the natural gas composition is firstly evaluated.

$$LHV_{NG} = y_{CH_4} \cdot LHV_{CH_4} + y_{C_2H_6} \cdot LHV_{C_2H_6} + y_{C_3H_8} \cdot LHV_{C_3H_8} \qquad \left[\frac{MJ}{kg}\right] \tag{3}$$

Where y_i is the molar fraction of i-specie from Table 2 and LHV_i is the lower heating value of i-specie found in literature.

Applying the values reported in Table 2 inside equation (3) the LHV of natural gas used is:

$$LHV_{NG} = 47.75 \left[\frac{MJ}{kg}\right] = 9.82 \left[\frac{kWh}{Nm^3}\right]$$

The LHV value of natural gas used in this model slightly differs (3.3%) from the reference LHV of the datasheet. This small variation introduces a change in the exhaust mass flow rate [33].

In order to evaluate the exhaust gas flow rate in the model conditions, (which differs from the reference ones) some assumption have been performed.
In both conditions the exhaust flow rate is evaluated as the sum of fuel and air mass flows (5) by applying the principle of mass conservation (4) on the ICE in steady state condition as showed in Figure 13.

$$\left(\frac{\delta M}{\delta t}\right)_{C.V.} + \sum_{k=1}^{n^\circ\, flows} G_k = 0 \tag{4}$$

$$G_{exh,wet,CHP} = G_{fuel,CHP} + G_{air,CHP} \tag{5}$$

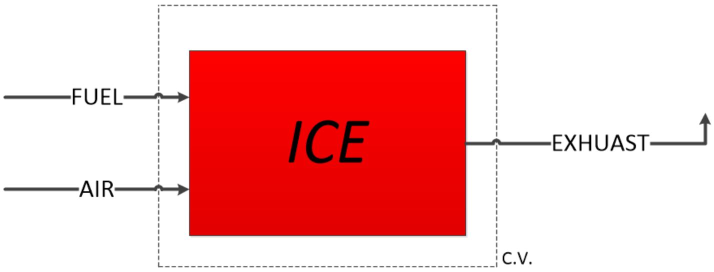

Figure 13 – ICE mass balance

To evaluate the exhaust flow rate in the model condition is needed to firstly evaluate all the mass flow rates in reference condition.

The datasheet provides, in full load condition, the air and exhaust mass flow rates while for the fuel a volumetric flow rate is given.
Is possible to evaluate the fuel mass flow (in the reference conditions) by applying the principle of mass conservation (4) on the ICE in steady state condition as showed in Figure 13 resulting in (6) using the values present in Table 3.

$$G_{fuel,CHP,ref} = G_{exh,wet,CHP,ref} - G_{air,CHP,ref} = 8064 - 7819 = 245 \qquad \left[\frac{kg}{h}\right] \tag{6}$$

The air dosage α_{ref} (in reference conditions) is defined as (7), so it is possible to evaluate it as (8).

$$\alpha = \frac{G_{air}}{G_{fuel}} \tag{7}$$

$$\alpha_{ref} = \frac{G_{air,CHP,ref}}{G_{fuel,CHP,ref}} = \frac{7819}{245} = 31.9 \tag{8}$$

For natural gas, a stoichiometric dosage α_{st} of 17 is supposed [34], so is possible to evaluate the air index n_{ref} (9).

$$n_{ref} = \frac{\alpha_{ref}}{\alpha_{st}} = \frac{31.9}{17} = 1.88 \tag{9}$$

Now is possible to calculate the flow rates in the model conditions using the results obtained for the reference conditions and performing some assumptions.

First, the fuel mass flow rate is evaluated. In reference condition a volumetric flow is given but, in the datasheet, consumption refers to the LHV [33] as defined as (10):

$$\dot{V}_{fuel} = \frac{\dot{F}}{LHV_{ref}} \tag{10}$$

Where $\dot{F}$ is the introduced power of fuel, defined in Table 3.

So, with the same amount of introduced power, the consumption of fuel can be expressed:

$$\dot{V}^*_{fuel} = \frac{\dot{F}}{LHV_{NG}} = \frac{3{,}417}{9.82} = 347.9 \qquad \left[\frac{Nm^3}{h}\right] \tag{11}$$

Once it is evaluated the corrected consumption of gas, is possible to evaluate the fuel mass flow rate as (12):

$$G^*_{fuel,CHP} = \dot{V}^*_{fuel,CHP} \cdot \frac{MW_{NG}}{22.414} = 347.9 \cdot \frac{16.598}{22.414} = 257.6 \qquad \left[\frac{kg}{h}\right] \tag{12}$$

Where MW_{NG} is the molar weight of natural gas evaluated with (13) using the values in Table 2.

$$MW_{NG} = y_{CH_4}MW_{CH_4} + y_{C_2H_6}MW_{C_2H_6} + y_{C_3H_8}MW_{C_3H_8} + y_{N_2}MW_{N_2} \qquad \left[\frac{g}{mol}\right] \tag{13}$$

Second, the air mass flow in real condition is evaluated assuming the air dosage, evaluated in reference conditions (8), as constant parameter (14) because it is considered the same working point but with different fuel mass flow, so the air mass flow can be evaluated as (15):

$$\alpha^* = \alpha_{ref} \tag{14}$$

$$G^*_{air,CHP} = G^*_{fuel,CHP} \cdot \alpha^* = 257.6 \cdot 31.9 = 8221.1 \qquad \left[\frac{kg}{h}\right] \tag{15}$$

When the real air flow is calculated the exhaust flow (16), in the new supply conditions, can be calculated using the mass balance on ICE (5).

$$G^*_{exh,wet,CHP} = G^*_{fuel,CHP} + G^*_{air,CHP} = 8221.1 + 257.6 = 8473.7 \qquad \left[\frac{kg}{h}\right] \tag{16}$$

Now with the information about the exhaust mass flow rate and the air index is possible evaluate the exhaust mixture composition to fully define the ICE exhaust inside the model.

A complete combustion reaction (17) is assumed [35].

$$\begin{gathered} 0.912CH_4 + 0.043N_2 + 0.044C_2H_6 + 0.001C_3H_8 + n \cdot x\left(O_2 + \frac{79}{21}N_2\right) \rightarrow \\ \rightarrow a \cdot CO_2 + b \cdot H_2O + n \cdot x \cdot \frac{79}{21}N_2 + 0.043N_2 + x(n-1)O_2 \end{gathered} \tag{17}$$

Where the coefficient *a, b*, and *x* are the stoichiometric coefficients of products evaluated in (18), (19) and (20) balancing reaction (17).

$$a = 0.912 + 2 \cdot 0.044 + 3 \cdot 0.001 = 1.003 \qquad \left[\frac{mol_{CO_2}}{mol_{NG}}\right] \tag{18}$$

$$b = 2 \cdot 0.912 + 3 \cdot 0.044 + 4 \cdot 0.001 = 1.960 \qquad \left[\frac{mol_{H_2O}}{mol_{NG}}\right] \tag{19}$$

$$x = a + \frac{b}{2} = 1.003 + \frac{1.960}{2} = 2.963 \qquad \left[\frac{mol_{O_2}}{mol_{NG}}\right] \tag{20}$$

In conclusion, from 1 mol of natural gas, the exhaust composition is reported in Table 4.

Table 4 – Exhaust composition

Specie	Mol	y	Vol [l]	% Vol. dry	% Vol. wet
CO_2	1.003	0.0378	53.592	4.076	3.775
H_2O	1.960	0.0738	104.727	/	7.377
O_2	2.607	0.0981	139.297	10.594	9.813
N_2	20.998	0.7903	1121.965	85.330	79.035
Total	26.568	1	dry: 1314.854 wet: 1419.581	100	100

The volume occupied by a mol v_{mol} is evaluated using relation (21):

$$v_{mol} = v_{mol@N.c} \cdot \frac{T_{exh}}{273.15} = 22.414 \cdot \frac{378 + 273.15}{273.15} = 53.432 \qquad \left[\frac{l}{mol}\right] \tag{21}$$

Where $v_{mol@N.c}$ is molar volume in normal condition and T_{exh} is exhaust temperature defined in Table 3.

As for the pollutants emissions the manufacturer guarantees for the reference oxygen content:

- NO_x<250 mg/Nm^3 (5%O_2)
- CO<300 mg/Nm^3 (5%O_2)

The corrected values of emissions e for an oxygen content of 8.79% are calculated using formula (22):

- NO_x<175 mg/Nm^3
- CO<210 mg/Nm^3

$$e = e_{ref} \frac{21 - \%O_2}{21 - \%O_{2,ref}} \qquad \left[\frac{mg}{Nm^3}\right] \tag{22}$$

Where e_{ref} are the emissions in reference condition and $\%O_2$ and $\%O_{2,ref}$ is the oxygen content of exhaust respectively in real condition and reference condition.

In this model the emissions of NO_x and CO are neglected due the low quantity (ppm) and thus are not interacting in the model because they are inert inside the fuel cell [14].

Once the ICE exhaust mass flow is determined, the other ones are dependent on the molar flow of CO_2 inside the ICE exhaust. In Figure 14 is reported a simplify version of the inlet flows involved in the MCFC.

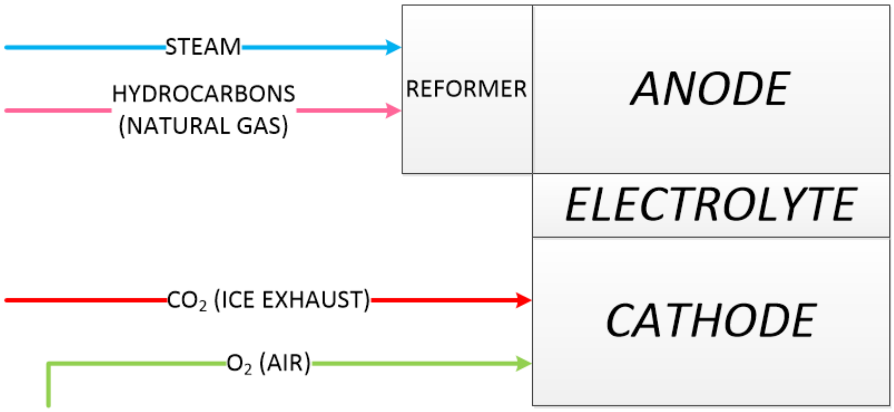

Figure 14 – MCFC inlet flows

On cathode side there is the reduction reaction (23) of air and flue gases of ICE producing carbonate ions.

$$\frac{1}{2}O_2 + CO_2 + 2e^- \rightarrow CO_3^= \tag{23}$$

In this model only a part of the CO_2 present in the exhaust is used as a fuel in the cell, the CO_2 utilization factor U_{CO_2} can be defined as the ratio between the flow rate of CO_2 transferred through the cell as carbonate $CO_3^=$ ions and the CO_2 flow rate introduced at the cathode inlet.

$$U_{CO_2} = \frac{\dot{n}_{CO_2,consumed}}{\dot{n}_{CO_2,in}} \tag{24}$$

In this case is chosen to apply a CO_2 utilization factor U_{CO_2} of 0.75 [9] in order to maintain an excess of cathodic reagent for the correct functioning of the cell and to limit losses due to the diffusion of reagents in the cell.

First, is evaluated the total current I_{tot} produced by the CO_2 flow (26) using the Faraday's law (25) where z_i is the charge number of a chemical specie i and F is the Faraday constant (96,487 C/mol).
Once the current is calculated using again the Faraday's law (25) the oxygen molar flow $\dot{n}_{O_2}$ is evaluated imposing a charge number of 4.

$$\dot{n}_i = \frac{I}{z_i \cdot F} \qquad \left[\frac{mol}{s}\right] \tag{25}$$

$$I_{tot} = U_{CO_2} \cdot \dot{n}_{CO_2,in} \cdot 2 \cdot F \qquad [A] \tag{26}$$

$$\dot{n}_{O_2} = \frac{I_{tot}}{z_{O_2} \cdot F} \qquad \left[\frac{mol}{s}\right] \tag{27}$$

At the cell anode the oxidation reaction of the reformed natural gas occurs. The natural gas mixture has different hydrocarbons that participate in the reforming reactions.

For each of them, the molar flow is evaluated with the Faraday's law (25).
As for the cathode, in the anode only a part of the fuel reacts inside the cell. The fuel utilization factor FU (32) is defined as the ratio between the stoichiometric molar flow needed for the

reaction and the total molar flow sent at the anode, as reported in equations (28), (29), and (30). In this model is chosen to have a FU of 0.75 [9] to maintain an excess of anodic reagent for the correct functioning of the cell and to limit losses due to fuel diffusion.

The charge numbers of hydrocarbons are evaluated with relation (31) and for methane, ethane and propane the charge numbers are respectively 8, 14 and 20.

The flow of fuel needed is calculated as a weighed contribution of each hydrocarbon in the mixture (33).

The molar flow of natural gas (34) is evaluated as the fuel molar flow (33) divided the molar fraction of hydrocarbons in the mixture considering that in natural gas there is also an inert (nitrogen) as reported in Table 2.

$$\dot{n}_{CH_4} = \frac{I_{tot}}{z_{CH_4} \cdot F \cdot FU} \qquad \left[\frac{mol}{s}\right] \tag{28}$$

$$\dot{n}_{C_2H_6} = \frac{I_{tot}}{z_{C_2H_6} \cdot F \cdot FU} \qquad \left[\frac{mol}{s}\right] \tag{29}$$

$$\dot{n}_{C_3H_8} = \frac{I_{tot}}{z_{C_3H_8} \cdot F \cdot FU} \qquad \left[\frac{mol}{s}\right] \tag{30}$$

$$z_{C_xH_y} = 4x + y \tag{31}$$

$$FU = \frac{\dot{n}_{fuel,st}}{\dot{n}_{fuel,tot}} \tag{32}$$

$$\dot{n}_{FUEL} = y_{CH_4} \cdot \dot{n}_{CH_4} + y_{C_2H_6} \cdot \dot{n}_{C_2H_6} + y_{C_3H_8} \cdot \dot{n}_{C_3H_8} \qquad \left[\frac{mol}{s}\right] \tag{33}$$

$$\dot{n}_{NG} = \frac{\dot{n}_{FUEL}}{y_{hc}} \qquad \left[\frac{mol}{s}\right] \tag{34}$$

3.5 Reformer

Inside the reformer, steam (produced onsite) react with the fuel (natural gas) in a set of reaction to produce mainly hydrogen, carbon dioxide and carbon monoxide. The main reactions of natural gas steam reforming are:

$$CH_4 + H_2O \leftrightarrow 3H_2 + CO \qquad \Delta H^0_{298\,K} = 206.4\ [kJ/mol] \tag{35}$$

$$C_nH_m + nH_2O \rightarrow \left(\frac{m}{2} + n\right) H_2 + nCO \qquad \Delta H^0_{298\,K} > 0 \tag{36}$$

$$CO + H_2O \leftrightarrow H_2 + CO_2 \qquad \Delta H^0_{298\,K} = -41.2\ [kJ/mol] \tag{37}$$

Reaction (36) represent the steam reforming of hydrocarbon heavier than methane contained in natural gas.

The concurrent water gas shift reaction (37) is a slightly exothermic reaction and convert the carbon monoxide produced in (35) and (36) into hydrogen and carbon dioxide. Globally the overall process is endothermic (heat is requested to support the reaction).

Because of the endothermic nature of natural gas steam reforming, a heat input is required.
The reformer reactor can be classified according to the heat source:

a. External: heat is supplied by an external source (e.g. heat recovery from system or with a dedicated NG-fed burner).
b. Internal indirect: heat is supplied by the fuel cell reaction, which is exothermic, but reforming does not take place on the cell anode. The two reactions are kept separated and are only thermally connected.
c. Internal direct: reforming reaction happens directly on the anode of the fuel cell. This could create cold areas on the anode and should be limited to around 50% maximum and the remaining part should be reformed with the previous options.

In steam reforming other reaction may occurs as CO_2 reforming or dry reforming (38), methane decomposition (39) and Boundouard reaction (40) [36]. The last two reactions produce carbon deposits.

$$CH_4 + CO_2 \rightarrow 2H_2 + 2CO \qquad \Delta H^0_{298\,K} = 247.3\ [kJ/mol] \tag{38}$$

$$CH_4 \rightarrow C + H_2 \qquad \Delta H^0_{298\,K} = 74.9\ [kJ/mol] \tag{39}$$

$$2CO \rightarrow C + CO_2 \qquad \Delta H^0_{298\,K} = -172.5\ [kJ/mol] \tag{40}$$

The reaction bed in which the reforming occurs normally contains a catalyst, mainly based on nickel, that improve kinetics of (35) and (36), decreasing the reformer temperature, but can be poisoned by sulfur compounds and carbon deposit (solid particles) causing the catalyst deactivation.
To avoid carbon deposition an oxygen carrier is added to the fuel, such as H_2O, CO_2 and O_2, the most used are water and oxygen.
This generate a mixture that is thermodynamically stable towards separation of C in solid form.
The Steam to Carbon ratio (S/C) (41) is a parameter defined to avoid carbon deposition in the cell, in this model is chosen a S/C of 3.5 [6]–[8]. A design specification tool is used to guarantee the defined S/C ratio.

$$S/C = \frac{\dot{n}_{H_2O}}{\dot{n}_{CH_4}} \tag{41}$$

In S/C definition is used the molar flow of methane due the fact that it is the prevalent hydrocarbon in the supposed mixture as reported in Table 2

In this model it is assumed that reactions (35) and (36) are completely moved on the product side thanks to the abundant quantity of steam added to the fuel mixture imposed by (41) and WGS (37) is supposed to reach the thermodynamic equilibrium at the operating temperature.

The main operating variables that influence the process are temperature, pressure and the molar Steam to Carbon ratio (S/C) (41).

In this model is chosen to adopt an internal indirect reformer, operating at $p = 1.013$ bar (atmospheric pressure) and $T = 640$ °C [37], [38].

The reformer is modeled using an isothermal Gibbs reactor (reactions are supposed to reach equilibrium in the component).

In this model is chosen to do an anodic recirculation of 10% of anode outlet and the remaining is sent to the carbon capture section, in this way the high temperature anodic exhaust is used to heat up the mixture of steam and natural gas with the optics of the heat recovery and to decrease the consumption of steam. In this design specification is manipulated the steam molar flow to guarantee the imposed S/C ratio.

3.6 Molten Carbonate Fuel Cell

At the cell anode the oxidation reaction (42) of the reformed fuel occurs, in this model it is assumed that the only fuel is hydrogen and the remaining carbon monoxide and hydrocarbons undergo a second reforming reaction on the anode thanks to the abundant quantity of steam used.

On cathode side there is the reduction reaction (43) of air and flue gases of ICE producing carbonate ions needed in reaction (42)

$$H_2 + CO_3^{=} \rightarrow H_2O + CO_2 + 2e^- \tag{42}$$

$$\frac{1}{2}O_2 + CO_2 + 2e^- \rightarrow CO_3^{=} \tag{43}$$

In Aspen Plus it is not possible to model the cell as a single component and use ions inside the simulation, so the carbonate ion $CO_3^{=}$ stream is divided in two streams, one for CO_2 and another for O_2 moving from cathode towards to anode.
The anode is simulated using an isothermal Gibbs reactor, at the operating conditions of 1.013 bar (ambient pressure) and 660 °C where the fuel oxidation occurs producing heat and power.
This temperature is chosen to simulate a temperature gradient of 20 °C inside the anode, due to the electrochemical reaction, and obtain an average temperature of 650 °C.
For the cathode, a separator block is used, which separate the components needed at the anode and send to the chimney (atmosphere) the other components not used.
In Figure 15 is reported the scheme of the MCFC with the reformer used in Aspen Plus.

The inlet molar flows are imposed by an Aspen calculator.
In the calculator is used directly the molar flow of CO_2 ($\dot{n}_{CO_2,consumed}$) sent to the anode (stream CO_2) because the utilization factor U_{CO_2} is imposed as the split fraction inside the separator definitions. In the calculator, I_{tot} is an export parameter evaluated using $\dot{n}_{CO_2,consumed}$ (imported variable of CO_2 stream) and $\dot{n}_{O_2}$ is an export block variable that overwrite the flow fraction of O_2 in the separator block (cathode). The molar flow of each hydrocarbon of the natural gas ($\dot{n}_{CH_4}$, $\dot{n}_{C_2H_6}$, $\dot{n}_{C_3H_8}$, and $\dot{n}_{FUEL}$) is evaluated as export parameters while $\dot{n}_{NG}$ is an export stream variable that overwrite the initial molar flow of natural gas (stream NG1).

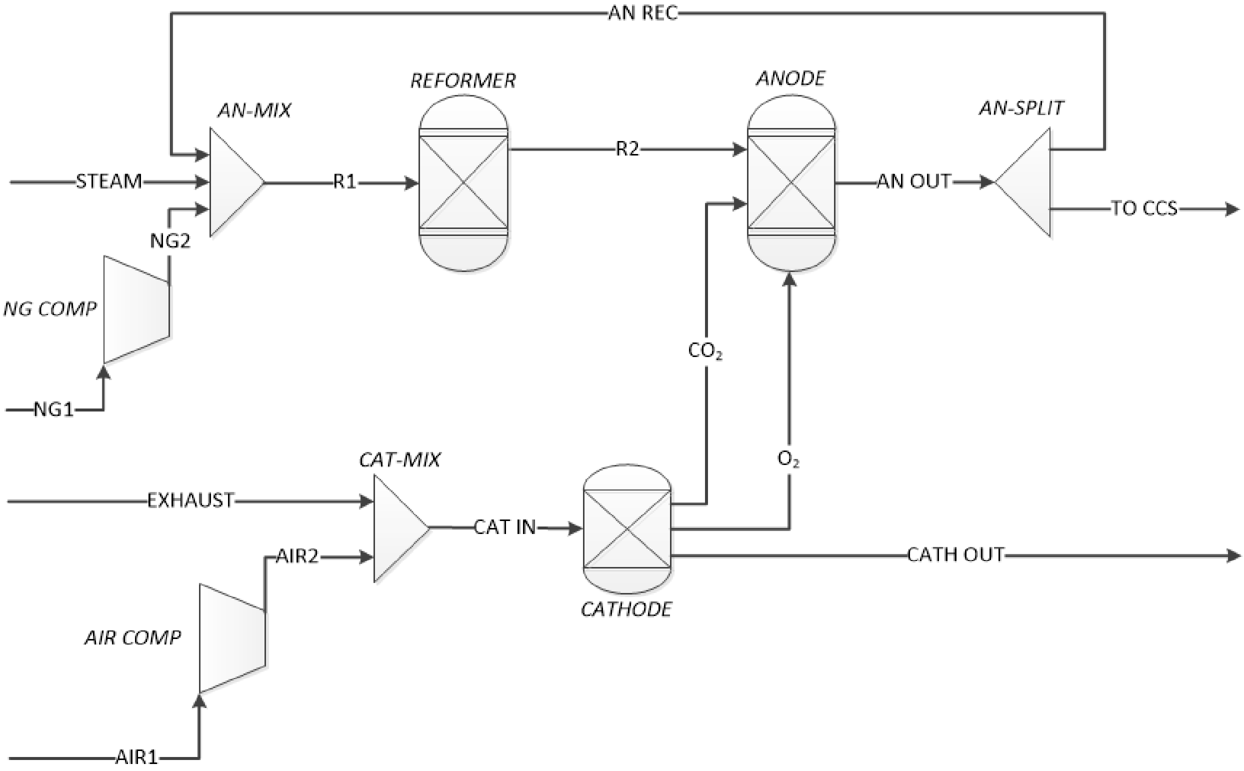

Figure 15 – MCFC in Aspen Plus

3.6.1 Electrochemical model

The cell voltage and performance in this model are evaluated by a calculator tool starting from reversible Nernst potential OCV_{Nernst} (44) [19].

$$OCV_{Nernst} = \frac{\Delta G}{z_i F} + \frac{RT}{z_i F} \ln \left[\frac{p_{H_2,an} \cdot (p_{O_2,cat})^{0.5} \cdot p_{CO_2,cat}}{p_{H_2O,an} \cdot p_{CO_2,an}} \right] \qquad [V] \qquad (44)$$

Where z_i is the charge number of chemical species i, in this case is equal 2 because the hydrogen dissociated, F is the Faraday constant, R is the gas constant, T the cell operating temperature and p_i is the partial pressure of chemical specie i.

The Gibbs free energy variation ΔG, which only depends on the thermodynamic properties of the chemical species involved in hydrogen oxidation, is calculated by the approximate relation (45) [39] depending on the cell operating temperature expressed in Kelvin.

$$\Delta G = 242{,}000 - 45.8 \cdot T \qquad \left[\frac{J}{mol \cdot K} \right] \qquad (45)$$

In literature various authors [13], [40]–[43] use the experimental model proposed by Campanari et al. [9], the same electrochemical model is adopted here.

In the model the cell losses are evaluated as a cell resistance divided among anode and cathode overpotential and the ohmic potential (46) [44]–[46]:

$$V_{cell} = OCV_{Nernst} - (R_{an} + R_{cat} + R_{ohm}) \cdot i_{cell} \qquad [V] \qquad (46)$$

Where R_{an} is the anodic resistance, R_{cat} is the cathodic resistance, R_{ohm} is the ohmic resistance and i_{cell} is the current density evaluated as (47):

$$i_{cell} = \frac{I_{tot}}{n_{cell}^{o} \cdot A_{cell}} \qquad \left[\frac{\Omega}{m^2}\right] \tag{47}$$

Where n_{cell}^{o} are the number of cell in a stack and A_{cell} is the cell area.

In this model is chosen to impose a current density and evaluate the number of stacks needed imposing a defined cell area.

The resistances are calculated according to equation (48), (49), and (50) proposed by Hao [45]:

$$R_{an} = 2.27 \cdot 10^{-9} \cdot \exp\left(\frac{E_{act,an}}{RT}\right) \cdot p_{H_2}^{-0.42} \cdot p_{CO_2}^{-0.17} \cdot p_{H_2O}^{-1.0} \qquad \left[\frac{\Omega}{m^2}\right] \tag{48}$$

$$R_{cat} = 7.505 \cdot 10^{-10} \cdot \exp\left(\frac{E_{act,cat}}{RT}\right) \cdot p_{O_2}^{-0.43} \cdot p_{CO_2}^{-0.09} \qquad \left[\frac{\Omega}{m^2}\right] \tag{49}$$

$$R_{ohm} = 0.5 \cdot 10^{-4} \cdot \exp\left[3016\left(\frac{1}{T} - \frac{1}{923}\right)\right] \qquad \left[\frac{\Omega}{m^2}\right] \tag{50}$$

$$p_i = \frac{y_i \cdot p_{tot}}{p_0} \tag{51}$$

Where

- p_k (51) is the partial pressure (non-dimensional with respect to 1 atm) of i-th specie.
- E_{act} is the anode and cathode activation energy (assumed $E_{act,an}$=53500 kJ/mol and $E_{act,cat}$=77229 kJ/mol [47]).
- T is the cell temperature calculated as the average value between the anode conditions at inlet and outlet, expressed in Kelvin.

The results of the electrochemical model are reported in Table 5. In the evaluation of R_{ohm} the coefficient 0.5 is modified to 1.1 to fit the model results found in [9].

Table 5 – Electrochemical model result

Parameter	**Value**	**Unit**
$p_{H_2,an}$	0.47	[-]
$p_{H_2O,an}$	0.46	[-]
$p_{CO_2,an}$	0.43	[-]
$p_{O_2,cat}$	0.10	[-]
$p_{CO_2,cat}$	0.04	[-]
R_{ohm}	1.10E-4	[Ω/m²]
R_{an}	8.24E-6	[Ω/m²]
R_{cat}	6.32E-5	[Ω/m²]
ΔG	199.7	[kJ/molK]
OCV_{Nernst}	0.97	[V]

The polarization curve of this model can be drawn by varying the current density, as reported in Figure 16, showing the typical linear behavior of MCFC that differs to the other fuel cell polarization curve.

The model curve is confronted with the results provided in Campanari et al. [9] to validate it.

The error between the two curves is evaluated as:

$$error = \frac{|V_{model,j} - V_{ref,j}|}{V_{ref,j}} \tag{52}$$

Where $V_{model,i}$ is the model voltage for a current density j and $V_{ref,j}$ is the voltage of Campanari reference for a current density j.

The average error between the two curves is 3.8% with a maximum value of 6.9%.

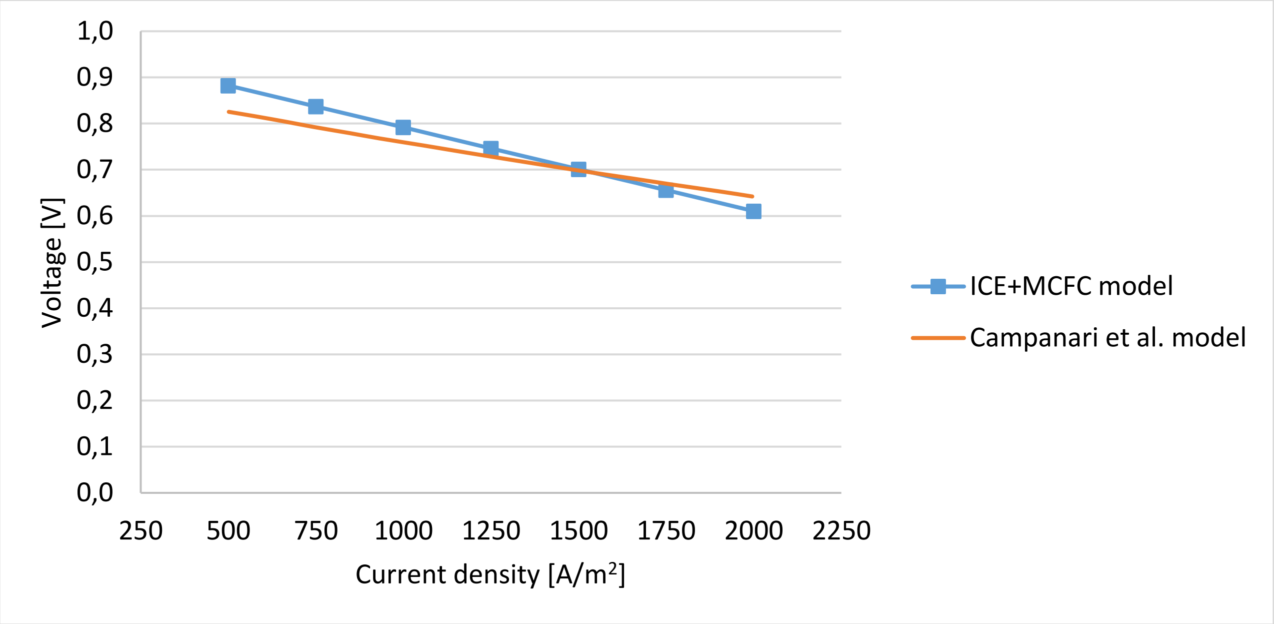

Figure 16 – Polarization curve

In this model the total current is imposed by the carbon dioxide molar flow through the Faraday's law (26), the number of stack necessary and the power produced by the cell are dependent on the imposed current density of the cell.
The electrical power (53), heat produced (54) and efficiency (55) of cell can be evaluated as:

$$W_{el,FC,DC} = V_{cell} \cdot I_{tot} \qquad [W] \tag{53}$$

$$\phi = \left(-\frac{\Delta\tilde{h}_{react}}{z_i F} - V_{cell} \right) \cdot I_{tot} = -\Delta H_{react} - V_{cell} \cdot I_{tot} \qquad [W] \tag{54}$$

$$\eta_{el,FC} = \frac{W_{el,FC,DC}}{G_{fuel,FC} \cdot LHV_{NG}} \tag{55}$$

Where ΔH_{react} is the net duty of the Gibbs reactor, used to simulate the anode, and is the global heat produced by the electrochemical reaction.

High power is obtained when using low current density and high voltage. Imposing a low current density means an increase of cells to obtain the same current output, so is necessary a tradeoff. In this model a cell area of 100 cm^2 is assumed, and each stack contain 100 cells.

From Figure 17, increasing the current density initially have a good response because there is a high decrease of number of stacks, compared to energy production, but for high current density there is a big drop in energy production despise the stack reduction, so in the model is choose to operate with a current density of 1300 A/m^2, in this way the number of stack is not excessive, 351 stacks, and the electric power produced is around 336 kW (DC).

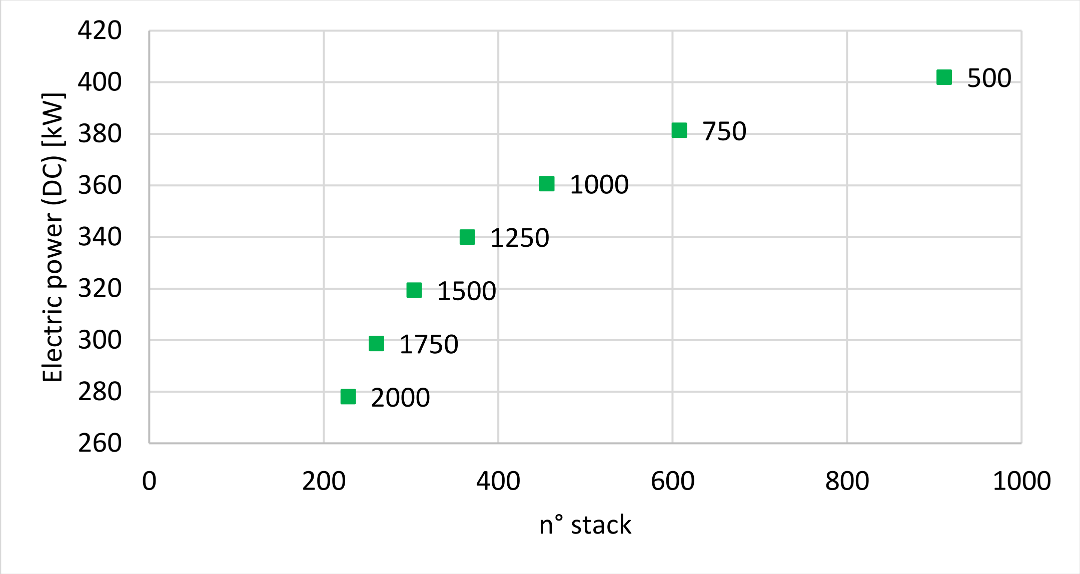

Figure 17 – Number of stack and electric power depending on the current density

In Table 6 the main feature of the fuel cell, working at the chosen current density of 1300 A/m², are reported.

Table 6 – Fuel Cell performance

Parameter	Value	Unit
V_{cell}	0.74	[V]
$W_{el,DC,FC}$	335.9	[kW]
ϕ_{cell}	236.6	[kW]
$n°\ cells$	35050	[-]
$n°\ stacks$	351	[-]
$\eta_{el,DC,FC}$	53.0 %	[-]

3.6.2 Thermal Balance

The electrochemical reaction is an exothermal process, some of this heat is used to sustain the reformer which is an endothermic process. The remaining heat need to be removed with an excess of air.

The heat removed by air ϕ_{air} is evaluated through a first principle balance (56) applied to the cell, it is also considered the heat used in the reformer.

$$\sum_{j=1}^{n} \phi_j - W_t - W_0 = \frac{\partial U^{tot}}{\partial t} + \sum_{k=1}^{nc} G_k \cdot h_k^{tot} \tag{56}$$

$$\phi_{air} = -\Delta H_{react} - \phi_{ref} - W_{el} \tag{57}$$

Where ΔH_{react} is the heat generated by the electrochemical reaction, ϕ_{ref} is the heat used in the reformer and W_{el} is the electric power generated by the cell.

The heat needed to be removed by air is evaluated with an Aspen calculator using a first principle balance (57) where ΔH_{react} and ϕ_{ref} are the net duty of Gibbs reactors for anode and reformer and W_{el} is imported from the excel calculator of electrochemical model.

When ϕ_{air} is calculated, a design specification is needed to apply a cathodic air mass flow able to remove it. To perform this manipulation a fictitious heat exchanger (HX-RAF in Figure 18) is added before the cathode to simulate the temperature gradient inside the cathode, in this model is set a temperature difference of 32 °C.

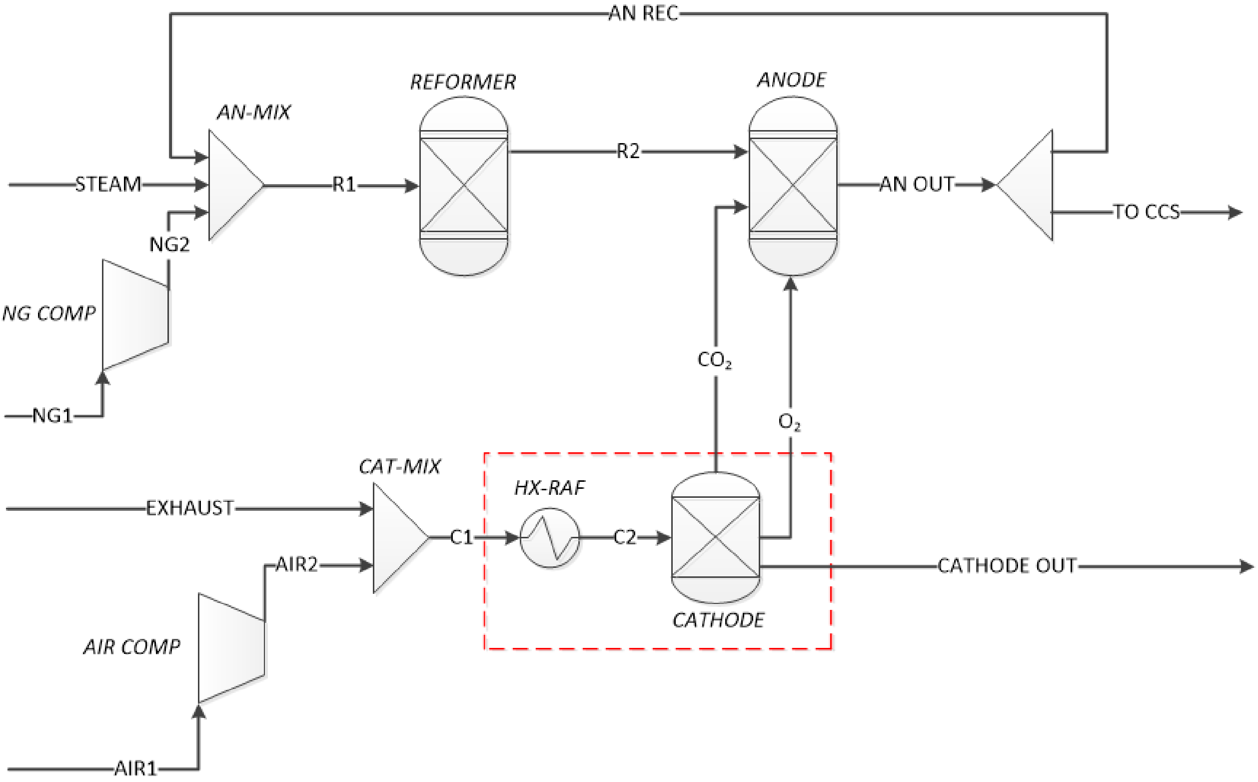

Figure 18 – Aspen layout

In the design specification the target is that the two heat flux are the same as (58), where ϕ_{HX} is the heat duty of the fictitious heat exchanger (HX-RAF)
The air flow needed $\dot{n}_{air,real}$ is evaluated as (59), where AU is the Air Utilization factor defined as (60). The design specification manipulates the AU factor.

$$\phi_{air} = \phi_{HX} \tag{58}$$

$$\dot{n}_{air,real} = AU \cdot \frac{\dot{n}_{O_2,st}}{0.21} \tag{59}$$

$$AU = \frac{\dot{n}_{air,real}}{\dot{n}_{air,st}} \tag{60}$$

With the same method used to defining U_{CO_2}, the O_2 utilization factor it can be defined as (61):

$$U_{O_2} = \frac{\dot{n}_{O_2\ consumed}}{\dot{n}_{O_2\ in}} \tag{61}$$

For a given composition at the cathode inlet, U_{O_2} and U_{CO_2} are related as half a mole of O_2 is required to react with one mole of CO_2 to originate a mole of $CO_3^{=}$ while $\dot{n}_{O_2\ in}$ are the total molar flow of oxygen sent to the cathode, in this simulation is obtained $U_{O_2} = 0.13$.

To conclude the MCFC section, Table 7 report all the inlet stream of the model.

Table 7 – Fuel cell inlet streams

Stream	**Symbol**	**Value**	**Unit**
Steam	G_{steam}	0.038	[kg/s]
Natural gas	$G_{fuel,FC}$	0.013	[kg/s]
Air	$G_{air,FC}$	0.093	[kg/s]
ICE flue gases	$G^{*}_{exh,wet,CHP}$	2.354	[kg/s]

3.7 Pressure drops evaluation

In this model a pressure drop of 500 mbar for both cathode and anode lines is set (assumption based on experience with real sites [48], [49]), so 2 compressors are added to the air stream and natural gas stream to compensate the pressure drops of the plant, making the assumption of electric-mechanical efficiency η_{el} of 0.98, isentropic efficiency η_c of 0.82 and mechanical efficiency η_m of 0.97. In the model, the pressure drop is assumed concentrated and modelled with a valve after the compressor.

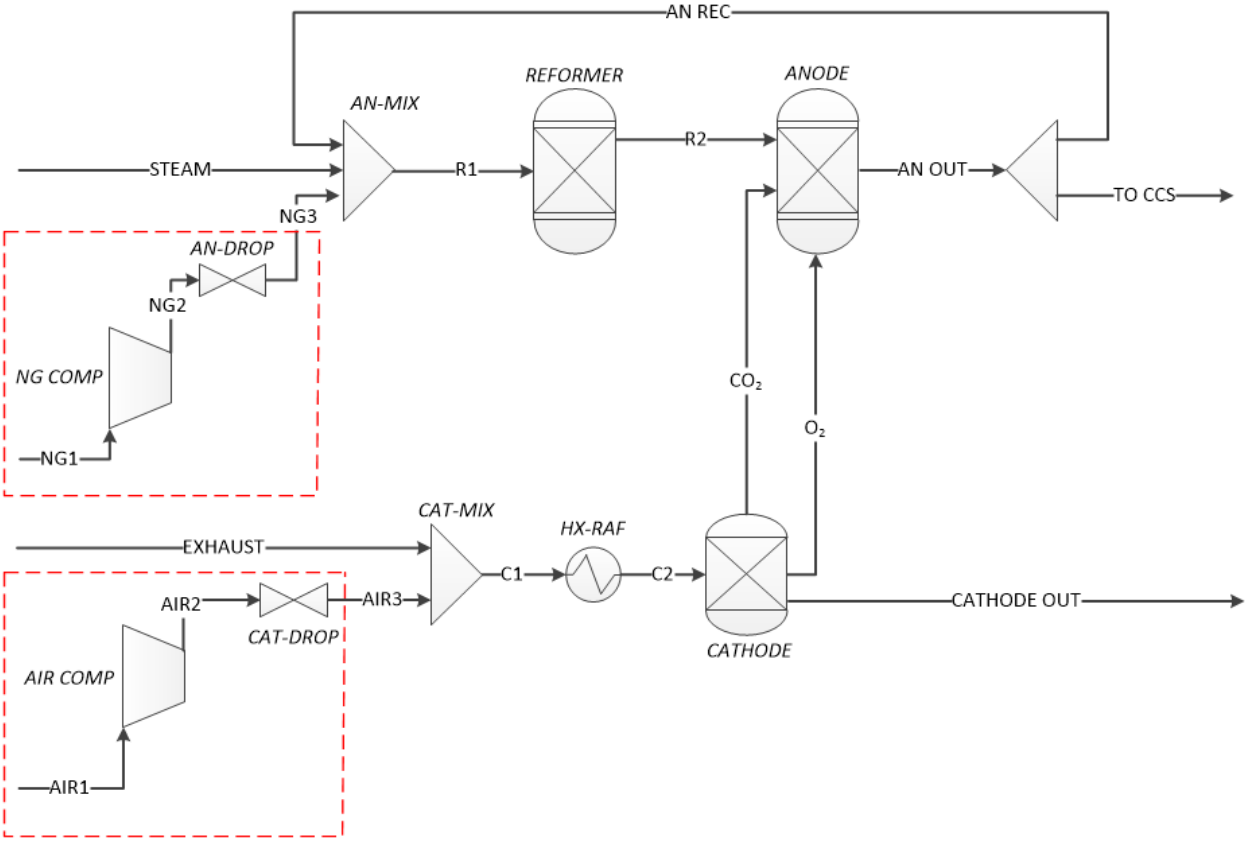

Figure 19 – Pressure drops in Aspen Plus

For the steam generation line, the pressure drop should be covered by a pump but it is neglected because the low energy consumption.

For the natural gas is assumed a supply pressure of 1.023 bar and temperature 15 °C, according to "Codice di Rete - Allegato 11/A" [50], while the air is assumed at 1.013 bar and 20 °C.

The mechanical and electric consumptions for each compressor are reported in Table 8.

Table 8 – Compressors consumptions

Parameter	**Name**	**Value**	**Unit**
$W_{m,air}$	Air compressor mechanical power	4.18	[kW]
$W_{el,air}$	Air compressor electrical power	4.26	[kW]
$W_{m,NG}$	NG compressor mechanical power	0.95	[kW]
$W_{el,NG}$	NG compressor electrical power	0.97	[kW]

3.8 Carbon capture section

The anode outlet that is not recirculated back to the reformer is sent to the carbon sequestration section. The composition of the anodic mixture is composed mainly of steam and carbon dioxide as anodic reaction products and a small fraction of residual unreacted fuel and nitrogen.

The stream S1 is at 660 °C and is cooled down to 102 °C with a heat exchanger, performing at the same time heat recovery, then the stream S2 enter in a condenser where the water is removed. The condenser works at 1.013 bar and in a range between 102 °C and 95 °C, the condensed water (W1) can be used again for the steam reforming reaction as the condensed water flow rate is greater than that needed by the reformer.
The outlet stream (S3) is composed mainly by CO_2 at 95 °C that need to be further cooled to 40 °C before entering in the compression unit.

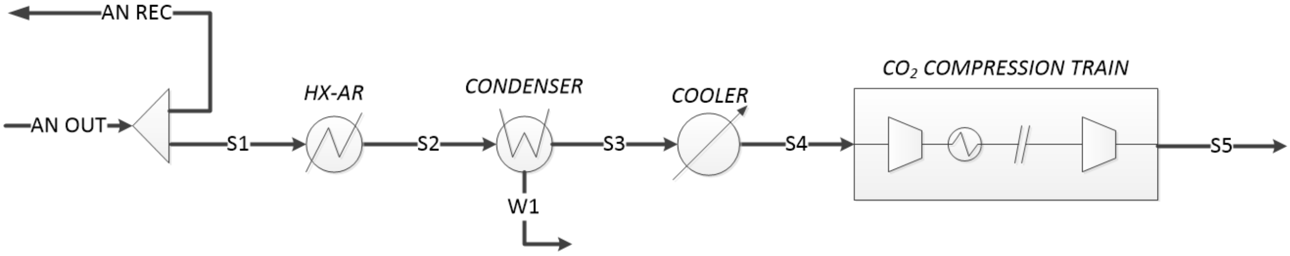

Figure 20 – Carbon Capture line

The stream S4 is compressed to 150 bar by a intercooled compression train. At the exit of the compression unit (S5) the CO_2 is still in gas form and can be injected in a pipeline or used inside the plant.

The intercooled compression train is composed by 4 radial compressors and 2 intercoolers that cool the stream to 40 °C, reducing the duty of the compressors. Table 9 shows the data used for the compressor train [51] in the Aspen Plus model

Table 9 – Compressors train data

Parameter	Name	Value	Unit
β	Pressure ratio	3.5	[-]
η_c	Isentropic efficiency	0.82	[-]
η_m	Mechanical efficiency	0.97	[-]
η_{el}	Electric-mechanic efficiency	0.98	[-]
p_{out}	Discharge pressure	150	[bar]

The discharge conditions are 150 bar and 40 °C following [52]: in this model is assumed that the plant is connected to a CO_2 pipeline where the compressed mixture is injected.

The CO_2 pipeline quality [19] are reported in Table 10:

Table 10 – Pipeline quality requirements

Component	Concentration	Related problems
H_2O	500 ppm	Corrosion (hydrates formation)
H_2S	200 ppm	Toxicity
CO	2000 ppm	Toxicity
CH_4	Aquifer < 4 vol.%, EOR < 2 vol.%	Increase compression work
N_2	<4 vol.% (all non-condensable gasses)	Increase compression work
Ar	<4 vol.% (all non-condensable gasses)	Increase compression work
H_2	<4 vol.% (all non-condensable gasses)	Increase compression work
CO_2	>95.5%	/

Two methods are studied to purify the CO_2: the first using a membrane and the second using an oxy-combustor.

3.8.1 Carbon capture section with H_2 membranes

Before entering the compressor train, the gas mixture is further purified through a membrane for hydrogen capture. In Figure 21 is reported the carbon capture line with membrane layout. The recovered hydrogen could be reused in the cell or for other applications (e.g. green mobility).

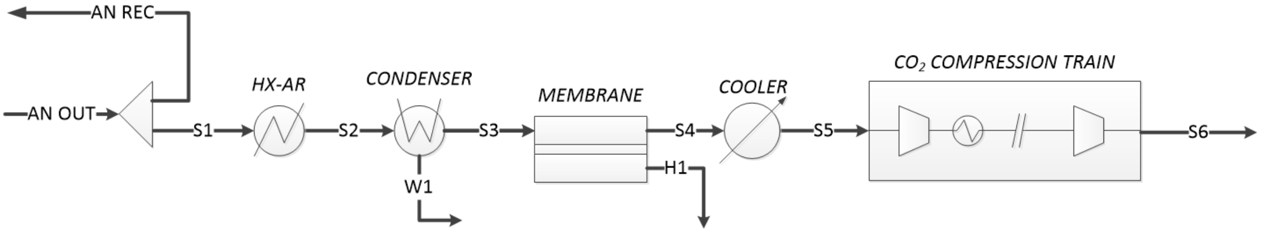

Figure 21 – Carbon Capture line with membrane

A hydrogen membrane is chosen because these technologies are the most common used while CO_2 membrane are yet under study and development. There are three categories of H_2-selective membrane [53].

The first are metallic membranes, generally based on palladium, can produce hydrogen with a purity of 99.99%, the diffusion of hydrogen inside the membrane is influenced by metal surface roughness, purity, metallic lattice, and temperature, Pd membrane usually work at high temperature. Pd membranes have some problems which reduce their application for large scale hydrogen separation. One is the phase change that happen at low temperature (< 300 °C) causing catastrophic failure due to hydrogen embrittlement. Another problem is the presence of contaminants that can damage the membrane. The biggest issues are the limited lifespan of Pd membrane, often months, and the cost due the fact that Pd is a precious metal.
The second category are porous membrane, they can be also applied to the separation of H_2 from CO_2. The range of inorganic materials used include alumina, zeolites, nitrides, oxides, and silica.

This type of membranes is based on the molecular size, so have a pore structure carefully controlled, hydrogen diffuse inside the membrane through the pores.
Usually they work at temperature between 100 °C and 450 °C and suffer from the presence of stream inside the mixture.

The last are polymeric membranes operating by the solution diffusion mechanism. In this type of membrane, the gas dissolves into the polymer at one face on the membrane, diffuse inside the membrane and then desorbed at the other face, the permeability is a function of both solubility and gas diffusivity. The H_2 selective polymeric membrane are characterized by high diffusivity exploited and limited low solubility, usually applied in hydrogen recovery in the refining and chemical industry, operating at temperatures lower than 100 °C. For hydrogen separation from CO_2 a wide range of polymeric membranes can be used, a type are glassy polymeric membranes, operating at temperature below the glass transition temperature, provide high H_2/CO_2 selectivity due to a larger void fraction within the polymeric matrix.

Between these categories, a polymeric membrane is the most suitable for the plant under study because the stream reaches low temperature before the compression stage with low molar flow.

In this model, the membrane is modeled in a simple way (as a separator), after the condenser, without considering any pressure gradient between the faces of the membrane or assuming a specific operating temperature because these conditions are related to the type and material of the membrane.

A parameter used to estimate the CO_2 capture efficiency is the Carbon Capture Ratio (CCR) which is defined as (62):

$$CCR = \frac{\dot{n}_{CO_2\,removed}}{\dot{n}_{C\,fuel}} \tag{62}$$

Where $\dot{n}_{C\,fuel}$ is the molar flow rate of carbon contained in the input fuel.

The plant is able to capture all the carbon contained in the natural gas introduced in the MCFC and the fraction U_{CO_2} of the fuel burnt in the ICE, the CCR can be also written as (63):

$$CCR = \frac{U_{CO_2} \cdot G_{fuel,ICE} + G_{fuel,FC}}{G_{fuel,ICE} + G_{fuel,FC}} \tag{63}$$

The carbon capture main results are reported in Table 11:

Table 11 – CO_2 parameters

Parameter	**Value**	**Unit**
$CO_2\,purity$	91.6 %	[-]
CCR	78.9 %	[-]
$G_{H_2,recovered}$	3.4	[kg/h]
$G_{H_2O,removed}$	204.2	[kg/h]

The CO_2 purity does not satisfy the pipeline requirements (Table 10). The biggest impurity inside the stream is the unreacted carbon monoxide in the cell anode (7%).

In Figure 22 and in Figure 23 is reported a sensitivity analysis of the CO_2 purity and CCR when FU (32) or U_{CO_2} is modified.

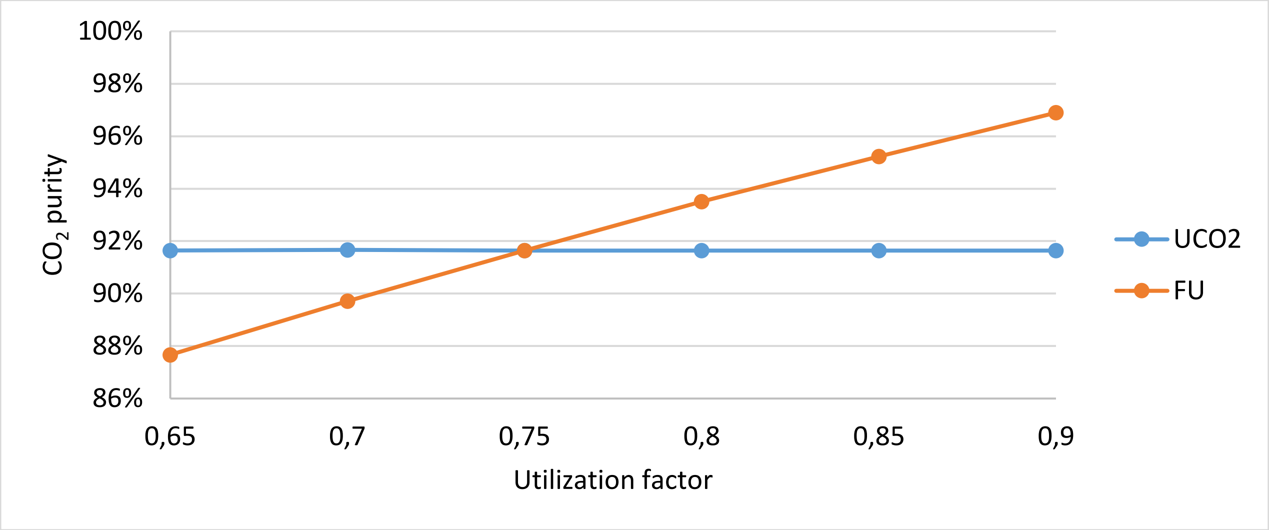

Figure 22 – CO_2 purity sensitivity

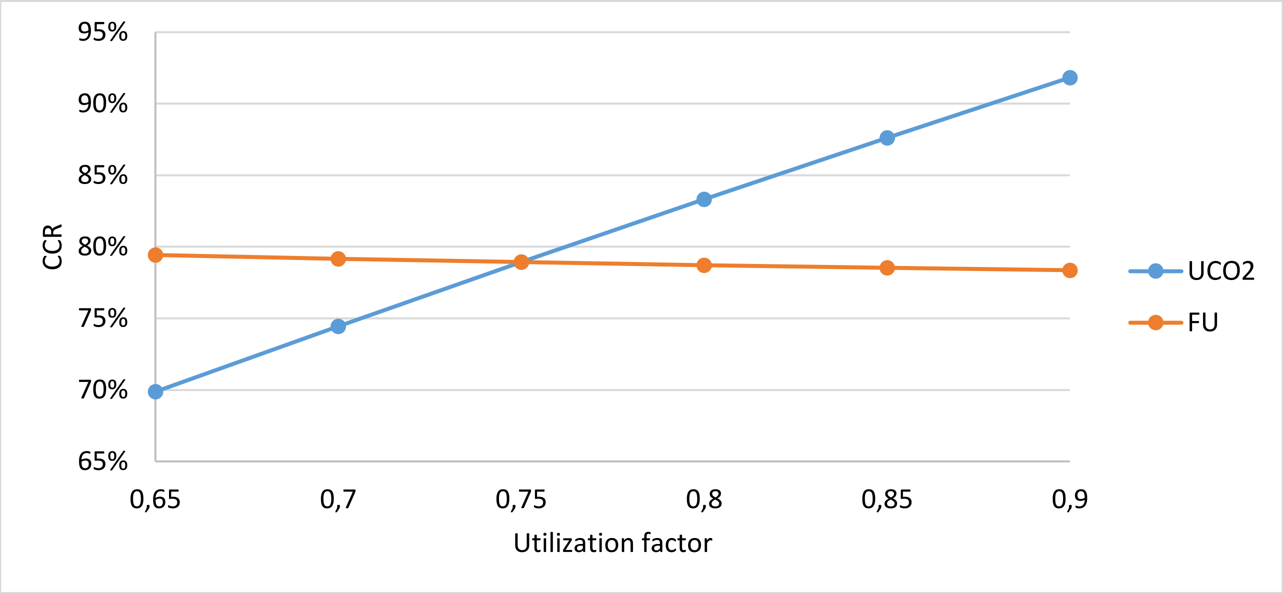

Figure 23 – CCR sensitivity

From the base point of 0.75 for both utilization ratios, the purity of carbon dioxide does not change when the utilization factor of CO_2 is changed (at a constant fuel utilization) but the CCR does because it is proportional to U_{CO_2}.

Vice versa changing the FU factor, the CCR decrease a bit because the consumption of natural gas in the fuel cell decreases but the purity increases up to 96.9% because less unreacted carbon monoxide reaches the CCS unit. The CO value is still too high (2.1%) compared to a pipeline requirement of 2000 ppm (0.2%).

3.8.2 Carbon capture section with oxy-combustion

In this option of CCS an oxy-combustor is installed, as reported in Figure 24, to convert all the unreacted fuel in water and carbon dioxide and recover the remaining chemical energy.

The oxygen needed is produced on site with an Air Separation Unit (ASU) with a purity of 98 vol.% and a power consumption of 0.295 $\left[\frac{kWh_{el}}{kg_{PURE\ O_2}}\right]$ [9].

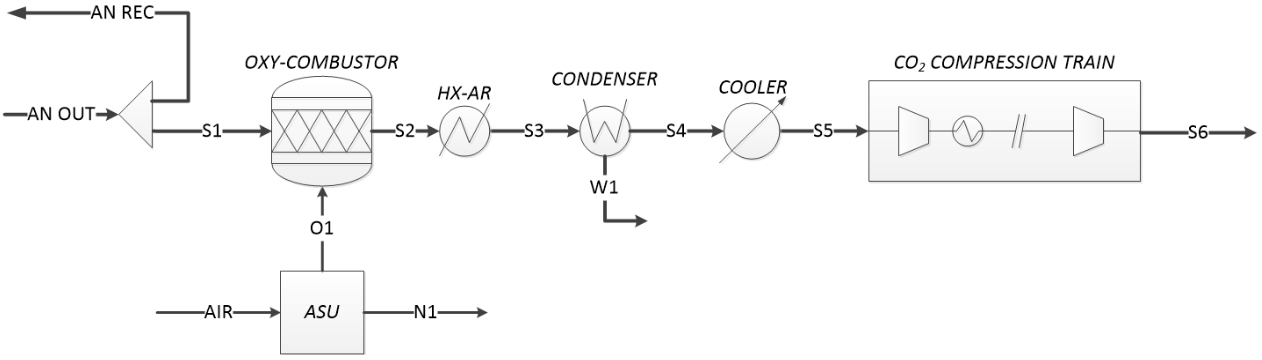

Figure 24 – Carbon capture with oxy-combustor

The reaction involved in the burner are:

$$H_2 + \frac{1}{2}\,O_2 \rightarrow H_2O \tag{64}$$

$$CO + \frac{1}{2}\,O_2 \rightarrow CO_2 \tag{65}$$

$$CH_4 + 2\,O_2 \rightarrow CO_2 + 2\,H_2O \tag{66}$$

$$C_3H_8 + 5\,O_2 \rightarrow 3\,CO_2 + 4\,H_2O \tag{67}$$

$$C_2H_6 + \frac{7}{2}\,O_2 \rightarrow 2\,CO_2 + 3\,H_2O \tag{68}$$

The burner operates in stoichiometric conditions but a small excess (5%) is added, the oxygen needed to be provided by the ASU unit is evaluated solving equation (69) with the calculator tool.

$$\dot{n}_{O_2} = 1.05 \cdot \left(\frac{1}{2}\cdot \dot{n}_{H_2} + \frac{1}{2}\cdot \dot{n}_{CO} + 3\cdot \dot{n}_{CH_4} + 5\cdot \dot{n}_{C_3H_8} + \frac{7}{2}\cdot \dot{n}_{C_2H_6}\right) \qquad \left[\frac{mol}{s}\right] \tag{69}$$

The oxygen mass flow needed is 42.1 $\frac{kg}{h}$ and the ASU energy consumption can be evaluated as:

$$W_{el,ASU} = 0.295 \cdot G_{O_2} = 0.295 \cdot 42.1 = 12.4 \qquad [kW] \tag{70}$$

The CCR is the same as the membrane case (78.9%) but the CO_2 purity is 97.9% with negligible CO residues (<700 ppm). In Figure 25 is reported a sensitivity analysis about the ASU consumption when FU or U_{CO_2} change. When the FU increase the fuel excess decrease, so less oxygen is needed and the ASU energy consumption decrease. When U_{CO_2} increase more fuel is needed but, with a fixed FU, the quantity of unreached fuel increase and more energy is required due to the higher quantity of oxygen needed.

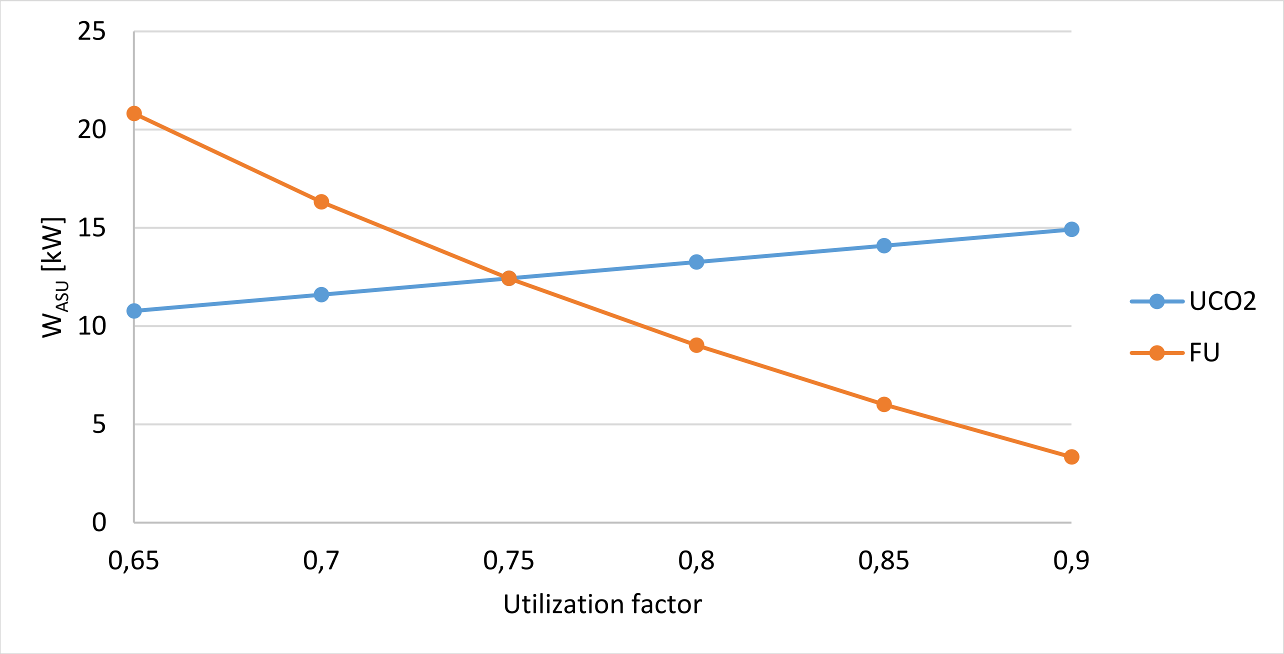

Figure 25 – ASU consumption sensitivity

3.9 Thermal integration with pinch analysis methodology

The model is now completed but there are some streams that need to be heated and other need to be cooled, as reported in Figure 26, so a pinch analysis [54] is performed to achieve heat recovery and decrease the consumption of external resources. The pinch analysis is applied firstly to the membrane case.

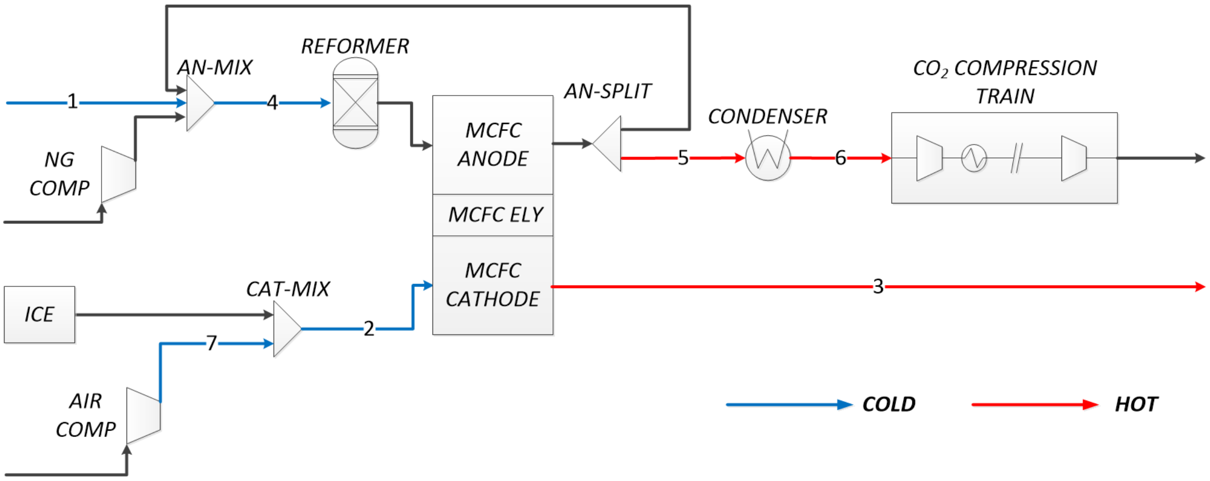

Figure 26 – Streams involved in the Pinch Analysis

The streams are:

1. The reforming reaction require steam that need to be produced from water.
2. The mixture of flue gases and air need to be heated up to the cell operating temperature.
3. The cathodic exhaust needs to be cooled down before reach the chimney.
4. The mixture of steam, fuel and anodic recirculation need to be heated up to the reforming temperature.
5. The anodic exhaust needs to be cooled down to remove water
6. The CO_2 stream need to be cooled before entering the compression train.
7. The cathodic air needs to be heated up before mixing with the ICE exhausts.

The streams list is reported in Table 12 with the corresponding temperature variation.

Table 12 – Stream list

Stream	**Type**	**T_{in} [°C]**	**T_{out} [°C]**
1	Cold	95	230
2	Cold	369.42	625
3	Hot	660	120
4	Cold	283.85	640
5	Hot	660	95
6	Hot	95	40
7	Cold	57.44	170

In the Aspen Plus model the heat requirement for each stream ϕ_i is known, the product $G \cdot c_i$ is evaluated as (71):

$$Gc_i = \frac{\phi_i}{T_{in,i} - T_{out,i}} \tag{71}$$

In this pinch analysis the analytic method is used, a minimum temperature difference ΔT_{min} of 15 °C is imposed. The corrected temperature T_i^* are calculated using (72) for cold fluids and (73) for hot fluids.

$$T_i^* = T_i + \frac{\Delta T_{min}}{2} \tag{72}$$

$$T_i^* = T_i - \frac{\Delta T_{min}}{2} \tag{73}$$

To consider the variation of the specific heat, each fluid is divided in subintervals to consider phase changes, when water is involved, or to split a large temperature variation. Table 13 report those, the corresponding Gc and the corrected temperature of each of them.

Table 13 – Fluids subdivisions

#	Type	T_{in} [°C]	T_{out} [°C]	Gc [kW/K]	ϕ [kW]	T^*_{in} [°C]	T^*_{out} [°C]
1a	F	95	102	12.89	-90.2	102.5	109.5
1b	F	102	230	0.07	-9.4	109.5	237.5
2a	F	370.65	450	2.77	-219.7	378.15	457.5
2b	F	450	628	2.85	-507.9	457.5	632.5
3a	C	660	470	2.71	514.4	652.5	462.5
3b	C	470	120	2.55	893.3	462.5	112.5
4a	F	283.85	450	0.15	-25.2	291.35	457.5
4b	F	450	640	0.17	-31.4	457.5	647.5
5a	C	660	300	0.29	103.9	652.5	292.5
5b	C	300	102	0.26	51.5	292.5	94.5
5c	C	102	95	19.37	135.6	94.5	87.5
6	C	95	40	0.18	9.7	87.5	32.5
7	F	63.17	170	0.09	-10.1	70.67	177.5

The thermal cumulative curve is obtained sorting in descending order the corrected temperatures and reporting all the fluid present in each interval with their Gc, as showed in Table 14.
For each temperature interval is supposed that all fluids are mixed together uniformly, so for each interval is evaluated the global Gc as (74):

$$Gc_{tot} = \sum_{hot} Gc_{hot} - \sum_{cold} Gc_{cold} \tag{74}$$

After, the heat flux of each temperature interval is calculated as (75):

$$\phi_i = Gc_{tot}(T^*_i - T^*_{i-1}) \tag{75}$$

The last step is to calculate the cumulative curve: this evaluation is useful to identify the minimum thermal energy requirements and the pinch point of the plant. This divide the plant in two parts: the hot one above this point and the cold one under this point.
In a pinch analysis a negative cumulative is unacceptable because one of its rules is to avoid heat exchange between the pinch point and having a negative value means breaking the rule.

The first try set 0 the initial value of the cumulative, as reported in the last column of Table 14, then for each interval the cumulative C_i is evaluated as (76):

$$C_i = C_{i-1} + \phi_i \tag{76}$$

Once the first cumulative is completed, the procedure is to identify the lowest value inside the cumulative, change its sign if negative and set as the first value of the next cumulative.
In this case the lowest value is 0 so the cumulative is already acceptable.
The pinch point of the plant is evaluated using the reverse formula of (72) and (73) obtaining $T_{pp,hot}$=660 °C and $T_{pp,cold}$=645 °C.

The first value of the cumulative represent the heat requirement from an external source while the last value represent the cooling requirement with an external source: in this case no heat is needed but 814.5 kW needed to be extracted from the plant by a cooling system. Part of this cooling requirement will be used to produce thermal energy while the remaining low temperature part will be dissipated.

In Figure 27 is reported the cumulative of the plant.

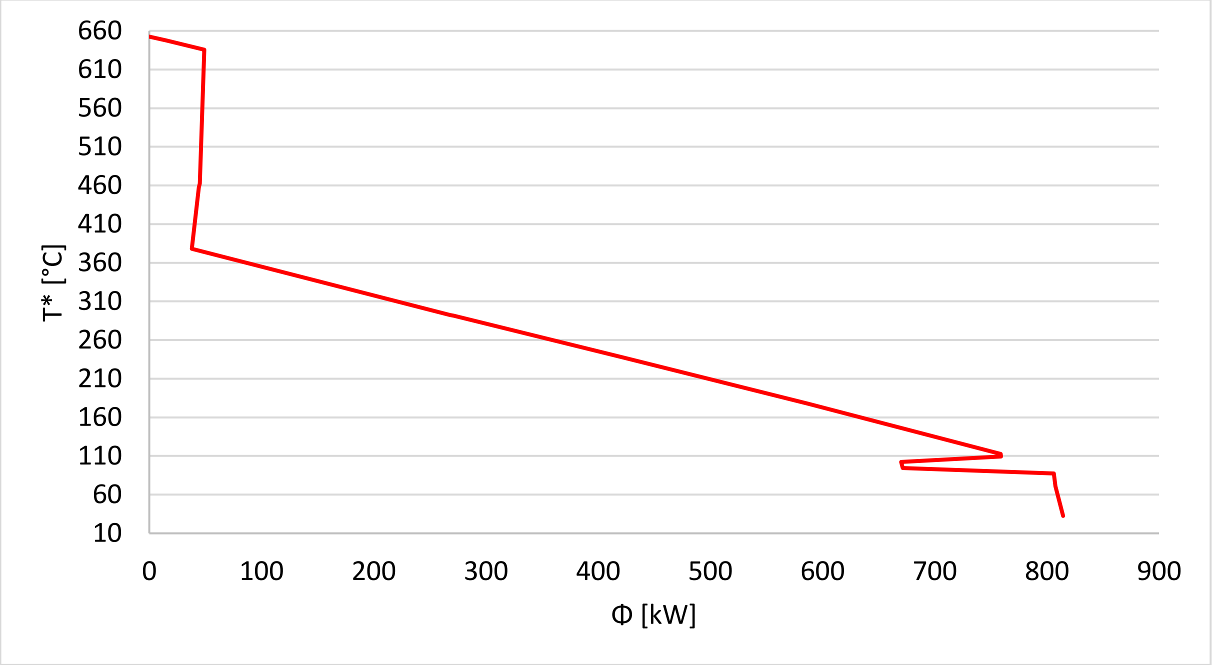

Figure 27 – Thermal Cumulative

Table 14 – Cumulative construction

T* [K]	**1a**	**1b**	**2a**	**2b**	**3a**	**3b**	**4a**	**4b**	**5a**	**5b**	**5c**	**6**	**7**	**Gc [kW/K]**	**ϕ [kW]**	**C**
652.50														-	-	0
647.50					↓				↓					3.00	15.0	15.0
635.50					↓			↑	↓					2.83	34.0	48.9
462.50				↑	↓			↑	↓					-0.02	-3.9	45.1
457.50				↑		↓		↑	↓					-0.18	-0.9	44.2
378.15			↑			↓	↑		↓					-0.08	-6.3	37.9
292.50						↓	↑		↓					2.69	230.3	268.2
291.35						↓	↑			↓				2.66	3.1	271.3
237.50						↓				↓				2.81	151.4	422.7
177.50		↑				↓				↓				2.74	164.3	587.1
112.50		↑				↓				↓			↑	2.64	171.9	758.9
109.50		↑								↓			↑	0.09	0.3	759.2
102.50	↑									↓			↑	-12.72	-89.1	670.2
94.50										↓			↑	0.17	1.3	671.5
87.50											↓		↑	19.27	134.9	806.4
70.67												↓	↑	0.08	1.4	807.8
32.50												↓		0.18	6.8	814.5

The network of heat exchangers is now drawn considering the following rules:

1. The Gc product must be:
   a. Above pinch point:
   $$Gc_{hot\ fluids} \leq Gc_{cold\ fluids}$$
   b. Under pinch point:
   $$Gc_{hot\ fluids} \geq Gc_{cold\ fluids}$$
2. The number of fluids must be:
   a. Above pinch point:
   $$n°_{hot\ fluids} \leq n°_{cold\ fluids}$$
   b. Under pinch point:
   $$n°_{hot\ fluids} \geq n°_{cold\ fluids}$$

3. Completely cooling of hot fluids above the pinch point and completely heating of cold fluids under the pinch point.

From the cumulative estimation the plant is all under the pinch point, for the drawing of the heat exchanger network are followed the rules regarding only the part under the pinch point.

Now are reported the calculations of the heat exchangers network while the complete heat exchangers network is reported in Figure 28.

$$\begin{gathered} \phi_{A1} = Gc_{2b}\left(T_{out,2b} - T_{in,2b}\right) = 507.9 \qquad [kW] \\ T_{out,3a,A1} = T_{in,3a} - \frac{\phi_{A1}}{Gc_{3a}} = 472.41 \qquad [°C] \end{gathered} \tag{77}$$

$$\begin{gathered} \phi_{A2} = Gc_{3a}\left(T_{in3a,A1} - T_{out,3a}\right) = 6.5 \qquad [kW] \\ T_{in,2a,A2} = T_{out,2a} - \frac{\phi_{A2}}{Gc_{2a}} = 447.64 \qquad [°C] \end{gathered} \tag{78}$$

$$\begin{gathered} \phi_{A3} = Gc_{2a}\left(T_{in,2a,A1} - T_{in,2a}\right) = 213.1 \qquad [kW] \\ T_{in,3b,A3} = T_{out,3b} - \frac{\phi_{A3}}{Gc_{3b}} = 386.52 \qquad [°C] \end{gathered} \tag{79}$$

$$\begin{gathered} \phi_{B1} = Gc_{4b}\left(T_{out,4b} - T_{in,4b}\right) = 31.4 \qquad [kW] \\ T_{out,5a,B1} = T_{in,5a} - \frac{\phi_{B1}}{Gc_{5a}} = 551.24 \qquad [°C] \end{gathered} \tag{80}$$

$$\begin{gathered} \phi_{B2} = Gc_{4a}\left(T_{out,4a} - T_{in,4a}\right) = 25.2 \qquad [kW] \\ T_{out,5a,B2} = T_{out,5a,B1} - \frac{\phi_{B2}}{Gc_{5a}} = 463.96 \qquad [°C] \end{gathered} \tag{81}$$

$$\begin{gathered} \phi_{D} = Gc_{1a}\left(T_{out,1a} - T_{in,1a}\right) = 90.2 \qquad [kW] \\ T_{out,3b,D} = T_{out,3b,A3} - \frac{\phi_{D}}{Gc_{3b}} = 351.17 \qquad [°C] \end{gathered} \tag{82}$$

$$\phi_E = Gc_{1b}\left(T_{out,1b} - T_{in,1b}\right) = 9.4 \qquad [kW]$$

$$T_{out,5a,E} = T_{out,5a,B2} - \frac{\phi_E}{Gc_{5a}} = 431.36 \qquad [°C] \tag{83}$$

$$\phi_F = Gc_7\left(T_{out,7} - T_{in,7}\right) = 10.1 \qquad [kW]$$

$$T_{out,5a,F} = T_{out,5a,E} - \frac{\phi_F}{Gc_{5a}} = 396.38 \qquad [°C] \tag{84}$$

In the evaluation of heat exchanger A3 (79) and D (82), the rule 1.b. about Gc is broken but having a sufficient difference between the fluids temperatures guarantee that both side of the heat exchangers the minimum temperature difference of 15 °C is respected.

Once all the cold fluids are heated, coolers are introduced for hot fluids.

$$Cooler_1 = Gc_{3b}\left(T_{out,3b,D} - T_{out,3b}\right) = 590.0 \qquad [kW] \tag{85}$$

$$Cooler_{2a} = Gc_{5a}\left(T_{out,5a,F} - T_{out,5a}\right) = 27.8 \qquad [kW] \tag{86}$$

$$Cooler_{2b} = Gc_{5b}\left(T_{in,5b} - T_{out,5b}\right) = 51.5 \qquad [kW] \tag{87}$$

$$Cooler_{2c} = Gc_{5c}\left(T_{in,5c} - T_{out,5c}\right) = 135.6 \qquad [kW] \tag{88}$$

$$Cooler_3 = Gc_6\left(T_{in,6} - T_{out,6}\right) = 9.7 \qquad [kW] \tag{89}$$

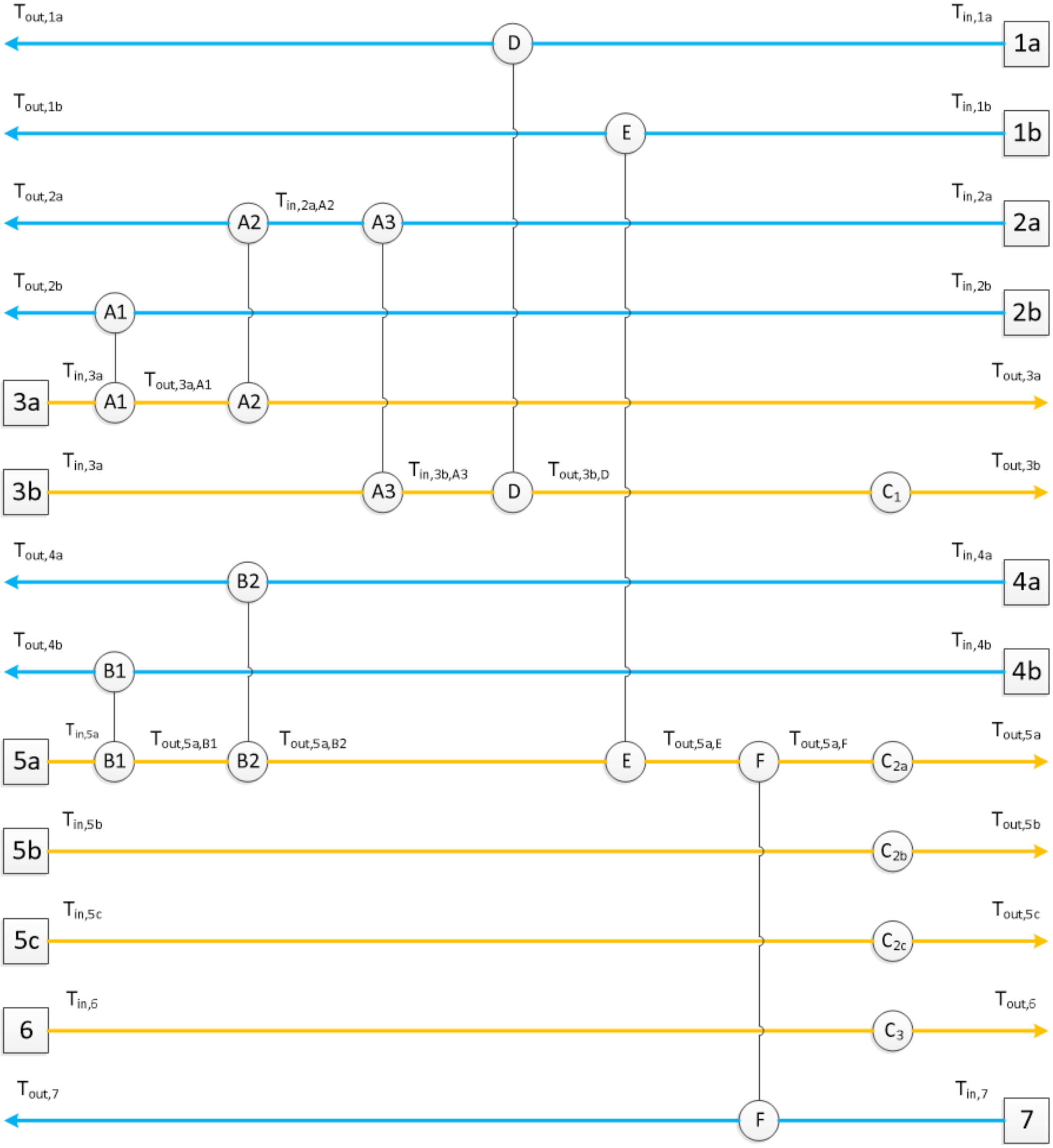

Figure 28 – Heat exchangers network

The first three heat exchangers named A_1, A_2 and A_3, evaluated in (77), (78) and (79), link together the streams 2a, 2b, 3a and 3b that in reality are stream 2 and 3 so these heat exchangers became one, called A.

Same story for heat exchanger B_1 and B_2, evaluated in (80) and (81), that became B and Cooler$_{2a}$ and Cooler$_{2b}$, evaluated in (86) and (87).

The values find are under the hypothesis of constant specific heat, so in Aspen Plus is needed to slightly correct those values because the specific heat is a temperature function.

In conclusion the real heat exchanger network is reported in Figure 29 (Pinch Analysis result) and Figure 30 (Aspen Plus layout) with a thermal power recovered of:

$$\phi_{REC,FC} = \phi_{REC1} + \phi_{REC2} + \phi_{COND} = 804.8 \qquad [kW] \qquad (90)$$

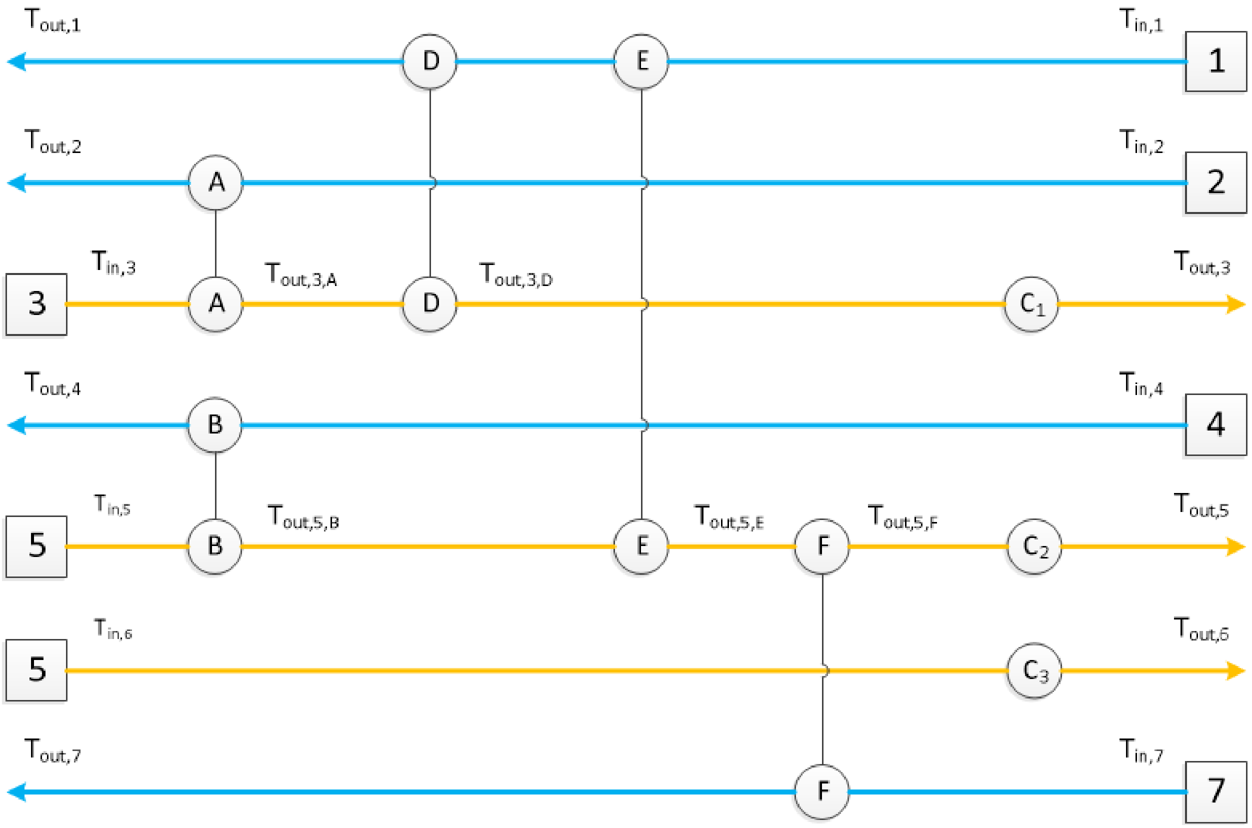

Figure 29 – Real heat exchangers network

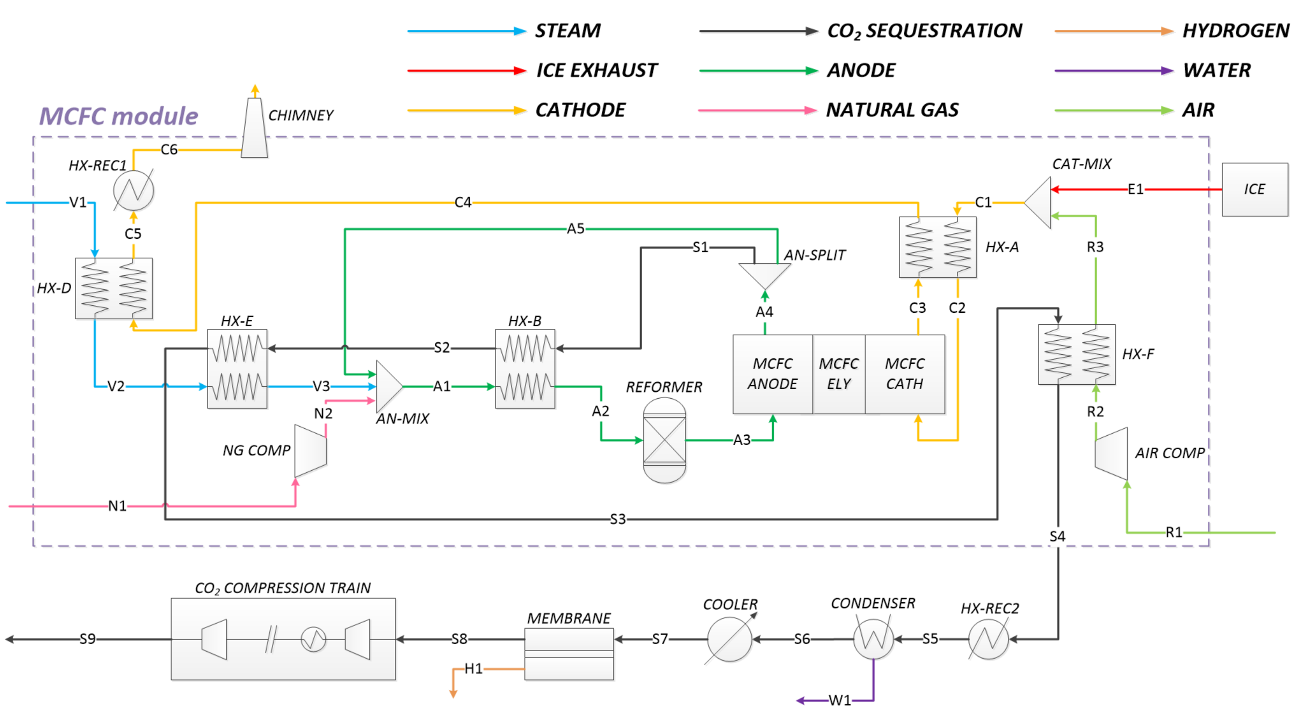

Figure 30 – Complete Aspen Plus layout with pinch analysis (membrane case)

For the second case with the oxy-combustor, the burner increases only the temperature of the anodic exhaust (stream 5 in Figure 29) not affecting the heat exchanger network but only shifting the temperature along all the stream. In this model is considered that the oxy-combustor is placed at the end of the module (Figure 31), where the exhaust temperature are still high, because is a part of the CCS line and it is a component not foreseen within the traditional MCFC module.

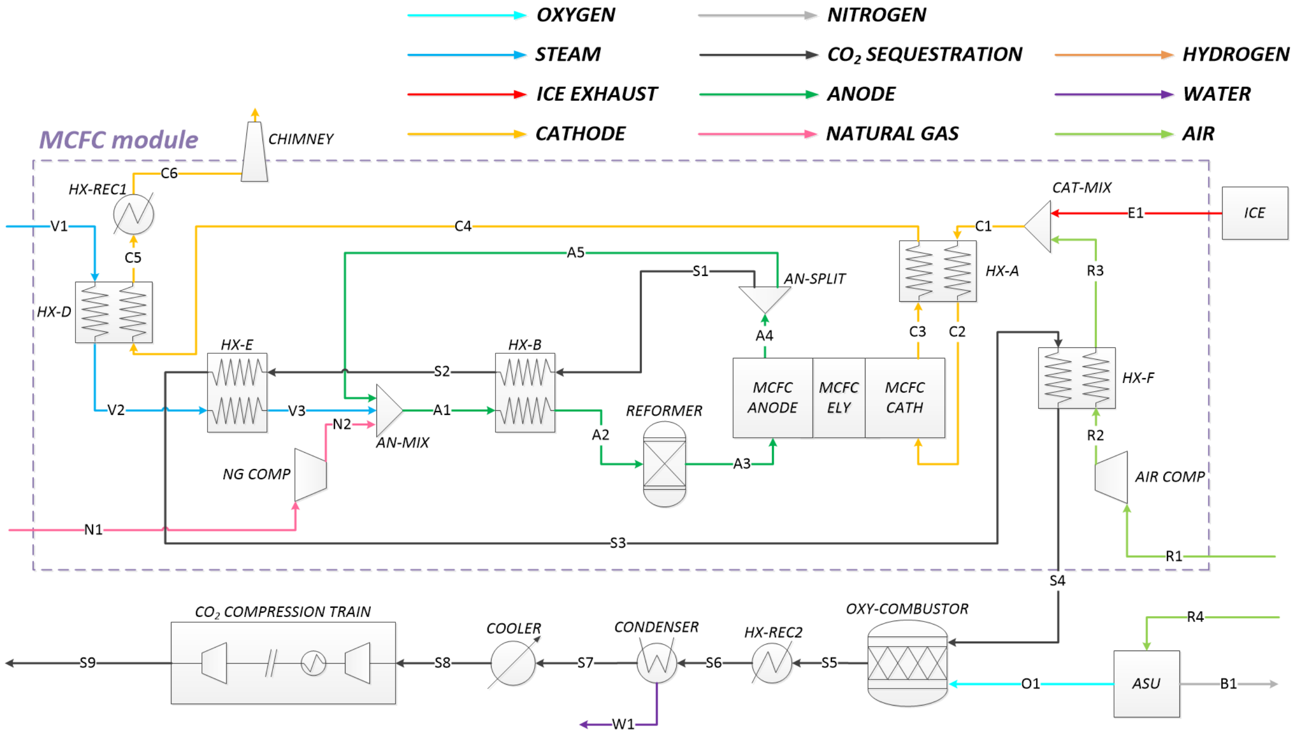

Figure 31 – Aspen Plus layout with pinch analysis (oxy-combustor case)

However, placing it before the heat recovery unit can reach a recover thermal power of 1168.1 kW.

3.10 Plant performance

Before addressing the energy analysis, the main results obtained and some considerations on the overall performance, regarding the two analyzed configurations, are reported in this section.

In the system CHP+MCFC+CCS, the CHP works continuously in full load mode. From the Appendix I: JMS 420 G8 B02 datasheet the main energy data are reported in Table 15.

Table 15 – JMS 420 performance data

Parameter	Value	Unit
$W_{el,CHP}$	1413	[kW]
$\phi_{th,CHP}$	897	[kW]
$\phi_{th,CHP,exhaust\ cooled\ @\ 120\ °C}$	641	[kW]
$\phi_{th,CHP,tot}$	1538	[kW]
$\eta_{el,CHP}$	41.4 %	[-]
$\eta_{th,CHP}$	45.0 %	[-]
$\eta_{g,CHP}$	86.4 %	[-]
$G^{*}_{fuel,CHP}$	257.6	[kg/h]

For the MCFC module the energy consumptions are resumed in Table 16:

Table 16 – MCFC module performance

Parameter	**Value**	**Unit**
V_{cell}	0.74	[V]
$W_{el,DC,FC}$	336	[kW]
$n°\ stacks$	351	[-]
$\eta_{el,DC,FC}$	53.0 %	[-]
$G_{fuel,FC}$	0.013	[kg/s]
$W_{el,air}$	4.63	[kW]
$W_{el,NG}$	0.97	[kW]

The net electric power of the MCFC module $W_{el,net,FC}$ is given by (91):

$$W_{el,net,FC} = W_{el,DC,FC} \cdot \eta_{inv} - W_{el,air} - W_{el,NG} = 314 \qquad [kW] \tag{91}$$

Where η_{inv} is the inverter efficiency used for DC/AC conversion assumed 0.95.

The MCFC module support the electric energy demand of the CCS unit. The two CCS option influence the compression train work because is related to the purity of the CO_2 stream. Also, the CCS configuration determine the quantity of heat recovered. In the heat recovery unit, the maximum value achievable is when the flue gases are cooled down to 120 °C for both configurations.

For the first case, membrane case, the compression train energy demand and the heat recovered are reported in Table 17.

Table 17 – Performance of CCS with membrane

Parameter	**Name**	**Value**	**Unit**
$W_{m,ct}$	Mechanical work compression train	68.7	[kW]
$W_{el,ct}$	Electrical power compression train	70.1	[kW]
ϕ_{cool}	Heat removed	92.9	[kW]
$\phi_{rec,max,FC}$	Maximum heat recovered	805	[kW]

The useful electric power output of the MCFC module is evaluated as:

$$W_{el,MCFC} = W_{el,DC,FC} \cdot \eta_{inv} - W_{el,air} - W_{el,NG} - W_{el,ct} = 244 \qquad [kW] \tag{92}$$

For the second case, oxy-combustor case, the heat recovered, the compression train and ASU energy demand are reported in Table 18.

Table 18 – Performance of CCS with oxy-combustion

Parameter	Value	Unit
$W_{m,ct}$	68.6	[kW]
$W_{el,ct}$	70.0	[kW]
ϕ_{cool}	97.5	[kW]
$W_{el,ASU}$	12.4	[kW]
$\phi_{rec,max,FC}$	1168	[kW]

The useful electric power of the MCFC module, in this configuration, is evaluated as:

$$W_{el,MCFC} = W_{el,DC,FC} \cdot \eta_{inv} - W_{el,air} - W_{el,NG} - W_{el,ct} - W_{el,ASU} = 232 \quad [kW] \tag{93}$$

The global electric efficiency of the plant $\eta_{el,p}$ is evaluated as (94):

$$\eta_{el,pl} = \frac{W_{el,CHP} + W_{el,MCFC}}{(G^*_{fuel,CHP} + G_{fuel,FC}) \cdot LHV_{NG}} \tag{94}$$

Where $W_{el,CHP}$ and $W_{el,MCFC}$ are the electric power of CHP and MCFC module, $G^*_{fuel,CHP}$ and $G_{fuel,FC}$ are the fuel mass flow of CHP and MCFC and LHV_{NG} is the Lower Heating Value of the fuel (natural gas).

The global thermal efficiency of the plant $\eta_{th,p}$ is evaluated as (95):

$$\eta_{th,max,pl} = \frac{\phi_{th,CHP} + \phi_{rec,max,FC}}{(G^*_{fuel,CHP} + G_{fuel,FC}) \cdot LHV_{NG}} \tag{95}$$

Where $\phi_{th,CHP}$ is the heat recovered in the CHP unit and $\phi_{rec,max,FC}$ is the maximum heat recovered achievable from the exhausts of the MCFC module.

The global efficiency of the plant is evaluated as (96):

$$\eta_{g,max,pl} = \frac{W_{el,CHP} + W_{el,MCFC} + \phi_{th,CHP} + \phi_{rec,max,FC}}{(G^*_{fuel,CHP} + G_{fuel,FC}) \cdot LHV_{NG}} \tag{96}$$

To conclude, in Table 19 are reported the main results when both configurations operate in the same conditions.

Table 19 – Global performance

Parameter	Membrane	Oxy-combustor	Unit
$W_{el,MCFC}$	244	232	[kW$_{el}$]
$\phi_{rec,max,FC}$	805	1168	[kW$_{th}$]
$\eta_{el,pl}$	40.9 %	40.6 %	[-]
$\eta_{th,max,pl}$	42.0 %	51.0 %	[-]
$\eta_{g,max,pl}$	82.9 %	91.9 %	[-]
$CO_2\ purity$	91.6 %	97.9 %	[-]
$G_{CO_2,em}$	34.6	34.6	[g/s]
$G_{CO_2,seq}$	128.1	137.9	[g/s]

When working in the same condition, the second case achieves a lower electric power, due to ASU consumption, but obtain a higher purity of CO_2 that can be injected in the pipeline or used, while the first case has a not negligible quantity of CO in the stream that need to be removed before entering in the pipeline. The oxy-combustor can increase the heat production of the system, with a maximum of 1168 kW$_{th}$, consequently the maximum thermal and global efficiency are higher than the other case.

4 Energy analysis

In this section an energy index analysis is carried to better understand the performance of the model respect to other configurations that can be chosen for cogeneration applications.

4.1 Primary Energy Saving (PES)

The Primary Energy Saving (PES) is the most used index to evaluate the energetic performance of a cogeneration plant.
The PES indicator expresses the amount of energy savings achieved by a CHP plant, with respect to the separate production of the same quantity of heat and electricity.
It was introduced with the Directive 2004/08/EC [55] and it is defined as (97).

$$PES = \frac{\Delta E_p}{\frac{E_{el,CHP}}{\eta_{el,s}} + \frac{E_{th,CHP}}{\eta_{th,s}}} = 1 - \frac{E_{f,CHP}}{\frac{E_{el,CHP}}{\eta_{el,s}} + \frac{E_{th,CHP}}{\eta_{th,s}}} = 1 - \frac{1}{\frac{\eta_{el,CHP}}{\eta_{el,s}} + \frac{\eta_{th,CHP}}{\eta_{th,s}}} \tag{97}$$

Where ΔE_p is the avoided primary energy consumption respect to the separated production and it is defined as (98):

$$\Delta E_p = \left(\frac{E_{el,CHP}}{\eta_{el,s}} + \frac{E_{th,CHP}}{\eta_{th,s}}\right) - E_{f,CHP} \tag{98}$$

Where $E_{f,CHP}$ is the total energy of fuel input in CHP in the reference period, $E_{el,CHP}$ is the electricity produced (net of auxiliaries) and $E_{el,CHP}$ is the useful thermal energy recovered from the CHP unit, measured at the CHP outlet, in the same period.
$\eta_{el,CHP}$ and $\eta_{th,CHP}$ are the CHP electric efficiency and the CHP thermal efficiency respectively defined as (99) and (100):

$$\eta_{el,CHP} = \frac{E_{el,CHP}}{E_{f,CHP}} \tag{99}$$

$$\eta_{th,CHP} = \frac{E_{th,CHP}}{E_{f,CHP}} \tag{100}$$

The electric efficiency of separated production $\eta_{el,s}$ is defined as (101), following the instruction of attachment I and IV of "Regolamento Delegato (UE) 2015/2402" (Appendix II: Regolamento Delegato (UE) 2015/2402), corrected with the percentages of electric energy injected in the grid and electric energy auto consumed.

$$\eta_{el,s} = \eta_{el,s,ref} \cdot \left(C_{f,ext} \cdot \%Grid\ injected + C_{f,int} \cdot \%Auto\ comsumption\right) \tag{101}$$

Where $\eta_{el,s,ref}$ is the harmonized reference efficiency for separate electric power generation defined in attachment I. In this case for a plant using natural gas (category G10) and built after 2016, $\eta_{el,s,ref} = 53.0\%$.

$C_{f,ext}$ and $C_{f,int}$ are the correction factors related to the avoided grid losses related to the connection voltage defined in attachment IV. In this case for the energy injected in Low Voltage (LV) $C_{f,ext} = 0.888$ while for the energy auto consumed in LV $C_{f,int} = 0.851$.
For each scenario is defined $\eta_{el,s}$ depending to the percentage of electricity auto consumed and grid injected.
The thermal efficiency of separated production $\eta_{th,s}$ is defined following the instruction of attachment II of "Regolamento Delegato (UE) 2015/2402".
In this analysis is assumed that both hot water and steam are generated, so it is chosen $\eta_{th,s}$ equal 90%.

4.2 Energy Utilization Factor (EUF)

Another index that can be introduced is the total Energy Utilization Factor (EUF) of a CHP plant defined as (102) [56]:

$$EUF = \frac{E_{th,CHP} + E_{el,CHP}}{E_{f,CHP}} = \eta_{el,CHP} + \eta_{th,CHP} \tag{102}$$

The combined production is recognized by European Parliament as an important measure among those required to meet the achievement of the Kyoto Protocol targets.
The concept of "High Efficiency Cogeneration (HEC)" is introduced by the Directive 2004/8/EC. HEC is obtained when the combined production of electric and thermal energy guarantees a significant Primary Energy Savings compared to traditional production.

For CHP units composed by an Internal Combustion Engine (ICE) or a fuel cell technology or a combination of both technologies and rated higher than 1 MW_{el}, the requirements to obtain the HEC status are PES>10% and EUF>75% [57].

4.3 CO_2 emissions factors

The CO_2 specific emission is an important value to compare different scenario considering the mass of CO_2 released and the energy produced by the system.
For a better evaluation between different CHP systems, two different emission factors are considered: one regarding only the electric energy production (103) and the other the overall energy production (104) (electric and thermal).

$$e_{CO_2,el} = \frac{G_{CO_2,el}}{E_{el}} \qquad \left[\frac{g_{CO_2}}{kWh_{el}}\right] \tag{103}$$

$$e_{CO_2,g} = \frac{G_{CO_2}}{E_{el} + E_{th}} \qquad \left[\frac{g_{CO_2}}{kWh}\right] \tag{104}$$

4.4 Scenarios analyzed

Five scenarios have been analyzed considering traditional options and different configuration of the MCFC+CHP system. The scenarios are:

1. *Separated production*
2. *CHP system*
3. *MCFC+CHP system*
4. *MCFC+CHP+CCS with membrane*
5. *MCFC+CHP+CCS with oxy-combustion*

To perform this analysis some assumptions are made to better compare different configuration:

- All scenarios have the same capacity factor (h_{work} 7000 hours/year).
- The plant energy demand is the same for all the scenarios. The energy analysis is focused on CCS scenarios, for which the energy requirement of the plant is chosen using these scenarios as a reference. In order not to favor a scenario too much, it was chosen to use the electrical production of the scenario with oxy-combustion as the electrical demand, while for the thermal demand the annual thermal production of the scenario with the membrane was taken as reference.
  The electric energy demand is 11.5 GWh_{year} and the thermal energy demand is 11.9 GWh_{year}.
- If the thermal production is higher than the demand, the excess is not used and is dissipated by modifying the outlet temperature of the exhaust gas heat recovery (in case of MCFC the cathodic exhaust heat recovery).
- If the electric energy production is higher than the demand the surplus is introduced in the grid, if the production is lower than the requested demand the deficit is grid supplied.
- For separated energy production the efficiencies are defined following the indications found in "Regolamento Delegato (UE) 2015/2402", assuming an annual average temperature of 15 °C.
- For separated production, the CO_2 emission factors are chosen according to the ISPRA 2020 report [58] and assuming a boiler efficiency of 94.5%.

4.4.1 Separated production

In this scenario all the energy demand is produced separately: the electric energy demand ($E_{el} = 11.5\,GWh_{year}$) is supplied from the national grid while the thermal energy demand ($E_{th} = 11.9\,GWh_{year}$) is covered by a boiler as showed in Figure 32.

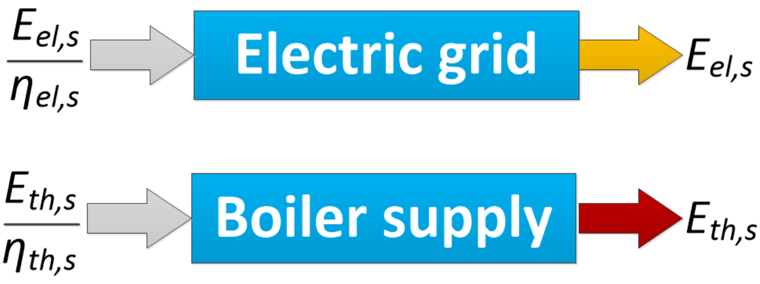

Figure 32 – Scenario 1: separated production

The electric efficiency of separated production $\eta_{el,s}$ is defined as (101), following the instruction of attachment I and IV of “Regolamento Delegato (UE) 2015/2402”, corrected with the percentages of electric energy injected in the grid and electric energy auto consumed.
In this case all the energy is auto consumed in LV so only $C_{f,int} = 0.851$ is considered. The electric efficiency $\eta_{el,s}$ of this scenario is 45.1%.

The thermal efficiency of separated production $\eta_{th,s}$ is 90% defined following the instruction of attachment II of “Regolamento Delegato (UE) 2015/2402”.

In this case, the fuel consumption for electric energy production $E_{f,el}$ and the fuel consumption for thermal energy production $E_{f,th}$ are evaluated as (105) and (106):

$$E_{f,el} = \frac{E_{el}}{\eta_{el,s}} = \frac{11.5}{0.451} = 25.5 \qquad \left[kWh_f\right] \tag{105}$$

$$E_{f,th} = \frac{E_{th}}{\eta_{th,s}} = \frac{11.9}{0.9} = 13.2 \qquad \left[kWh_f\right] \tag{106}$$

The avoided primary energy consumption ΔE_p in this case is 0, consequently the PES is also 0.

For this scenario is possible to evaluate a corrected definition of EUF, called Overall Energy Utilization Factor (OEUF) [56] defined as (107):

$$OEUF = \frac{E_{el} + E_{th}}{E_{f,el} + E_{f,th}} = \frac{11.5 + 11.9}{25.5 + 13.2} = 60.4\% \tag{107}$$

The CO2 emission factors and the quantity of CO2 emitted are now evaluated.

For separated production, the emission factors are defined according to ISPRA.

The emission factor for electric energy production is $e_{CO_2,el} = 284.50 \; \frac{g_{CO_2}}{kWh_{el}}$.

The emission factor related to natural gas used for thermal energy production is $e_{CO_2,f} = 206.88 \; \frac{g_{CO_2}}{kWh_{el}}$ (assuming a boiler efficiency of 94.5%).

The quantity of CO2 produced in a year by the electric energy production can be evaluated as (108):

$$M_{CO_2,el} = e_{CO_2,el} \cdot E_{el} = 284.50 \cdot 11.5 \cdot 10^3 = 3.3 \cdot 10^6 \qquad \left[kg_{CO_2}\right] \tag{108}$$

The quantity of CO2 produced in a year by the thermal energy production can be evaluated as (109):

$$M_{CO_2,th} = e_{CO_2,f} \cdot E_{f,th} = 206.88 \cdot 13.2 \cdot 10^3 = 2.7 \cdot 10^6 \qquad \left[kg_{CO_2}\right] \tag{109}$$

To conclude, the CO2 emission factor related to electric and thermal energy production is:

$$e_{CO_2,g} = \frac{M_{CO_2,el} + M_{CO_2,th}}{E_{el} + E_{th}} = \frac{(3.3 + 2.7) \cdot 10^3}{11.5 + 11.9} = 256.7 \qquad \left[\frac{g_{CO_2}}{kWh}\right] \tag{110}$$

4.4.2 CHP system

In this scenario a CHP system is installed, the CHP used is the JMS 420 G8 B02 adopted in the MCFC+CHP model.

In this configuration the CHP can produce an electric power $W_{el,CHP}$ of 1413 kW and a thermal power $\phi_{th,CHP,tot}$ of 1538 kW.

The thermal production in this case consider also the heat recovered from the flue gases cooled to 120 °C.

The electric energy (111) and thermal energy (112) produced by the CHP system are:

$$E_{el,CHP} = h_{work} \cdot W_{el,CHP} = 7000 \cdot 1413 = 9.9 \qquad [GWh_{el}] \tag{111}$$

$$E_{th,CHP} = h_{work} \cdot \phi_{th,CHP,tot} = 7000 \cdot 1538 = 10.8 \qquad [GWh_{th}] \tag{112}$$

This system is not sufficient to fully cover the energy needs, so is necessary to cover the difference with a separate production of electric energy (113) and thermal energy (114).

$$E_{el,s} = E_{el} - E_{el,CHP} = 11.5 - 9.9 = 1.6 \qquad [GWh_{el}] \tag{113}$$

$$E_{th,s} = E_{th} - E_{th,CHP} = 11.9 - 10.8 = 1.1 \qquad [GWh_{th}] \tag{114}$$

Figure 33 shows how the energy demand is covered.

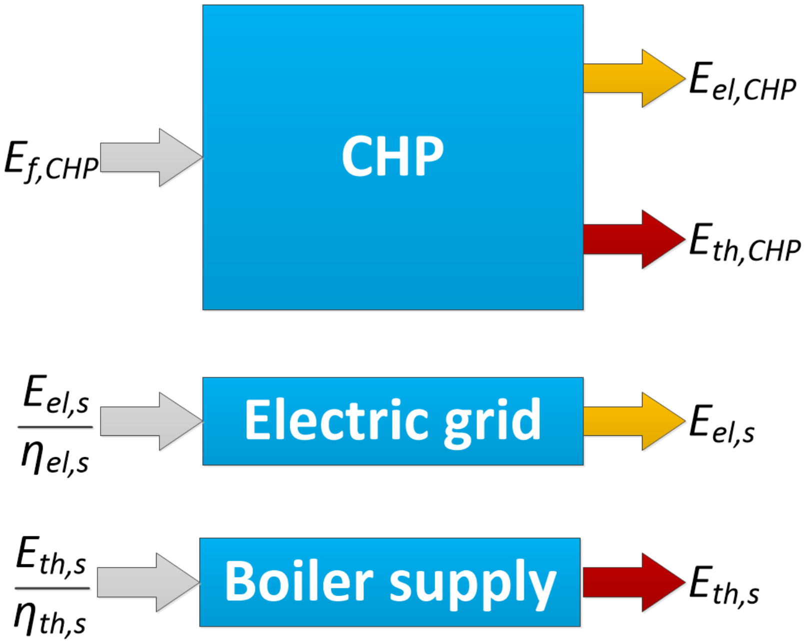

Figure 33 – Scenario 2: CHP system

In this scenario, for separated production, are used the same electric efficiency $\eta_{el,s} = 45.1\%$ and thermal efficiency $\eta_{th,s} = 90\%$ of previous scenario because the operating conditions are the same.

As before, the fuel consumptions for separated production of electricity and heat are:

$$E_{f,el,s} = \frac{E_{el,s}}{\eta_{el,s}} = \frac{1.6}{0.451} = 3.6 \quad [GWh_f] \tag{115}$$

$$E_{f,th,s} = \frac{E_{th,s}}{\eta_{th,s}} = \frac{1.1}{0.9} = 1.3 \quad [GWh_f] \tag{116}$$

The CHP system operate in the same conditions adopted in the model, so the fuel consumption is G^*_{fuel} evaluated in section 3.4 using (12).

The fuel energy consumed in a year is evaluated as (117):

$$E_{f,CHP} = G^*_{fuel,CHP} \cdot LHV_{NG} \cdot h_{work} = 0.0716 \cdot 47.7 \cdot 7 \cdot 10^6 = 23.9 \quad [GWh_f] \tag{117}$$

The electric and thermal efficiencies of CHP plant are evaluated as (118) and (119):

$$\eta_{el,CHP} = \frac{E_{el,CHP}}{E_{f,CHP}} = \frac{9.9}{23.9} = 41.4\% \tag{118}$$

$$\eta_{th,CHP} = \frac{E_{th,CHP}}{E_{f,CHP}} = \frac{10.8}{23.9} = 45.0\% \tag{119}$$

For the CHP part of the system are also evaluated the cogeneration ratio λ (120) and the specific net consumption $q_{f,net,CHP}$ (121).

$$\lambda_{CHP} = \frac{E_{th,CHP}}{E_{el,CHP}} = \frac{10.8}{9.9} = 1{,}1 \tag{120}$$

$$q_{f,net,CHP} = \frac{E_{f,CHP} - \frac{E_{th,CHP}}{\eta_{th,s}}}{E_{el,CHP}} = \frac{23.9 - \frac{10.8}{0.9}}{9.9} = 1{,}2 \tag{121}$$

The avoided primary energy consumption ΔE_p of this scenario is evaluated in (122) considering only the electric energy and thermal energy produced by the CHP unit.

$$\Delta E_p = \left(\frac{E_{el,CHP}}{\eta_{el,s}} + \frac{E_{th,CHP}}{\eta_{th,s}}\right) - E_{f,CHP} = \left(\frac{9.9}{0.451} + \frac{10.8}{0.9}\right) - 23.9 = 10.0 \quad [GWh] \tag{122}$$

The PES and the EUF of the CHP unit can be evaluated using (123) and (124).

$$PES_{CHP} = 1 - \frac{1}{\frac{\eta_{el,CHP}}{\eta_{el,s}} + \frac{\eta_{th,CHP}}{\eta_{th,s}}} = 1 - \frac{1}{\frac{41.4}{45.1} + \frac{45.0}{0.9}} = 29.4\% \tag{123}$$

$$EUF_{CHP} = \eta_{el,CHP} + \eta_{th,CHP} = 41.4 + 45.0 = 86.4\% \tag{124}$$

These evaluations do not clearly represent the scenario's performance because part of the energy is produced separately.

The PES definition (97) need to be modified in order to take into account the separated production contribution, the Overall Primary Energy Saving [56] is introduced (125):

$$OPES = \frac{\Delta E_p}{\frac{E_{el,CHP} + E_{el,s}}{\eta_{el,s}} + \frac{E_{th,CHP} + E_{th,s}}{\eta_{th,s}}} = \frac{10.0}{\frac{9.9 + 1.6}{0.451} + \frac{10.8 + 1.1}{0.9}} = 25.7\% \qquad (125)$$

Also, the EUF definition (102) need to be modified to introduce the Overall Energy Utilization Factor (126):

$$OEUF = \frac{E_{th} + E_{el}}{E_{f,CHP} + E_{f,el,s} + E_{f,th,s}} = \frac{11.5 + 11.9}{23.9 + 3.6 + 1.3} = 81.4\% \qquad (126)$$

Now the CO2 emission factors are evaluated.

For separated production, the emission factors are defined according to ISPRA. The emission factor for electric energy production is $e_{CO_2,el} = 284.50 \frac{g_{CO_2}}{kWh_{el}}$ and the emission factor related to natural gas used for thermal energy production is $e_{CO_2,f} = 206.88 \frac{g_{CO_2}}{kWh_{el}}$ (assuming a boiler efficiency of 94.5%).

For the CHP unit the CO2 mass flow $G_{CO_2,CHP}$ is the same used in the Aspen model.

The quantity of CO2 produced in a year by the CHP unit can be evaluated as:

$$M_{CO_2,CHP} = G_{CO_2,CHP} \cdot h_{work} = 0.139 \cdot 7000 \cdot 3600 = 3.5 \cdot 10^6 \qquad [kg_{CO_2}] \qquad (127)$$

The quantity of CO2 produced in a year for the electric energy due to separated production can be evaluated as:

$$M_{CO_2,el} = e_{CO_2,el} \cdot E_{el} = 284.50 \cdot 1.6 \cdot 10^3 = 4.6 \cdot 10^5 \qquad [kg_{CO_2}] \qquad (128)$$

The quantity of CO2 produced in a year by the thermal energy due to separated production can be evaluated as:

$$M_{CO_2,th} = e_{CO_2,f} \cdot E_{f,th} = 206.88 \cdot 1.3 \cdot 10^3 = 2.6 \cdot 10^5 \qquad [kg_{CO_2}] \qquad (129)$$

The total quantity of CO2 produced in a year is:

$$M_{CO_2} = M_{CO_2,CHP} + M_{CO_2,el} + M_{CO_2,th} = 3.5 + 0.49 + 0.26 = 4.2 \cdot 10^6 \, [kg_{CO_2}] \qquad (130)$$

To conclude, the CO2 emission factor related to only electric production and both electric and thermal energy production are:

$$e_{CO_2,el} = \frac{M_{CO_2,CHP} + M_{CO_2,el}}{E_{el}} = \frac{(3.5 \cdot 10^6 + 4.6 \cdot 10^5) \cdot 10^3}{11.5 \cdot 10^6} = 343.4 \quad \left[\frac{g_{CO_2}}{kWh_{el}}\right] \qquad (131)$$

$$e_{CO_2,g} = \frac{M_{CO_2}}{E_{el} + E_{th}} = \frac{4.2 \cdot 10^3}{11.5 + 11.9} = 180.4 \qquad \left[\frac{g_{CO_2}}{kWh}\right] \qquad (132)$$

4.4.3 MCFC+CHP system

In this scenario a CHP unit and a MCFC module without CCS is installed.
The MCFC module is a modified version of the Aspen model (Figure 34). The MCFC module operate in the same condition of the CCS cases but in this scenario both anode and cathode exhausts are mixed and burn together to recover the remaining chemical energy present in the exhausts. The burnt exhaust is used to perform a heat recovery.

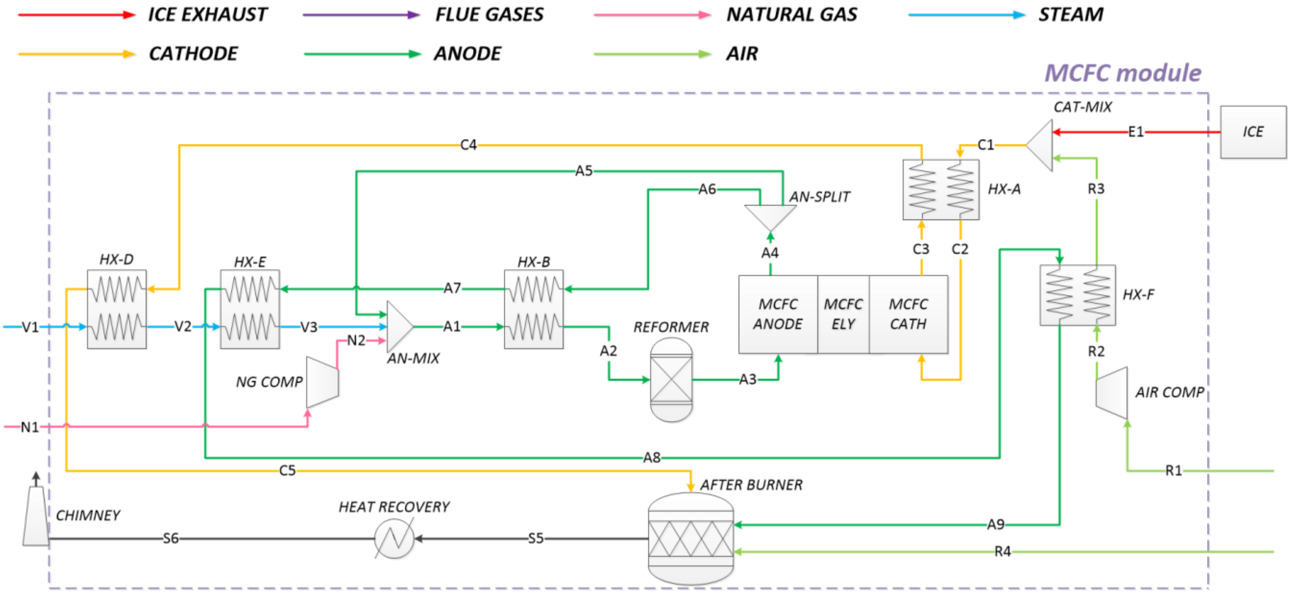

Figure 34 – MCFC-CHP layout

In this configuration the CHP unit operate in the same conditions of CCS cases with a net electric power $W_{el,CHP}$ of 1413 kW and a thermal power $\phi_{th,CHP}$ of 897 kW.
The electric energy (133) and thermal energy (134) yearly produced by the CHP unit are:

$$E_{el,CHP} = h_{work} \cdot W_{el,CHP} = 7000 \cdot 1413 = 9.9 \qquad [GWh_{el}] \tag{133}$$

$$E_{th,CHP} = h_{work} \cdot \phi_{th,CHP} = 7000 \cdot 897 = 6.3 \qquad [GWh_{th}] \tag{134}$$

As for the MCFC module the net electric power $W_{el,MCFC}$ is 314 kW and the thermal power $\phi_{th,MCFC}$ is 805 kW.
The electric energy (135) and thermal energy (136) yearly produced by the MCFC are:

$$E_{el,MCFC} = h_{work} \cdot W_{el,MCFC} = 7000 \cdot 314 = 2.2 \qquad [GWh_{el}] \tag{135}$$

$$E_{th,MCFC} = h_{work} \cdot \phi_{th,MCFC} = 7000 \cdot 805 = 5.6 \qquad [GWh_{th}] \tag{136}$$

The electric energy (137) and thermal energy (138) yearly produced by the system are:

$$E_{el,MCFC+CHP} = E_{el,CHP} + E_{el,MCFC} = 9.9 + 2.2 = 12.1 \qquad [GWh_{el}] \tag{137}$$

$$E_{th,MCFC+CHP} = E_{th,CHP} + E_{th,MCFC} = 6.3 + 5.6 = 11.9 \qquad [GWh_{th}] \tag{138}$$

In this case the electric energy produced is higher than the plant demand ($11.5\ GWh_{el}$), this surplus of electricity is introduced into the electric grid.

$$E_{el,surplus} = E_{el,MCFC+CHP} - E_{el} = 12.1 - 11.5 = 0.6 \qquad [GWh_{el}] \tag{139}$$

The fuel consumption of the two units can be evaluated as:

$$E_{f,MCFC} = G_{fuel,FC} \cdot LHV_{NG} \cdot h_{work} = 0.013 \cdot 47.7 \cdot 7 \cdot 10^6 = 4.43 \quad [GWh_f] \tag{140}$$

$$E_{f,CHP} = G^*_{fuel,CHP} \cdot LHV_{NG} \cdot h_{work} = 0.072 \cdot 47.7 \cdot 7 \cdot 10^6 = 23.92 \quad [GWh_f] \tag{141}$$

Where $G_{fuel,FC}$ is fuel mass flow rate of MCFC evaluated from Aspen plus (Table 16) and $G^*_{fuel,CHP}$ is the fuel mass flow rate of CHP, evaluated in (12).

The fuel consumption of the system E_f can be evaluated as:

$$E_f = E_{f,MCFC} + E_{f,CHP} = 4.43 + 23.92 = 28.4 \qquad [GWh_f] \tag{142}$$

In Figure 35 is reported the electric and thermal energy flux of the plant.

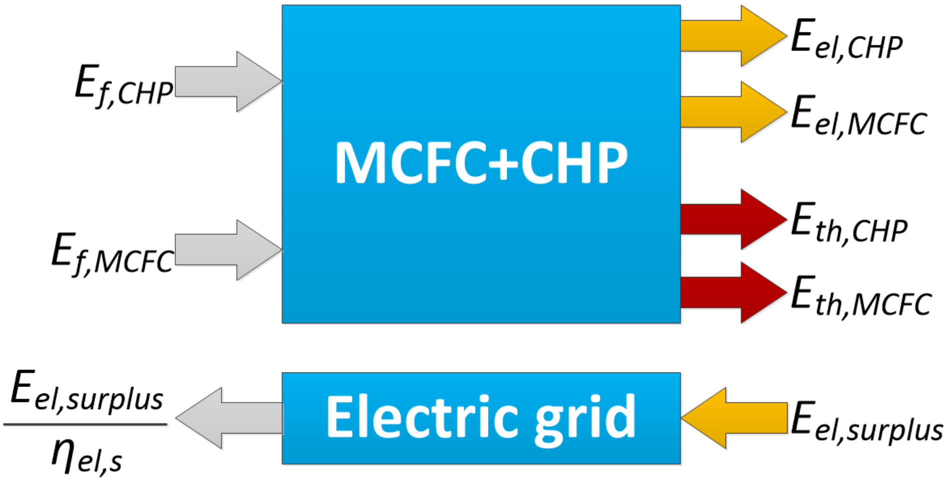

Figure 35 – Scenario 3: MCFC+CHP system

The efficiencies of this scenario are now estimated.

The electric efficiency of the plant η_{el} can be calculated using (143):

$$\eta_{el} = \frac{E_{el,MCFC+CHP}}{E_f} = \frac{12.1}{28.4} = 42.6\% \tag{143}$$

The thermal efficiency of the plant η_{th} can be calculated using (144):

$$\eta_{th} = \frac{E_{th,MCFC+CHP}}{E_f} = \frac{11.9}{28.4} = 42.0\% \tag{144}$$

For this scenario is needed to evaluate the electric efficiency for separated production using (101) considering the electric energy auto consumed and the electric energy injected in the grid, those fractions are: $\%Grid\ injected = 4.8\%$ and $\%Auto\ comsumption = 95.2\%$.

The electric efficiency for separated production $\eta_{el,s}$ is 45.2%, considering $\eta_{el,s,ref} = 53.0\%$, $C_{f,ext} = 0.888$ and $C_{f,int} = 0.851$.

The thermal efficiency for separated production $\eta_{th,s}$ is 0.9 as used in the other scenarios.

For the system MCFC+CHP are also evaluated the cogeneration ratio λ (145) and the specific net consumption $q_{f,net}$ (146).

$$\lambda = \frac{E_{th,MCFC+CHP}}{E_{el,MCFC+CHP}} = \frac{11.9}{12.1} = 0.99 \tag{145}$$

$$q_{f,net} = \frac{E_{f,MCFC+CHP} - \dfrac{E_{th,MCFC+CHP}}{\eta_{th,s}}}{E_{el,MCFC+CHP}} = \frac{28.4 - \dfrac{11.9}{0.9}}{12.1} = 1{,}3 \tag{146}$$

The avoided primary energy consumption ΔE_p of this scenario is evaluated in (147) considering the electric energy and thermal energy produced by the system.

$$\begin{aligned} \Delta E_p &= \left(\frac{E_{el,MCFC+CHP}}{\eta_{el,s}} + \frac{E_{th,MCFC+CHP}}{\eta_{th,s}}\right) - E_{f,MCFC+CHP} = \\ &= \left(\frac{12.1}{0.452} + \frac{11.9}{0.9}\right) - 28.4 = 11.6 \qquad [GWh] \end{aligned} \tag{147}$$

In this scenario the OPES and OEUF are directly evaluated because all the energy is produced by the cogeneration system.

The OPES is evaluated using the PES definition (97) without modifications

$$OPES = \frac{\Delta E_p}{\dfrac{E_{el,MCFC+CHP}}{\eta_{el,s}} + \dfrac{E_{th,MCFC+CHP}}{\eta_{th,s}}} = \frac{11.6}{\dfrac{12.1}{0.452} + \dfrac{11.9}{0.9}} = 29.1\% \tag{148}$$

Also, the OEUF is evaluated using definition (102) without modification

$$OEUF = \eta_{el,MCFC+CHP} + \eta_{th,MCFC+CHP} = 42.6 + 42.0 = 84.6\% \tag{149}$$

Now the CO_2 emission factors are evaluated.

For the MCFC+CHP system the CO_2 mass flow $G_{CO_2,MCFC+CHP}$ is evaluated from the Aspen model as the quantity of CO_2 present in the flue gases of the afterburner.

The quantity of CO_2 produced in a year by the MCFC+CHP system can be evaluated as:

$$M_{CO_2} = G_{CO_2,MCFC+CHP} \cdot h_{work} = 0.172 \cdot 7000 \cdot 3600 = 4.5 \cdot 10^6 \qquad \left[kg_{CO_2}\right] \tag{150}$$

To conclude, the CO_2 emission factor related to only electric production and both electric and thermal energy production are:

$$e_{CO_2,el} = \frac{M_{CO_2}}{E_{el,MCFC+CHP}} = \frac{4.5 \cdot 10^3}{12.1} = 359.6 \quad \left[\frac{g_{CO_2}}{kWh_{el}}\right] \tag{151}$$

$$e_{CO_2,g} = \frac{M_{CO_2}}{E_{el,MCFC+CHP} + E_{th,MCFC+CHP}} = \frac{4.5 \cdot 10^3}{12.1 + 11.9} = 181.1 \qquad \left[\frac{g_{CO_2}}{kWh}\right] \tag{152}$$

4.4.4 MCFC+CHP+CCS with membrane

In this scenario a CHP system and a MCFC module is installed with CCS, in this case a hydrogen membrane is used to purify the carbon dioxide.
In this configuration the CHP unit operate in full mode condition with a net electric power $W_{el,CHP}$ of 1413 kW and a thermal power $\phi_{th,CHP}$ of 897 kW.
The electric energy (153) and thermal energy (154) yearly produced by the CHP unit are:

$$E_{el,CHP} = h_{work} \cdot W_{el,CHP} = 7000 \cdot 1413 = 9.9 \qquad [GWh_{el}] \tag{153}$$

$$E_{th,CHP} = h_{work} \cdot \phi_{th,CHP} = 7000 \cdot 897 = 6.3 \qquad [GWh_{th}] \tag{154}$$

In this scenario the MCFC module fed the electric energy needed of the CCS unit, the net electric power $W_{el,MCFC}$ is 244 kW and the thermal power $\phi_{th,MCFC}$ is 805 kW.
The electric energy (155) and thermal energy (156) yearly produced by the fuel cell unit are:

$$E_{el,MCFC} = h_{work} \cdot W_{el,MCFC} = 7000 \cdot 244 = 1.7 \qquad [GWh_{el}] \tag{155}$$

$$E_{th,MCFC} = h_{work} \cdot \phi_{th,MCFC} = 7000 \cdot 805 = 5.6 \qquad [GWh_{th}] \tag{156}$$

The electric energy (157) and thermal energy (158) yearly produced by the system are:

$$E_{el} = E_{el,CHP} + E_{el,MCFC} = 9.9 + 1.7 = 11.6 \qquad [GWh_{el}] \tag{157}$$

$$E_{th} = E_{th,CHP} + E_{th,MCFC} = 6.3 + 5.6 = 11.9 \qquad [GWh_{th}] \tag{158}$$

In this case the electric energy produced is higher than the plant demand $(11.5\ GWh_{el})$, the small surplus of electricity is introduced into the electric grid.

$$E_{el,surplus} = E_{el,MCFC+CHP} - E_{el} = 11.6 - 11.5 = 0.1 \qquad [GWh_{el}] \tag{159}$$

The fuel consumption of the units can be evaluated as the previous scenario:

$$E_{f,MCFC} = G_{fuel,FC} \cdot LHV_{NG} \cdot h_{work} = 0.013 + 47.7 \cdot 7 \cdot 10^6 = 4.43 \quad \left[GWh_f\right] \tag{160}$$

$$E_{f,CHP} = G^*_{fuel,CHP} \cdot LHV_{NG} \cdot h_{work} = 0.072 \cdot 47.7 \cdot 7 \cdot 10^6 = 23.92 \quad \left[GWh_f\right] \tag{161}$$

The fuel consumption of the system can be evaluated as:

$$E_f = E_{f,MCFC} + E_{f,CHP} = 4.43 + 23.92 = 28.4 \qquad \left[GWh_f\right] \tag{162}$$

In Figure 36 is reported the electric and thermal energy flux of this scenario.

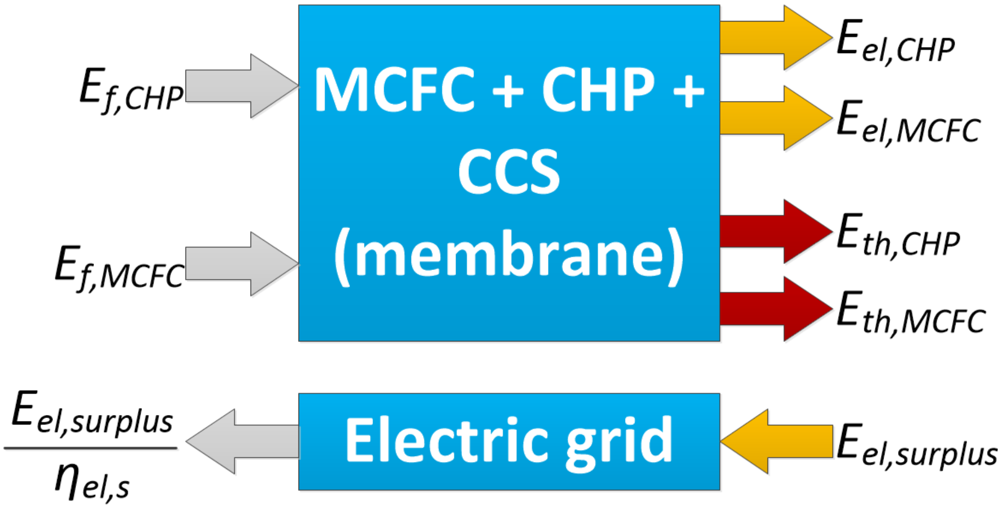

Figure 36 – Scenario 4: MCFC+CHP+CCS (membrane)

Now the efficiencies of this scenario are reported.

The electric efficiency of the plant η_{el} can be calculated using (163) while the thermal efficiency of the plant η_{th} can be calculated using (164):

$$\eta_{el} = \frac{E_{el}}{E_f} = \frac{11.6}{28.4} = 40.9\% \tag{163}$$

$$\eta_{th} = \frac{E_{th}}{E_f} = \frac{11.9}{28.4} = 42.0\% \tag{164}$$

For this scenario is needed to evaluate the electric efficiency for separated production using (101) considering the electric energy auto consumed and the electric energy injected in the grid, those fractions are: $\%Grid\ injected = 0.7\%$ and $\%Auto\ comsumption = 99.3\%$.

The electric efficiency for separated production $\eta_{el,s}$ is 45.1%, considering $\eta_{el,s,ref} = 53.0\%$, $C_{f,ext} = 0.888$ and $C_{f,int} = 0.851$.

The thermal efficiency for separated production $\eta_{th,s}$ is 0.9 as used in the other scenarios.

Also, for this scenario are evaluated the cogeneration ratio λ (165) and the specific net consumption $q_{f,net}$ (166).

$$\lambda = \frac{E_{th}}{E_{el}} = \frac{11.9}{11.6} = 1.03 \tag{165}$$

$$q_{f,net} = \frac{E_f - \frac{E_{th}}{\eta_{th,s}}}{E_{el}} = \frac{28.4 - \frac{11.9}{0.9}}{11.6} = 1{,}3 \tag{166}$$

The avoided primary energy consumption ΔE_p of this scenario is evaluated in (167):

$$\Delta E_p = \left(\frac{E_{el}}{\eta_{el,s}} + \frac{E_{th}}{\eta_{th,s}}\right) - E_f = \left(\frac{11.6}{0.451} + \frac{11.9}{0.9}\right) - 28.4 = 10.6 \qquad [GWh] \tag{167}$$

In this scenario the OPES and OEUF are directly evaluated, as done in the previous scenario, because all the energy is produced by the cogeneration system.

The OPES is evaluated using the PES definition (97) without modifications

$$OPES = \frac{\Delta E_p}{\frac{E_{el}}{\eta_{el,s}} + \frac{E_{th}}{\eta_{th,s}}} = \frac{10.6}{\frac{11.6}{0.451} + \frac{11.9}{0.9}} = 27.2\% \tag{168}$$

Also, the OEUF is evaluated using definition (102) without modification

$$OEUF = \eta_{el} + \eta_{th} = 40.9 + 42.0 = 82.9\% \tag{169}$$

Now the CO_2 emission factors are evaluated.

In this scenario the MCFC+CCS unit permits to achieve a reduction of 75% of the CO_2 present in the CHP (ICE) exhaust.

The remaining part that cannot be sequestrated is emitted, this mass flow $G_{CO_2,em}$ is evaluated from the Aspen model as the quantity of CO_2 present in the cathode exhaust (Table 19).

The quantity of CO_2 released in a year can be evaluated as:

$$M_{CO_2} = G_{CO_2,em} \cdot h_{work} = 0.035 \cdot 7000 \cdot 3600 = 8.8 \cdot 10^5 \qquad [kg_{CO_2}] \tag{170}$$

To conclude, the CO_2 emission factor related to only electric production and both electric and thermal energy production are:

$$e_{CO_2,el} = \frac{M_{CO_2}}{E_{el}} = \frac{8.8 \cdot 10^2}{11.6} = 75.3 \quad \left[\frac{g_{CO_2}}{kWh_{el}}\right] \tag{171}$$

$$e_{CO_2,g} = \frac{M_{CO_2}}{E_{el} + E_{th}} = \frac{8.8 \cdot 10^2}{12.1 + 11.9} = 37.1 \qquad \left[\frac{g_{CO_2}}{kWh}\right] \tag{172}$$

4.4.5 MCFC+CHP+CCS with oxy-combustion

In this scenario a CHP system and a MCFC module is installed with CCS, in this case an oxy-combustion is used to purify the carbon dioxide.
In this configuration the CHP unit operate in the same conditions of the last two cases with a net electric power $W_{el,CHP}$ of 1413 kW and a thermal power $\phi_{th,CHP}$ of 897 kW, consequently the energy production is the same ($E_{el,CHP} = 9.9\ GWh_{el}$ and $E_{th,CHP} = 6.3\ GWh_{th}$).
As for the MCFC module, in this scenario the CCS unit is fed by the fuel cell determining a net electric power $W_{el,MCFC}$ is 232 kW and the thermal power $\phi_{th,MCFC}$ is 805 kW.
The electric energy (173) and thermal energy (174) yearly produced by the MCFC are:

$$E_{el,MCFC} = h_{work} \cdot W_{el,MCFC} = 7000 \cdot 232 = 1.6 \qquad [GWh_{el}] \tag{173}$$

$$E_{th,MCFC} = h_{work} \cdot \phi_{th,MCFC} = 7000 \cdot 805 = 5.6 \qquad [GWh_{th}] \tag{174}$$

The electric energy (175) and thermal energy (176) produced by the system in a year are:

$$E_{el} = E_{el,CHP} + E_{el,MCFC} = 9.9 + 1.6 = 11.5 \qquad [GWh_{el}] \tag{175}$$

$$E_{th} = E_{th,CHP} + E_{th,MCFC} = 6.3 + 5.6 = 11.9 \qquad [GWh_{th}] \tag{176}$$

The two units, MCFC and CHP, operate in the same condition of the previous scenarios, consequently the fuel consumption $E_{f,CHP}$ is the same amount ($28.4\ GWh_f$) with $E_{f,MCFC} = 4.43\ GWh_f$ and $E_{f,CHP} = 23.92\ GWh_f$.
Figure 37 represent the energy flux of this scenario.

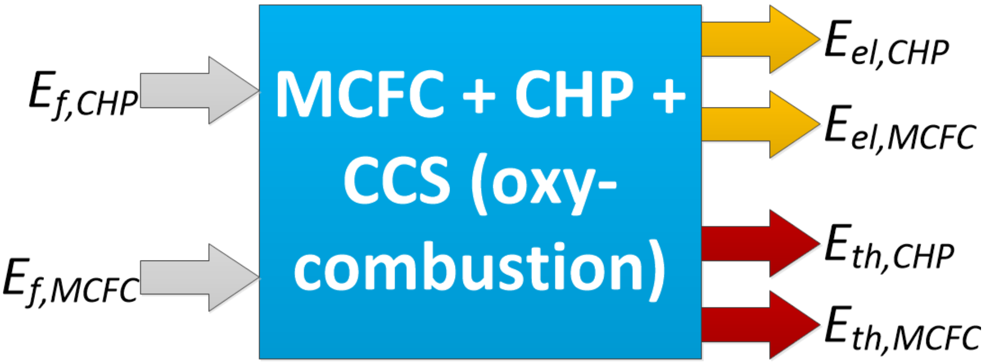

Figure 37 – Scenario 5: MCFC+CHP+CCS (oxy-combustion)

Now the efficiencies of this scenario are reported.
The electric efficiency of the plant η_{el} can be calculated using (177) while the thermal efficiency of the plant η_{th} can be calculated using (178):

$$\eta_{el} = \frac{E_{el}}{E_f} = \frac{11.5}{28.4} = 40.6\% \tag{177}$$

$$\eta_{th} = \frac{E_{th}}{E_f} = \frac{11.9}{28.4} = 42.0\% \tag{178}$$

In this scenario the electric efficiency for separated production can be evaluated as done in scenario 1 and scenario 2, considering only auto consumption, determining $\eta_{el,s} = 45.1\%$
The thermal efficiency for separated production $\eta_{th,s}$ is 0.9 as used in the other scenarios.

Also, for this scenario are evaluated the cogeneration ratio λ (179) and the specific net consumption $q_{f,net}$ (180).

$$\lambda = \frac{E_{th}}{E_{el,MCFC+CHP+CCS_{oxy}}} = \frac{11.9}{11.5} = 1.03 \tag{179}$$

$$q_{f,net} = \frac{E_f - \frac{E_{th}}{\eta_{th,s}}}{E_{el,MCFC+CHP+CCS_{oxy}}} = \frac{28.4 - \frac{11.9}{0.9}}{11.5} = 1,3 \tag{180}$$

The avoided primary energy consumption ΔE_p of this scenario is evaluated in (181):

$$\Delta E_p = \left(\frac{E_{el}}{\eta_{el,s}} + \frac{E_{th}}{\eta_{th,s}}\right) - E_f = \left(\frac{11.5}{0.451} + \frac{11.9}{0.9}\right) - 28.4 = \\ = 10.4 \qquad [GWh] \tag{181}$$

The OPES is evaluated using the PES definition (97) with no modifications:

$$OPES = \frac{\Delta E_p}{\frac{E_{el}}{\eta_{el,s}} + \frac{E_{th}}{\eta_{th,s}}} = \frac{10.4}{\frac{11.5}{0.451} + \frac{11.9}{0.9}} = 26.9\% \tag{182}$$

Also, the OEUF is evaluated using definition (102) with no modifications as done with the PES.

$$OEUF = \eta_{el} + \eta_{th} = 40.6 + 42.0 = 82.6\% \tag{183}$$

Now the CO2 emission factors are evaluated.

As the previous scenario with CCS, a reduction of 75% of the CO2 present in the CHP (ICE) exhaust is achieved and the remaining mass flow $G_{CO_2,em}$ is released in atmosphere.

The quantity of CO2 released in a year by the system is:

$$M_{CO_2} = G_{CO_2,em} \cdot h_{work} = 0.035 \cdot 7000 \cdot 3600 = \\ = 8.8 \cdot 10^5 \qquad [kg_{CO_2}] \tag{184}$$

To conclude, the CO2 emission factor related to only electric production and both electric and thermal energy production are:

$$e_{CO_2,el} = \frac{M_{CO_2}}{E_{el}} = \frac{8.8 \cdot 10^2}{11.5} = 75.8 \quad \left[\frac{g_{CO_2}}{kWh_{el}}\right] \tag{185}$$

$$e_{CO_2,g} = \frac{M_{CO_2}}{E_{el} + E_{th}} = \frac{8.8 \cdot 10^2}{11.5 + 11.9} = 37.3 \qquad \left[\frac{g_{CO_2}}{kWh}\right] \tag{186}$$

4.4.6 Scenarios comparison

After all the scenarios have been analyzed, a comparison of the obtained results is done.

First, a brief recap of the electric and thermal energy supplying is reported in Figure 38.

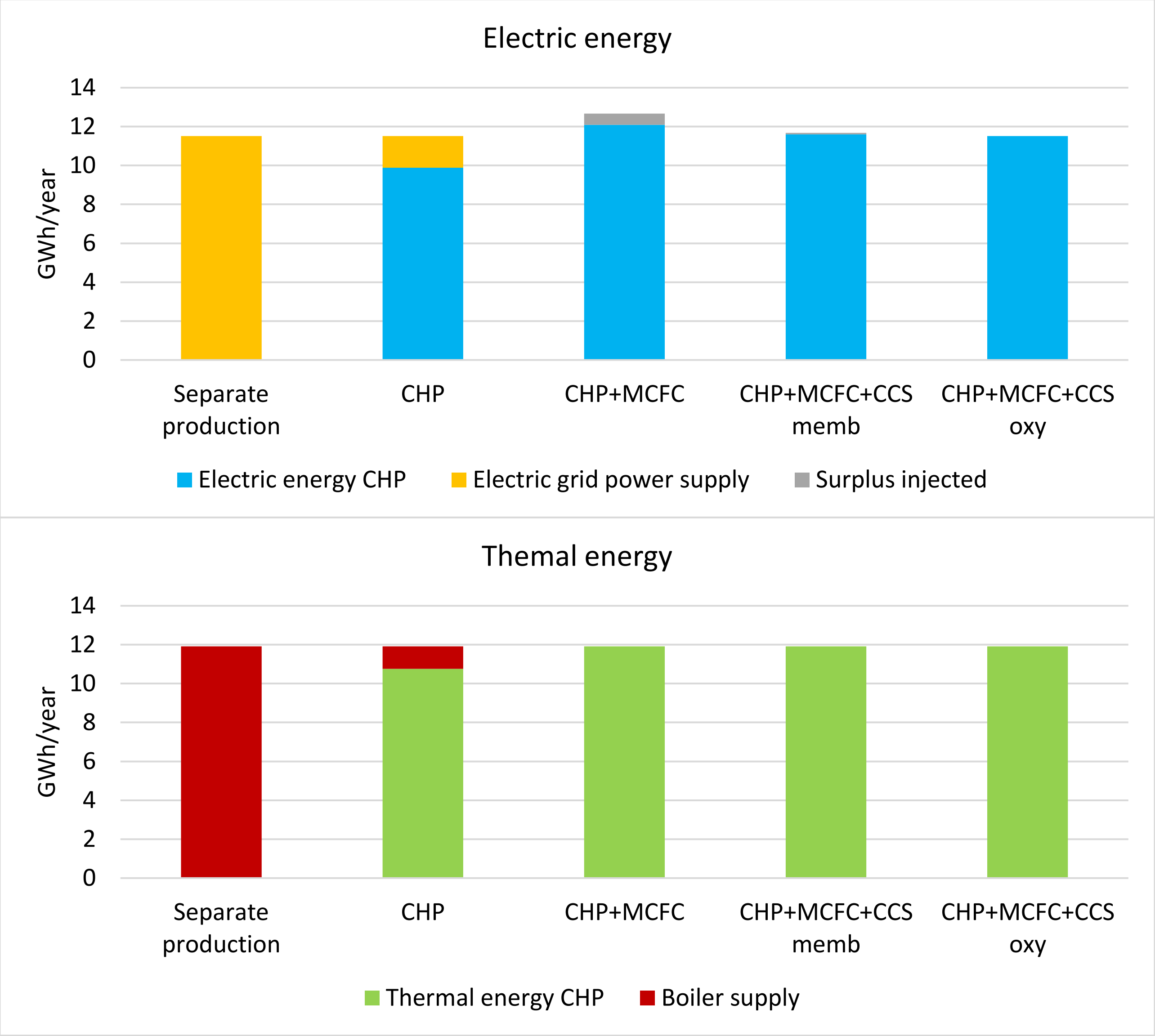

Figure 38 – Electric and thermal energy demand supplying

In the next charts are reported the energy index evaluated for each scenario.

In Figure 39 is reported the electric efficiency of the scenarios, for the separate production is used the electric efficiency evaluated according to “Regolamento Delegato (UE) 2015/2402”.

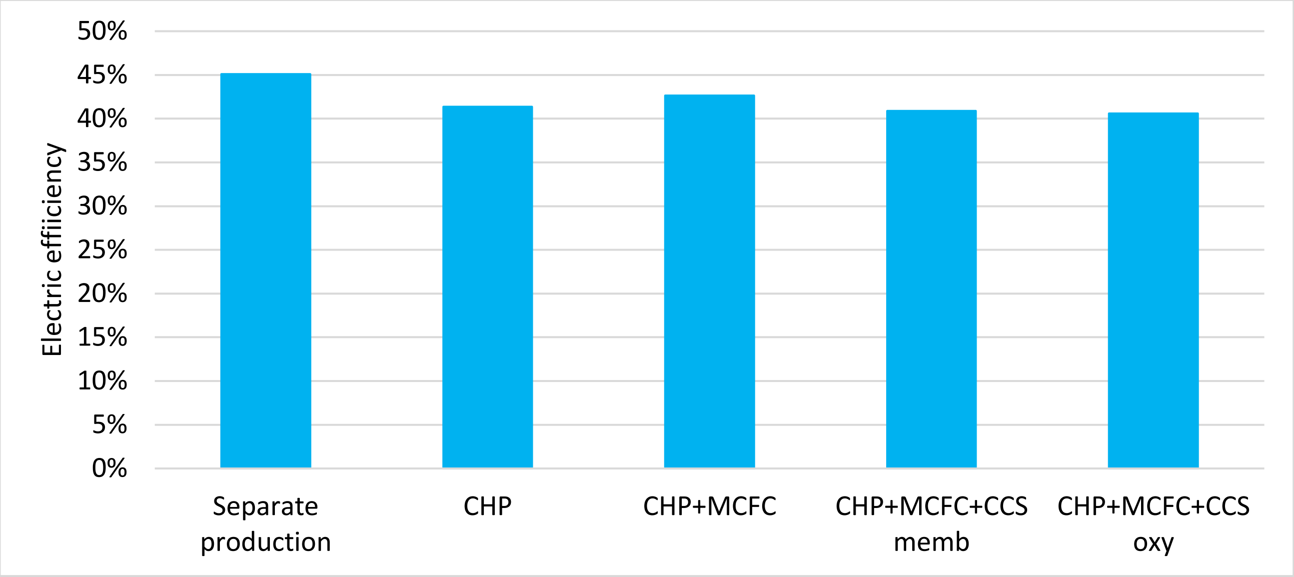

Figure 39 – Electric efficiency of cogeneration unit

The electric efficiency of the MCFC+CHP system is higher (+1.2%) respect to the CHP unit ($\eta_{el,CHP} = 41.4\%$) due to the high electric efficiency of the fuel cell technology but is the same system with a CCS unit have a lower efficiency compared to the traditional CHP due to the extra energy consumption needed to treat the CO_2.

The electric penalty introduced by the CCS energy consumption can be estimated introducing the ELectric Penalty factor (ELP) (187) [16]:

$$ELP = 1 - \frac{\eta_{el,CHP\ with\ CCS}}{\eta_{el,CHP\ ref}} \tag{187}$$

Where $\eta_{el,CHP\ with\ CCS}$ is the electric efficiency of the system with the CCS unit and $\eta_{el,CHP\ ref}$ is the reference system without the CCS unit. In this case the refence system is the MCFC+CHP scenario.
For the two scenarios, respectively CCS with membrane (188) and CCS with oxy-combustor (189), the electric penalty is:

$$ELP_{MCFC+CHP+CCS_{membrane}} = 1 - \frac{\eta_{el,MCFC+CHP+CCS_m}}{\eta_{el,MCFC+CHP}} = 1 - \frac{40.9}{42.6} = 4.1\% \tag{188}$$

$$ELP_{MCFC+CHP+CCS_{oxy-combustor}} = 1 - \frac{\eta_{el,MCFC+CHP+CCS_{oxy}}}{\eta_{el,MCFC+CHP}} = 1 - \frac{40.6}{42.6} = 4.8\% \tag{189}$$

The penalty introduced by the oxy-combustion system is higher due to the ASU electric energy consumption.

In Figure 40 is reported the avoided primary energy consumption and in Figure 41 the Overall Primary Energy Saving (OPES).

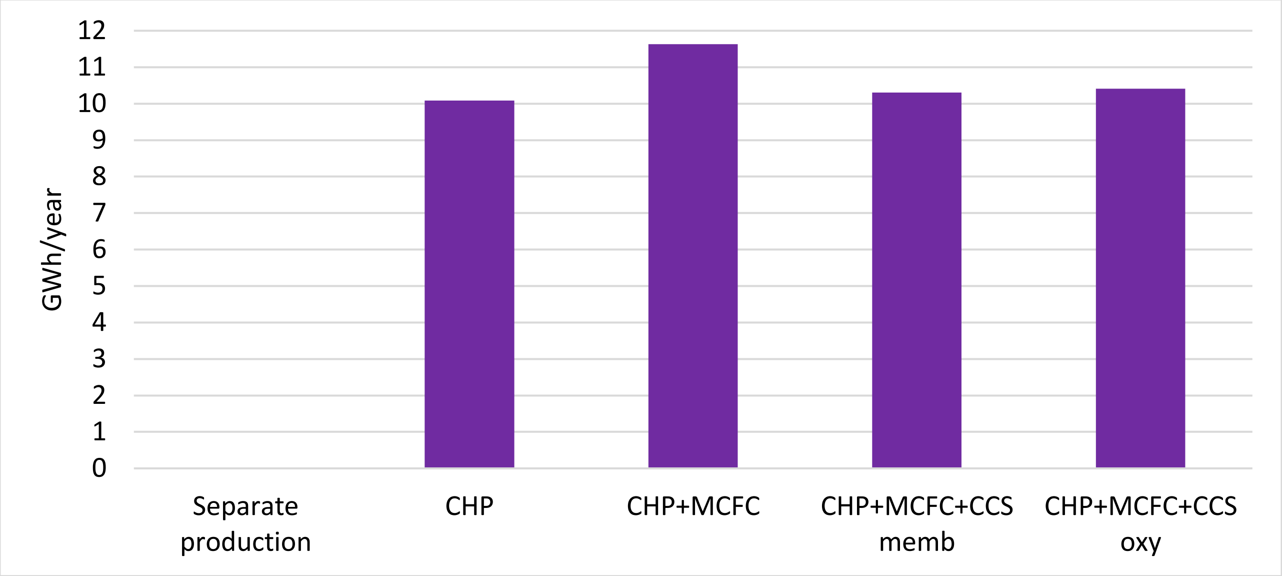

Figure 40 – Avoided primary energy consumption

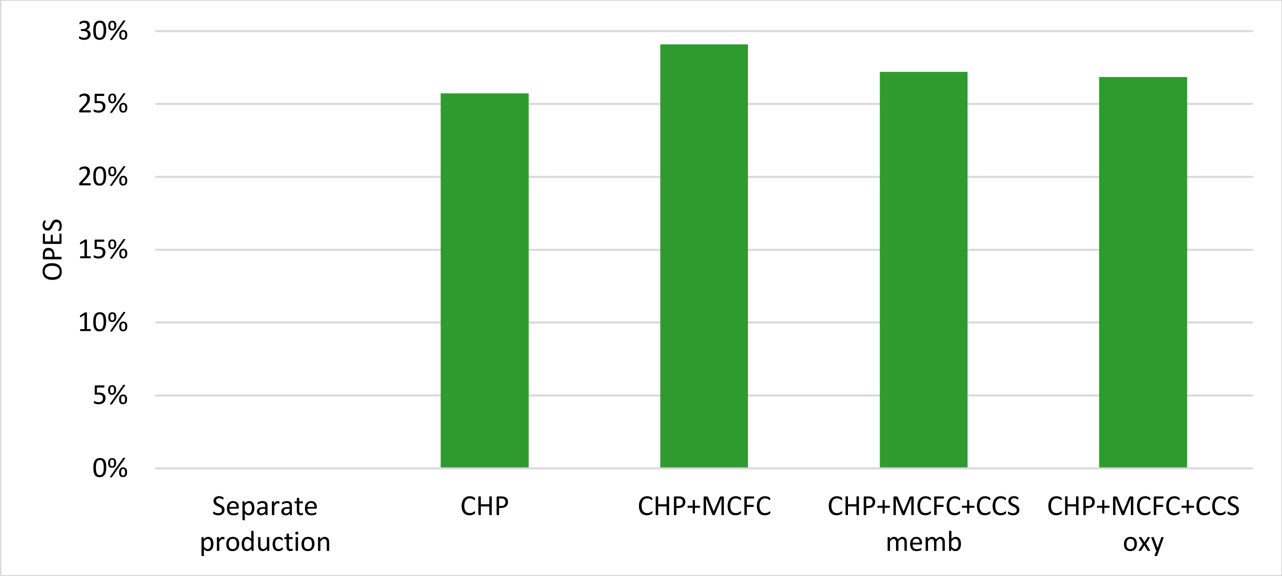

Figure 41 – Overall Primary Energy Saving

All the four cogeneration options can achieve more than 10 GWh of energy saving per year, respect to the separated production, and OPES higher than 25%

The MCFC+CHP is the best option with 11.6 GWh of primary energy saved and with OPES equal 29.1%.

The two configurations of MCFC+CHP with CCS are better than the CHP solution with OPES around 27%.

The CHP scenario has the lower primary energy consumption avoided. The PES of the CHP unit is higher than the other solutions (29.4%) but the energy demand of the plant require a supply from separated production, this introduce a penalty in the OPES (-3.8%) that make this option the worse among the four.
In Figure 42 the Overall Energy Utilization Factor (OEUF) is reported for all the five options

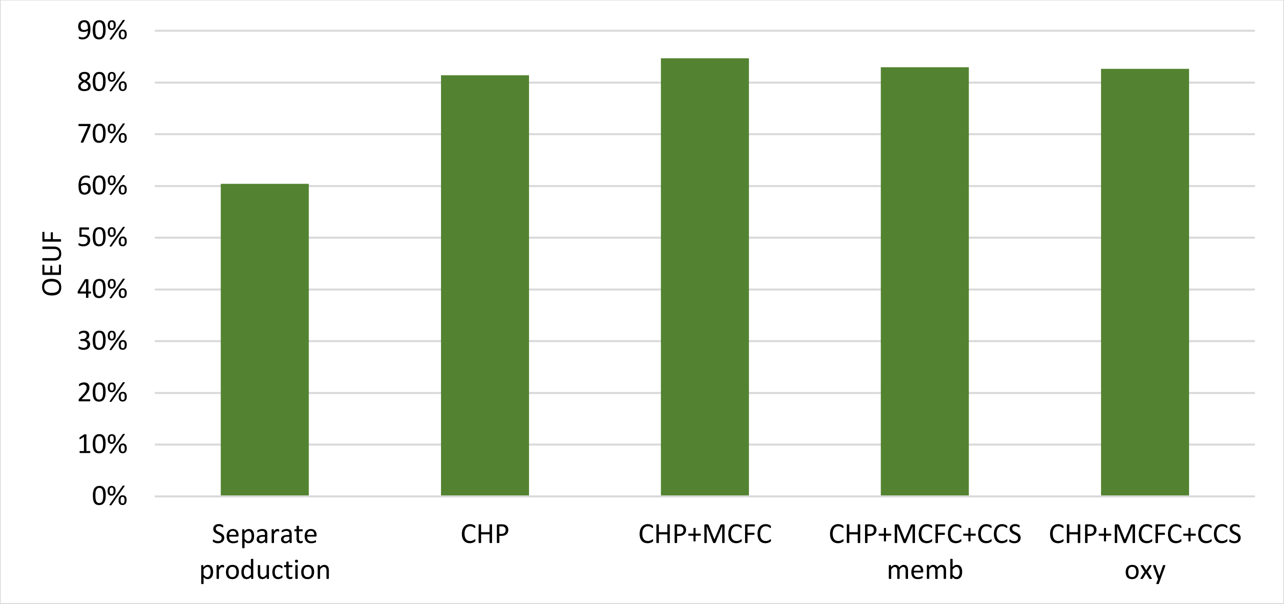

Figure 42 – Overall Energy Utilization Factor

The OEUF index can also be considered as the global efficiency of the plant, the scenarios involving a MCFC are the best, with OEUF slightly higher (4% in case of only MCFC and 1% in case of MCFC+CCS) than the CHP solution.

As before, the CHP option has a EUF higher between the scenarios, but the separated production penalized the overall value.

Also, for the separated production the OEUF is evaluated considering the two different way of energy production and the related fuel consumption.

Lastly, the CO_2 emission are reported in Figure 43 and Figure 44.

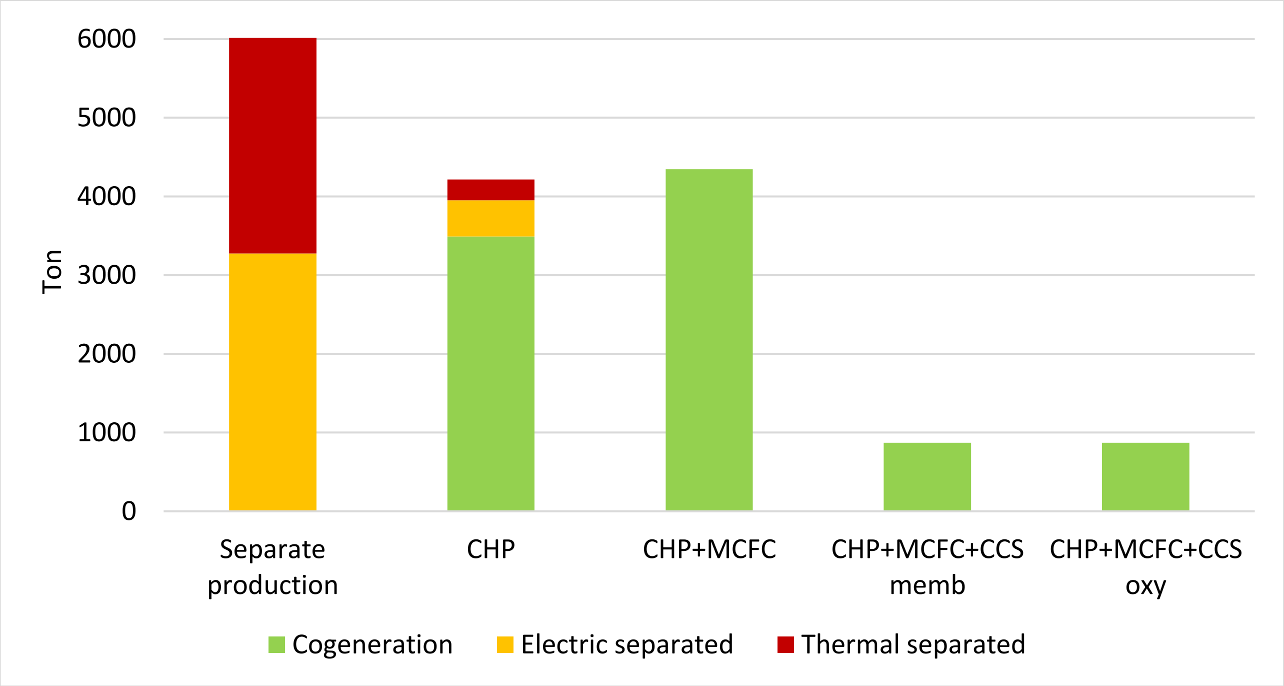

Figure 43 – Tons of CO_2 emitted in a year by the different components of each scenario.

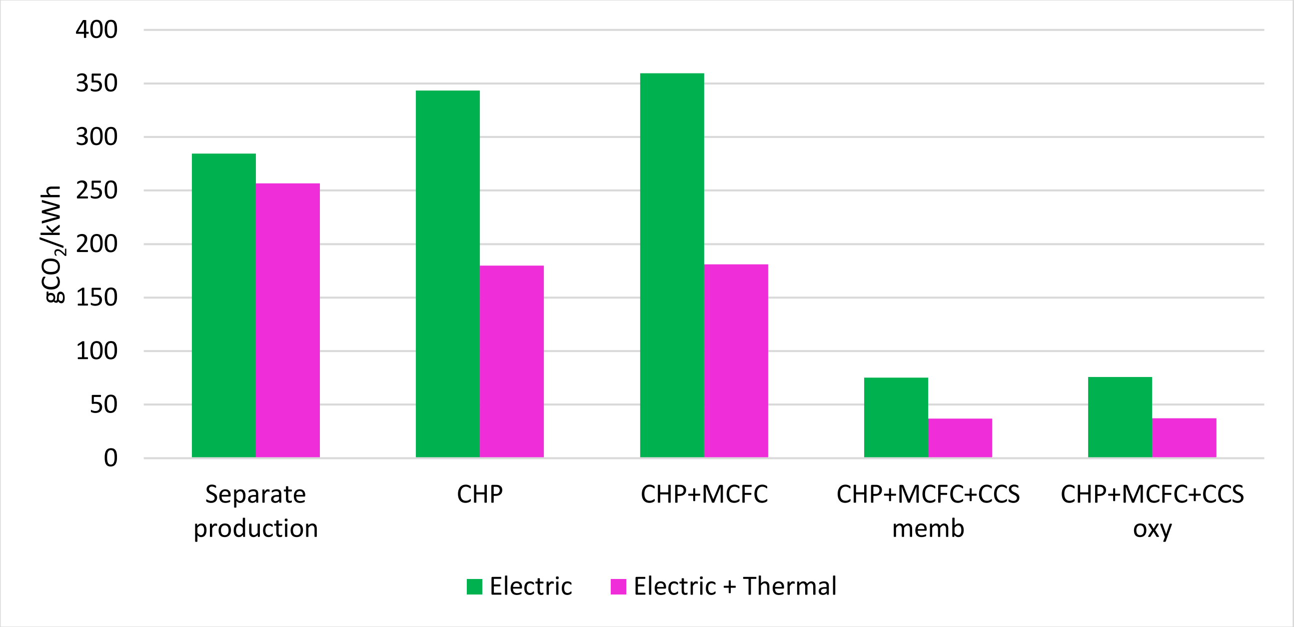

Figure 44 – CO_2 emission factors

Between all the options, the separated production is the one that produce the highest quantity of CO_2 (more than 6000 tons) and has the higher emission factor.

The MCFC+CHP, between the cogeneration options, is the one with the highest CO_2 production (around 4347 tons) and emissions 181.1 $\frac{g_{CO_2}}{kWh}$ (359.6 $\frac{g_{CO_2}}{kWh_{el}}$), but slightly higher than the CHP option with an emission of CO_2 around 4240 tons (considering also the separated production) and emission factor of 180.4 $\frac{g_{CO_2}}{kWh}$ (342.9 $\frac{g_{CO_2}}{kWh_{el}}$).

The last two options with CCS show how the emission of CO_2 can be reduced, the first case (membrane) is the best with 873 tons of CO_2 and 37.1 $\frac{g_{CO_2}}{kWh}$ (75.3 $\frac{g_{CO_2}}{kWh_{el}}$) emitted.

The other option (oxy-combustion) is slightly worse because there is a lower energy production. This option is still a good one with 873 tons of CO_2 and 37.3 $\frac{g_{CO_2}}{kWh}$ (75.8 $\frac{g_{CO_2}}{kWh_{el}}$) emitted.

For the options with CCS is possible to introduce the Specific Primary Energy Consumption for CO_2 Avoided (SPECCA) index to indicate the plant achievement in terms of electric efficiency and CO_2 specific emissions. SPECCA is defined as:

$$SPECCA = \frac{\frac{1}{\eta} - \frac{1}{\eta_{ref}}}{e_{ref} - e} \cdot 3600 \qquad \left[\frac{MJ}{kg_{CO_2}}\right] \tag{190}$$

Where η is the net electric efficiency of the plant and e is the CO_2 specific emission $\frac{kg_{CO_2}}{MWh_{el}}$ of the system with CCS while η_{ref} and e_{ref} are the electric efficiency and CO_2 specific emission of the reference plant. In this evaluation the reference plant is the scenario MCFC+CHP.

For the membrane scenario the SPECCA is 1.26 $\frac{MJ}{kg_{CO_2}}$ and for the oxy-combustion case the SPECCA is 1.49 $\frac{MJ}{kg_{CO_2}}$.

To conclude, all the four option for cogeneration achieve great results obtaining the HEC status but implementing the CCS can drastically reduce the CO_2 emissions of the plant making those system much cleaner compared to the traditional ones. In addition, between the two CCS option, the oxy-combustor is the best because can achieve higher thermal energy recovery reducing the overall CO_2 emission factor to 34.0 $\frac{g_{CO_2}}{kWh}$ and increasing the energy performance with an OPES of 31.6 %, OEUF of 91.9% and SPECCA of 1.30 $\frac{MJ}{kg_{CO_2}}$.

5 Conclusions

In this work we wanted to analyze how the application of an MCFC for CO_2 capture could affect the performance of a traditional CHP plant, in this case consisting of an ICE. It was chosen to analyze two different configurations for CO_2 capture: the first involves the use of a membrane for hydrogen capture while the second involves the use of an oxy-combustor.

After reviewing the literature inert to the topics covered, it was possible to build and validate a MCFC model with Aspen Plus and develop a complete model for both chosen configurations. For both cases, the pinch analysis methodology was applied for heat recovery within the plant and minimizing thermal energy requirements.

The two configurations were analyzed and the comparison showed that the second one (oxy-combustor) is the best because achieve a quality of CO_2 that satisfies the requirements to be injected into a pipeline for final sequestration, while in the first option there are non-negligible residues of CO (2.1%).

The MCFC module has a power output of 314 kW without considering the CCS unit. In both cases the energy consumption of CCS unit is supplied by the module, the compression train require 70 kW (in both cases) and for the second case the ASU requires 12.4 kW.
For the membrane case, the system can achieve an electrical efficiency of 40.9% and a thermal efficiency of 42.0%. In this case the installation of a MCFC module and a CCS unit increase the electric energy production of 244 kW (+17.2% compared to the CHP electric power). The MCFC installation require to remove the exhaust gas heat recovery from the CHP unit but the MCFC heat recovery increase the thermal production up to 805 kW, +25.6% compared to the exhaust gas heat recovery of the CHP.
For the other case, the net power provided by the MCFC is 232 kW, increasing the plant power of 16.4%, with a plant electric efficiency of 40.6%, the presence of an oxy-combustion increase the thermal production up to 1168 kW (+82.2% compared to CHP exhaust gas heat recovery) with a plant thermal efficiency of 51.0%.

An energy analysis of the two configurations was also carried out and compared with other possible options that can be adopted in the context of cogeneration, under the assumption of equal energy demand. Both are energetically competitive, the membrane case achieves a primary energy saving of 27.2% and an energy utilization factor of 82.9% while the oxy-combustion case achieves a primary energy saving of 26.8% and an energy utilization factor of 82.6%. Both cases can obtain the status of high efficiency cogeneration (HEC).
The reference system made of MCFC+CHP is the best with a primary energy saving of 29.1% and an energy utilization factor of 84.7%. The CCS unit penalize the plant, compared to the reference, the membrane case has an electrical penalty of 4.1% while for the oxy-combustion the electric penalty is 4.8%.
Despite the penalty introduced by the CCS unit, the two cases are still energetically better than the CHP scenario. The CHP performance is the best but the energy integration with separate production penalizes the CHP reducing the primary energy saving to 25.7% (-3.8% of the CHP value) and the energy utilization factor to 81.4% (-5% of the CHP value).

Compared to the other scenarios (separated production, CHP, CHP+MCFC), the application of CCS reduces the CO_2 emissions above 78%. From the analysis, the membrane case has the lowest emission factor (37.1 $\frac{g_{CO_2}}{kWh}$) with a SPECCA of 1.26 $\frac{MJ}{kg_{CO_2}}$ while the oxy combustion the emissions are slightly higher (37.3 $\frac{g_{CO_2}}{kWh}$) with a SPECCA of 1.49 $\frac{MJ}{kg_{CO_2}}$.

In conclusion, the energy analysis has demonstrated that the membrane option has higher energy performance than the case in which an oxy-combustion is used. Despite the higher performance, the membrane has non-negligible CO residues, not allowing the insertion of the captured CO_2 inside a pipeline for transport to the sequestration site. The second option is therefore better overall, having slightly worse performances, it still manages to capture the same amount of CO_2 ensuring an acceptable purity for transport in the pipeline. It should be added that in the case of oxy-combustion, the thermal production was limited during the energy analysis, so this option can further improve the results (already excellent) in the case of a greater thermal energy demand.

The application of MCFCs to CCS has showed to achieve optimistic performance as a measure against the GHG emissions, but further research is needed to improve the maturity of this technology. The economic part was not dealt with in this work, as it would be interesting to start from a load curve of a real plant, apply the model developed and analyze the economic feasibility of the plant as its ones of the main barrier needed to overcome.

6 References

[1] IPCC, "IPCC Fifth Assessment Synthesis Report-Climate Change 2014 Synthesis Report," *IPCC Fifth Assess. Synth. Report-Climate Chang. 2014 Synth. Rep.*, 2014.

[2] Intergovernmental Panel on Climate Change, "Special Report on Global Warming of 1.5C," *Glob. Warm. 1.5 °C Spec. Rep.*, 2018.

[3] "Our World In Data." https://ourworldindata.org/.

[4] L. Caprile, B. Passalacqua, and A. Torazza, "Carbon capture: Energy wasting technologies or the MCFCs challenge?," 2011, doi: 10.1016/j.ijhydene.2010.10.028.

[5] F. Wang *et al.*, "A comprehensive review on high-temperature fuel cells with carbon capture," *Appl. Energy*, vol. 275, no. May, p. 115342, 2020, doi: 10.1016/j.apenergy.2020.115342.

[6] L. Duan, K. Xia, T. Feng, S. Jia, and J. Bian, "Study on coal-fired power plant with CO2 capture by integrating molten carbonate fuel cell system," *Energy*, vol. 117, pp. 578–589, 2016, doi: 10.1016/j.energy.2016.03.063.

[7] L. Duan, S. Sun, L. Yue, W. Qu, and Y. Yang, "Study on a new IGCC (Integrated Gasification Combined Cycle) system with CO2 capture by integrating MCFC (Molten Carbonate Fuel Cell)," *Energy*, vol. 87, pp. 490–503, 2015, doi: 10.1016/j.energy.2015.05.011.

[8] L. Duan, J. Zhu, L. Yue, and Y. Yang, "Study on a gas-steam combined cycle system with CO2 capture by integrating molten carbonate fuel cell," *Energy*, vol. 74, no. C, pp. 417–427, 2014, doi: 10.1016/j.energy.2014.07.006.

[9] S. Campanari, P. Chiesa, and G. Manzolini, "CO2 capture from combined cycles integrated with Molten Carbonate Fuel Cells," *Int. J. Greenh. Gas Control*, 2010, doi: 10.1016/j.ijggc.2009.11.007.

[10] S. Campanari, G. Manzolini, and P. Chiesa, "Using MCFC for high efficiency CO2 capture from natural gas combined cycles: Comparison of internal and external reforming," *Appl. Energy*, vol. 112, pp. 772–783, 2013, doi: 10.1016/j.apenergy.2013.01.045.

[11] M. Spinelli *et al.*, "Molten Carbonate Fuel Cells for Retrofitting Postcombustion CO2 Capture in Coal and Natural Gas Power Plants," *J. Electrochem. Energy Convers. Storage*, 2018, doi: 10.1115/1.4038601.

[12] M. Spinelli, D. Di Bona, M. Gatti, E. Martelli, F. Viganò, and S. Consonni, "Assessing the potential of molten carbonate fuel cell-based schemes for carbon capture in natural gas-fired combined cycle power plants," *J. Power Sources*, vol. 448, no. September 2019, 2020, doi: 10.1016/j.jpowsour.2019.227223.

[13] F. Sartori da Silva and J. A. Matelli, "Exergoeconomic analysis and determination of power cost in MCFC – steam turbine combined cycle," *Int. J. Hydrogen Energy*, vol. 44, no. 33, pp. 18293–18307, 2019, doi: 10.1016/j.ijhydene.2019.05.156.

[14] U. Desideri, S. Proietti, P. Sdringola, G. Cinti, and F. Curbis, "MCFC-based CO2 capture system for small scale CHP plants," *Int. J. Hydrogen Energy*, vol. 37, no. 24, pp. 19295–19303, 2012, doi: 10.1016/j.ijhydene.2012.05.048.

[15] G. Rinaldi, D. McLarty, J. Brouwer, A. Lanzini, and M. Santarelli, “Study of CO2 recovery in a carbonate fuel cell tri-generation plant,” *J. Power Sources*, vol. 284, pp. 16–26, 2015, doi: 10.1016/j.jpowsour.2015.02.147.

[16] M. Badami, M. Cipriano, G. Kowalski, A. Portoraro, and M. Zenouzi, “Molten carbonate fuel cells for carbon capture from a cogeneration system: A comparative analysis of performance to other separation technologies,” *ASME Int. Mech. Eng. Congr. Expo. Proc.*, vol. 6, pp. 1–15, 2017, doi: 10.1115/IMECE2017-70519.

[17] N. Gaurina-Međimurec, K. Novak-Mavar, and M. Majić, “Carbon capture and storage (CCS): Technology, projects and monitoring review,” *Rud. Geol. Naft. Zb.*, vol. 33, no. 2, pp. 1–14, 2018, doi: 10.17794/rgn.2018.2.1.

[18] R. Y. Surampalli *et al.*, *Carbon capture and storage: Physical, chemical, and biological methods*. 2015.

[19] M. Santarelli, A. Lanzini, and G. Marta, “Polygeneration and Advanced Energy System - Theory lectures.” 2019.

[20] M. Bui *et al.*, “Carbon capture and storage (CCS): The way forward,” *Energy and Environmental Science*. 2018, doi: 10.1039/c7ee02342a.

[21] S. Mekhilef, R. Saidur, and A. Safari, “Comparative study of different fuel cell technologies,” *Renewable and Sustainable Energy Reviews*. 2012, doi: 10.1016/j.rser.2011.09.020.

[22] S. J. Mcphail, P. H. Hsieh, and J. R. Selman, “Molten Carbonate Fuel Cells,” *Mater. High-Temperature Fuel Cells*, pp. 341–371, 2012, doi: 10.1002/9783527644261.ch9.

[23] P. Tomczyk, “MCFC versus other fuel cells-Characteristics, technologies and prospects,” *J. Power Sources*, 2006, doi: 10.1016/j.jpowsour.2006.04.071.

[24] C. Yuh, M. Farooque, and F. Energy, “Materials and Life Considerations,” *Encycl. Electrochem. Power Sources*, no. January 2009, 2009.

[25] I. Dincer and M. A. Rosen, “Exergy Analysis of Fuel Cell Systems,” in *Exergy*, 2013.

[26] “MWM site.” https://www.mwm.net/mwm-chp-gas-engines-gensets-cogeneration/press/press-releases/bund-hessen-launches-chp-information-campaign-that-brings-together-chp-plant-man/.

[27] “Northern utilities site.” http://northernutilities.co.uk/combined-heat-and-power/.

[28] L. Zhao, M. Weber, and D. Stolten, “Comparative investigation of polymer membranes for post-combustion capture,” *Energy Procedia*, vol. 37, pp. 1125–1134, 2013, doi: 10.1016/j.egypro.2013.05.210.

[29] P. Shao, M. M. Dal-Cin, M. D. Guiver, and A. Kumar, “Simulation of membrane-based CO2 capture in a coal-fired power plant,” *J. Memb. Sci.*, vol. 427, pp. 451–459, 2013, doi: 10.1016/j.memsci.2012.09.044.

[30] K. Ramasubramanian, H. Verweij, and W. S. Winston Ho, “Membrane processes for carbon capture from coal-fired power plant flue gas: A modeling and cost study,” *J. Memb. Sci.*, vol. 421–422, pp. 299–310, 2012, doi: 10.1016/j.memsci.2012.07.029.

[31] H. Zhai and E. S. Rubin, “The effects of membrane-based CO2 capture system on pulverized coal power plant performance and cost,” *Energy Procedia*, vol. 37, pp. 1117–1124, 2013, doi: 10.1016/j.egypro.2013.05.209.

[32] "Jenbacher site." https://www.innio.com/en/products/jenbacher.

[33] A. Poggio, "Impianti di cogenerazione - Appunti del corso." 2018.

[34] P. Nuccio, "Complementi di macchine - Appunti del corso." 2019.

[35] A. Carpignano, R. Testoni, M. Montrucchio, and R. Gerboni, "Localizzazione e Impatto Ambientale dei Sistemi Energetici - Appunti del corso." 2019.

[36] L. García, "Hydrogen production by steam reforming of natural gas and other nonrenewable feedstocks," in *Compendium of Hydrogen Energy*, 2015.

[37] M. Lusardi, B. Bosio, and E. Arato, "An example of innovative application in fuel cell system development: CO2 segregation using Molten Carbonate Fuel Cells," *J. Power Sources*, vol. 131, no. 1–2, pp. 351–360, 2004, doi: 10.1016/j.jpowsour.2003.11.091.

[38] M. Mehrpooya, S. Sayyad, and M. J. Zonouz, "Energy, exergy and sensitivity analyses of a hybrid combined cooling, heating and power (CCHP) plant with molten carbonate fuel cell (MCFC) and Stirling engine," *J. Clean. Prod.*, vol. 148, pp. 283–294, 2017, doi: 10.1016/j.jclepro.2017.01.157.

[39] M. Baranak and H. Atakül, "A basic model for analysis of molten carbonate fuel cell behavior," *J. Power Sources*, 2007, doi: 10.1016/j.jpowsour.2007.05.027.

[40] S. Samanta and S. Ghosh, "A thermo-economic analysis of repowering of a 250 MW coal fired power plant through integration of Molten Carbonate Fuel Cell with carbon capture," *Int. J. Greenh. Gas Control*, vol. 51, pp. 48–55, 2016, doi: 10.1016/j.ijggc.2016.04.021.

[41] J. Yazdanfar, M. Mehrpooya, H. Yousefi, and A. Palizdar, "Energy and exergy analysis and optimal design of the hybrid molten carbonate fuel cell power plant and carbon dioxide capturing process," *Energy Convers. Manag.*, vol. 98, pp. 15–27, 2015, doi: 10.1016/j.enconman.2015.03.076.

[42] A. Salehi, S. M. Mousavi, A. Fasihfar, and M. Ravanbakhsh, "Energy, exergy, and environmental (3E) assessments of an integrated molten carbonate fuel cell (MCFC), Stirling engine and organic Rankine cycle (ORC) cogeneration system fed by a biomass-fueled gasifier," *Int. J. Hydrogen Energy*, vol. 44, no. 59, pp. 31488–31505, 2019, doi: 10.1016/j.ijhydene.2019.10.038.

[43] S. Wu, H. Zhang, and M. Ni, "Performance assessment of a hybrid system integrating a molten carbonate fuel cell and a thermoelectric generator," *Energy*, vol. 112, pp. 520–527, 2016, doi: 10.1016/j.energy.2016.06.128.

[44] J. Brouwer, F. Jabbari, E. M. Leal, and T. Orr, "Analysis of a molten carbonate fuel cell: Numerical modeling and experimental validation," *J. Power Sources*, 2006, doi: 10.1016/j.jpowsour.2005.07.093.

[45] H. Hongliang, H. Zhang, S. Weng, and M. Su, "Dynamic numerical simulation of a molten carbonate fuel cell," *J. Power Sources*, 2006, doi: 10.1016/j.jpowsour.2006.04.109.

[46] C. Y. Yuh and J. R. Selman, "The Polarization of Molten Carbonate Fuel Cell Electrodes: I . Analysis of Steady-State Polarization Data," *J. Electrochem. Soc.*, 2019, doi: 10.1149/1.2085473.

[47] J. Larminie and A. Dicks, *Fuel cell systems explained: Second edition*. 2013.

[48] SOFCOM project, "Final Report Summary - SOFCOM (SOFC CCHP WITH POLY-

FUEL: OPERATION AND MAINTENANCE),” 2015. .

[49] Http://www.sofcom.eu., “SOFCOM Project, SOFC CCHP with Poly-fuel Operation and Maintenance.” .

[50] SNAM, *Codice di rete*, Rev VI. Infrastrutture Trasporto Gas S.p.A., 2020.

[51] P. Nuccio, “Fondamenti di macchine - Appunti del corso.” 2017.

[52] A. Alabdulkarem, Y. Hwang, and R. Radermacher, “Development of CO2 liquefaction cycles for CO2 sequestration,” *Appl. Therm. Eng.*, 2012, doi: 10.1016/j.applthermaleng.2011.09.027.

[53] C. A. Scholes, K. H. Smith, S. E. Kentish, and G. W. Stevens, “CO2 capture from pre-combustion processes - Strategies for membrane gas separation,” *International Journal of Greenhouse Gas Control*. 2010, doi: 10.1016/j.ijggc.2010.04.001.

[54] V. Verda and E. Guelpa, *Metodi termodinamici per l’uso efficiente delle risorse energetiche*. 2013.

[55] European Commission, *Directive 2004/8/EC on the promotion of cogeneration based on a useful heat demand in the internal energy market and amending Directive 92/42/EEC*. 2004.

[56] M. Badami, R. Gerboni, and A. Portoraro, “Determination and assessment of indices for the energy performance of district heating with cogeneration plants,” *Energy*, 2017, doi: 10.1016/j.energy.2017.03.136.

[57] GSE, *Guida alla Cogenerazione ad Alto Rendimento - CAR*, 1st ed. 2018.

[58] ISPRA; SNPA, *Fattori di emissione atmosferica di gas ad effetto serra nel settore elettrico nazionale e nei principali Paesi Europei*. 2020.

7 APPENDIX

7.1 Appendix I: JMS 420 G8 B02 datasheet

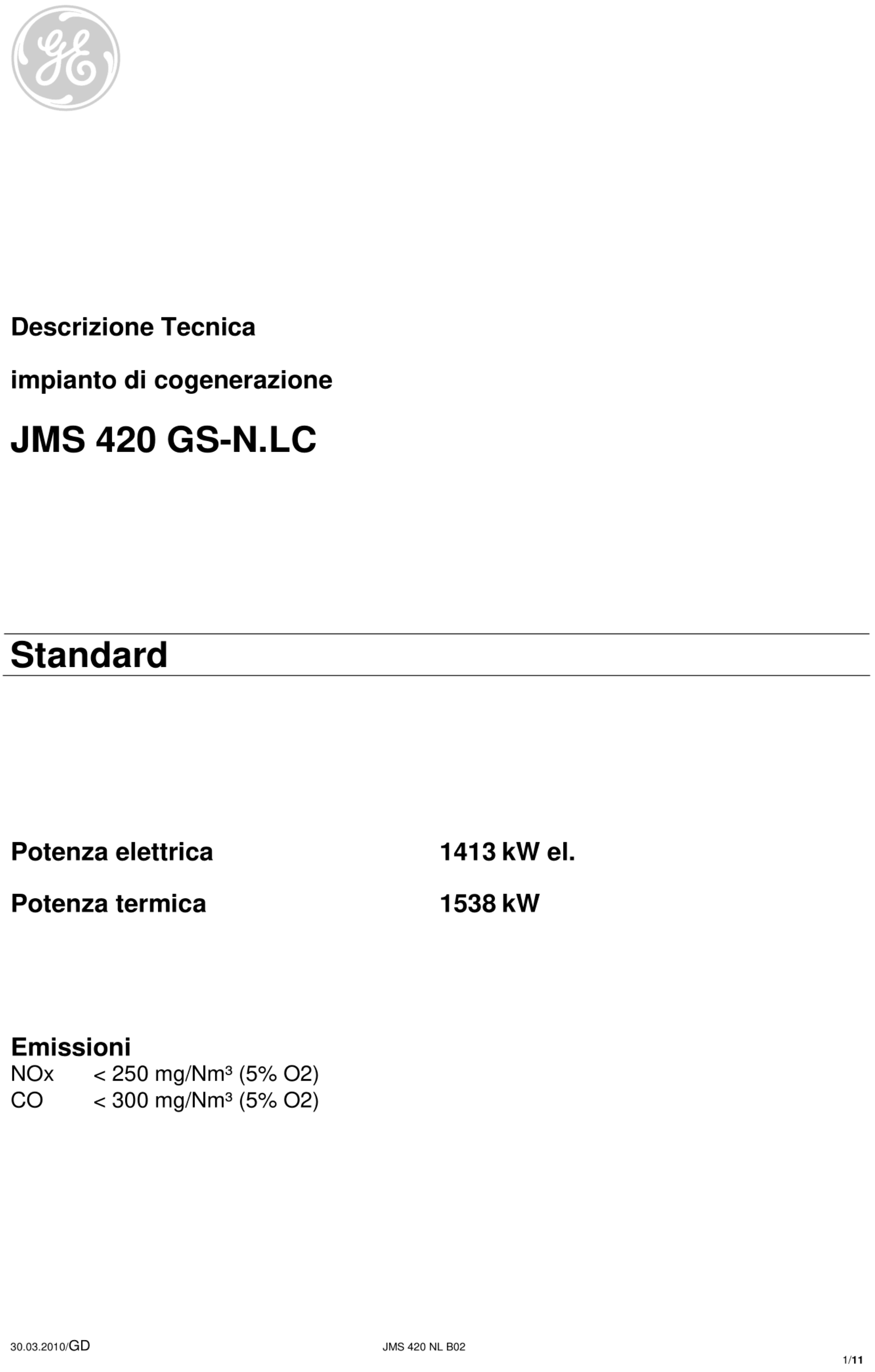

Descrizione Tecnica

impianto di cogenerazione

JMS 420 GS-N.LC

Standard

Potenza elettrica	**1413 kW el.**
Potenza termica	**1538 kW**

Emissioni
NOx < 250 mg/Nm³ (5% O2)
CO < 300 mg/Nm³ (5% O2)

0.01 Dati Tecnici (al modulo)

Dati con:				**Pieno carico**	**Carico parziale**	
Potere calorifico inferiore del gas (PCI)		kWh/Nm³		9,5		
				100%	75%	50%
Potenza introdotta		kW	[2]	3.417	2.636	1.856
Quantità di gas		Nm³/h	*)	360	277	195
Potenza meccanica		kW	[1]	1.451	1.088	726
Potenza elettrica		kW el.	[4]	1.413	1.060	704
Potenze termiche recuperabili						
~ Primo stadio intercooler		kW		309	153	44
~ Olio		kW		161	142	129
~ Acqua di raffreddamento motore		kW		427	390	325
~ Gas di scarico raffreddati a 120 °C		kW		641	534	402
Potenza termica complessiva		kW	[5]	1.538	1.219	900
Potenza erogata complessiva		kW totale		2.951	2.279	1.604
Potenza termica da dissipare						
~ Secondo stadio intercooler		kW		105	80	55
~ Olio		kW		~	~	~
~ Calore insuperficie	ca.	kW	[7]	98	75	57
~ Potenza termica rimanente		kW		34	26	19
Consumo specifico del motore		kWh/kWh	[2]	2,36	2,42	2,56
Consumo olio motore	ca.	kg/h	[3]	0,44	~	~
Rendimento elettrico		%		41,4%	40,2%	37,9%
Rendimento termico		%		45,0%	46,2%	48,5%
Rendimento complessivo		%	[6]	86,4%	86,4%	86,4%
Circuito acqua calda:						
Temperatura di mandata		°C		90,0	85,9	81,7
Temperatura di ritorno		°C		70,0	70,0	70,0
Portata nominale		m³/h		66,0	66,0	66,0

*) Valore indicativo per il dimensionamento della tubazione, Sm³=Nm³ x 1,055
[_] Spiegazioni: vedi voce 0.10 - Parametri tecnici

I dati termici si riferiscono alle condizioni di riferimento riportate nell'allegato 0.10. In caso di scostamenti da queste condizioni, possono esserci variazioni nei bilanci termici. Questi scostamenti devono essere considerati nel dimensionamento dei circuiti di dissipazione (emergenza, intercooler, ...). Sulla tolleranza del +/- 8% inerente la potenza termica recuperabile si consiglia di considerare per il progetto del recupero un'ulteriore tolleranza del + 10%.

Dimensioni prinipali e pesi (al modulo)

Lunghezza	mm	~ 7.100
Larghezza	mm	~ 1.800
Altezza	mm	~ 2.200
Peso a secco	kg	~ 15.000
Peso pronto per l'esercizio	kg	~ 15.700

Raccordi

Ingresso ed uscita acqua calda	DN/PN	100/10
Uscita gas di scarico	DN/PN	300/10
Gas di combustione (all'entrata linea gas)	DN/PN	80/16
Gas di combustione (al modulo)	DN/PN	125/10
Scarico acqua ISO 228	G	½''
Scarico condensa	DN/PN	50/10
Valvola di sicurezza acqua motore (ISO 228)	DN/PN	2x1½''/2,5
Valvola di sicurezza acqua calda	DN/PN	65/16
Riempimento olio lubrificante (tubo)	mm	28
Scarico olio lubrificante (tubo)	mm	28
Riempimento acqua motore (tubo flessibile)	mm	13
Acqua ingresso/uscita primo stadio intercooler	DN/PN	100/10
Acqua ingresso/uscita secondo stadio intercooler	DN/PN	65/10

Potenza / Consumo

Potenza standard ISO-ICFN	kW	1.451
Press. media eff. a carico nom. e velocità nom.	bar	19,00
Tipo di gas		Gas naturale
Numero metanico di riferimento|Numero metanico minimo	MZ d)	94|70
Rapporto di compressione	Epsilon	12,50
Range ammesso di pressione del gas all'entrata della rampa	mbar	120 - 200 c)
Range di pressione del flusso del gas di combustione ammesso	%	± 10
Velocitá massima di variazione pressione gas	mbar/sec	10
Temperatura massima raffreddamento intercooler 2°s tadio	°C	40
Consumo specifico del motore	kWh/kWh	2,36
Consumo specifico olio lubrificante	g/kWh	0,30
Temperatura olio mass.	°C	85
Temperatura mass. acqua raffreddamento motore	°C	90
Volume cambio olio	lit	~ 437

c) Pressione di gas inferiore su richiesta
d) Basato sul programma di calcolo del numero metanico AVL 3.1 (calcolato senza N2 e CO2)

0.02 Dati Tecnici del Motore

Costruttore		GE Jenbacher
Tipo di motore		J 420 GS-B02
Ciclo di funzionamento		4-tempi
Disposizione cilindri		V 70°
Numero cilindri		20
Alesaggio	mm	145
Corsa	mm	185
Cilindrata	lit	61,10
Velocità nominale	1/con	1.500
Velocitá media del pistone	m/s	9,25
Lunghezza	mm	3.750
Larghezza	mm	1.580
Altezza	mm	2.033
Peso a secco	kg	6.600
Peso pronto per l'esercizio	kg	7.300
Momento d'inerzia del volano	kgm²	11,64
Senso di rotazione (visto lato volano)		a sinistra
Attacco volano		SAE 18"
Livello dist. radio sec. VDE 0875		N
Motorino d'avviam.: pot.	kW	13
Motorino d'avviam.: tensione	V	24

Potenze termiche

Potenza introdotta	kW	3.417
Intercooler	kW	414
Olio	kW	161
Acqua di raffreddamento motore	kW	427
Gas di scarico totale	kW	868
Gas di scarico raffreddati a 180 °C	kW	496
Gas di scarico raffreddati a 100 °C	kW	689
Calore insuperficie	kW	60
Potenza termica rimanente	kW	34

Dati gas di scarico

Temperatura gas di scarico a pieno carico	°C [8]	378
Portata gas di scarico umido	kg/h	8.064
Portata gas di scarico secco	kg/h	7.512
Volume gas di scarico umido	Nm³/h	6.366
Volume gas di scarico secco	Nm³/h	5.703
Contropressione mass. gas di scarico all'uscita motore	mbar	50

Dati aria di combustione

Portata aria	kg/h	7.819
Volume aria	Nm³/h	6.048
Perdita di pressione mass. in aspirazione	mbar	10

Livello sonoro

Aggregato b)	dB(A) re 20µPa	97
31,5 Hz	dB	79
63 Hz	dB	87
125 Hz	dB	98
250 Hz	dB	95
500 Hz	dB	91
1000 Hz	dB	86
2000 Hz	dB	88
4000 Hz	dB	92
8000 Hz	dB	89
Gas di scarico a)	dB(A) re 20µPa	115
31,5 Hz	dB	95
63 Hz	dB	117
125 Hz	dB	115
250 Hz	dB	113
500 Hz	dB	108
1000 Hz	dB	105
2000 Hz	dB	108
4000 Hz	dB	109
8000 Hz	dB	107

Potenza sonora

Aggregato	dB(A) re 1pW	117
superficie di misura	m²	107
Gas di scarico	dB(A) re 1pW	123
superficie di misura	m²	6,28

a) I valori menzionati sono pressioni sonore misurate secondo DIN 45635, distanza 1 m, con propagazione semisferica in ambiente riflettente.
b) I valori menzionati sono pressioni sonore (riferite in condizioni di campo libero) secondo DIN 45635 classe di precisione 3 distanza di misura 1 m.
Con funzionamento a 1200 giri/min sono le stesse, con 1800 giri/min sono da aumentare di 3dB.
tolleranza macchina ± 3 dB

0.03 Dati Tecnici del Generatore

Costruttore		STAMFORD e)
Tipo		PE 734 E2 e)
Potenza omologata	kVA	1.770
Potenza meccanica introdotta	kW	1.451
Potenza attiva a cos phi = 1,0	kW	1.413
Potenza attiva a cos phi = 0,8	kW	1.397
Potenza apparente a cos phi = 0,8	kVA	1.747
Corrente nominale a cos phi = 0,8	A	2.521
Frequenza	Hz	50
Tensione	V	400
Giri	1/con	1.500
Velocità di fuga	1/con	2.250
Fattore di potenza ind.		0,8 - 1,0
Rendimento a cos phi = 1,0	%	97,4%
Rendimento a cos phi = 0,8	%	96,3%
Momento d'inerzia del volano	kgm²	44,49
Massa	kg	3.506
Livello dist. radio sec. VDE 0875		N
Forma costruttiva		B3/B14
Grado di protezione		IP 23
Classe d'isolamento		H
rialzo di temperatura (con potenza meccanica)		F
Temperatura ambientale massima	°C	40
Fattore di distorsione a vuoto tra neutro e fase	%	1,5

Reattanze e costanti di Tempo

xd Reattanza sincrona secondo l´asse diretto	p.u.	2,72
xd' Reattanza transitoria secondo l´asse diretto	p.u.	0,16
xd'' Reattanza subtransitoria secondo l´asse diretto	p.u.	0,12
Td'' Costante di tempo subtransitoria della corrente di c.to c.to	ms	20
Ta Costante di tempo - corrente continua	ms	20
Tdo' Costante di tempo transitoria a vuoto	s	2,46

e) GE Jenbacher si riserva il diritto di modificare il fornitore ed il tipo di generatore. I dati tecnici del generatore potranno essere soggetti a variazioni trascurabili. La potenza elettrica erogata dichiarata verrà garantita.

0.04 Dati Tecnici recupero calore

Dati generali - Circuito acqua calda

Potenza termica complessiva	kW	1.538
Temperatura di ritorno	°C	70,0
Temperatura di mandata	°C	90,0
Portata nominale	m³/h	66,0
Pressione nominale acqua calda	bar	10
Perdita di pressione nominale acqua calda	bar	0,90
Tolleranza massima ammissibile temperatura di ritorno	°C	+0/-20
Velocità di variazione mass. ammissibile	°C/min	10

Scambiatore di calore intercooler (1°stadio)

Tipo	Scambiatore di calore ad alette	
Pressione nominale acqua calda	bar	10
Perdita di pressione nominale acqua calda	bar	0,30
Raccordi acqua calda	DN/PN	100/10

Scambiatore di calore intercooler (2°stadio) (Scambiatore intercooler a parte)

Tipo	Scambiatore di calore ad alette	
Pressione nominale acqua calda	bar	10
Perdita di pressione nominale acqua calda	bar	0,80
Raccordi acqua calda	DN/PN	65/10

Scambiatore di calore olio

Tipo	Scambiatore di calore a piastre	
Pressione nominale acqua calda	bar	10
Perdita di pressione nominale acqua calda	bar	0,20
Raccordi acqua calda	DN/PN	100/10

Scambiatore di calore acqua motore

Tipo	Scambiatore di calore a piastre	
Pressione nominale acqua calda	bar	10
Perdita di pressione nominale acqua calda	bar	0,20
Raccordi acqua calda	DN/PN	100/10

Scambiatore di calore dei gas di scarico

Tipo	Scambiatore di calore a tubi	
PRIMARIO:		
Perdita di pressione gas di scarico ca.	bar	0,02
Raccordi gas di scarico	DN/PN	300/10
SECONDARIO:		
Pressione nominale acqua calda	bar	6
Perdita di pressione nominale acqua calda	bar	0,20
Raccordi acqua calda	DN/PN	100/10

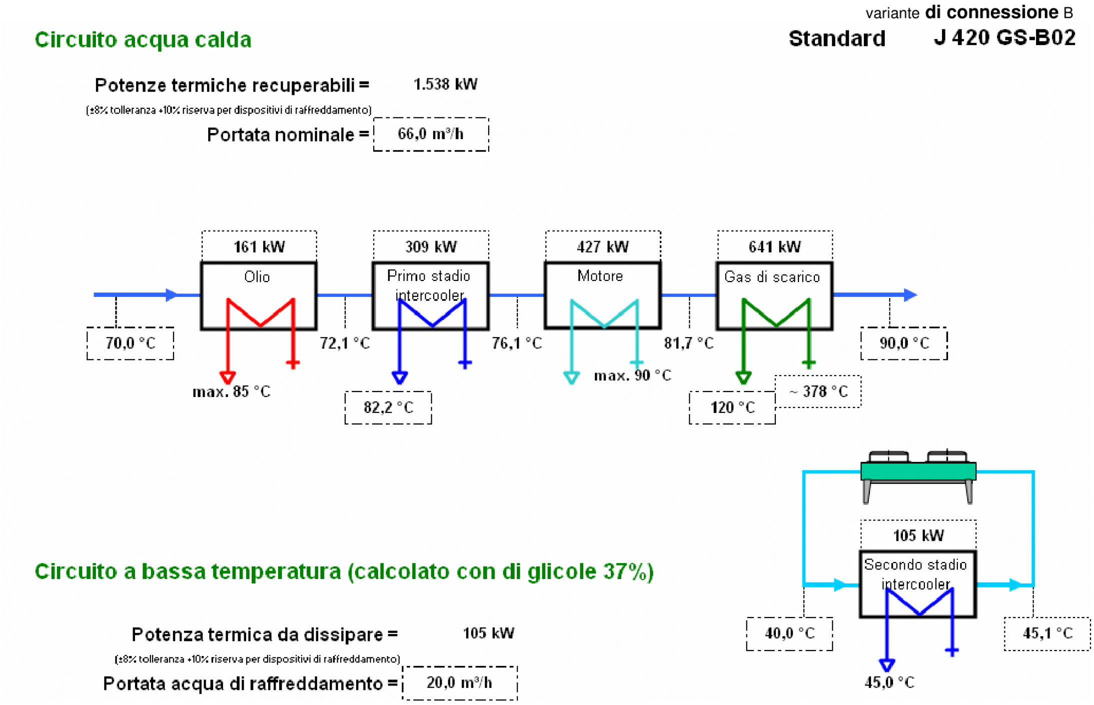

variante **di connessione** B

Standard **J 420 GS-B02**

Circuito acqua calda

Potenze termiche recuperabili = 1.538 kW

(±8% tolleranza +10% riserva per dispositivi di raffreddamento)

Portata nominale = 66,0 m³/h

Circuito a bassa temperatura (calcolato con di glicole 37%)

Potenza termica da dissipare = 105 kW

(±8% tolleranza +10% riserva per dispositivi di raffreddamento)

Portata acqua di raffreddamento = 20,0 m³/h

0.10 Condizioni di riferimento

I dati riportati nelle specifiche tecniche si riferiscono al funzionamento del motore a pieno carico, in accordo alle temperature e al numero metanico di riferimento indicati.
Lo sviluppo si riserva di poter apportare modifiche a tali prescrizioni.

Le indicazioni di pressione si intendono come sovrapressioni.
(1) Potenza ISO - standard limitata DIN-ISO 3046 e DIN 6271 riferita alle condizioni standard e a giri nominale.
(2) Secondo normativa DIN-ISO 3046 e DIN 6271 con tolleranza del + 5 %.
(3) Valore medio fra intervalli di cambio olio secondo il calendario di manutenzione, senza la quantità del cambio.
(4) Secondo normativa VDE 0530 REM / IEC-34.1 con relativa tolleranza , a fattore di potenza cos.phi = 1,0
(5) Per potenza complessiva con tolleranza del +/- 8 %.
(6) Secondo le condizioni di cui sopra da (1) a (5)
(7) Valido solo per il modulo (motore e alternatore), impianti periferici non considerati
(8) Temperatura gas di scarico con una tolleranza di +/-5 %

Disturbi radio
Grazie al dispositivo di accensione dei motori a gas vengono rispettati i limiti delle CISPR 12 (30-75 MHz, 75-400 MHz, 400-1000 MHz), e EN 55011, clase B (30-230 MHz, 230-1000 MHz) per i disturbi radio.

Definizione di potenza

- Potenza ISO-standard limitata:
  E' la potenza utilizzabile in via continuativa dichiarata dalla casa costruttrice per un motore funzionante secondo il numero di giri nominale nelle condizioni di manutenzione eseguite nei tempi e nei modi richiesti dalle indicazioni tecniche. Tale potenza viene misurata sperimentalmente dalla casa costruttrice in condizioni di funzionamento reali e calcolata per le condizioni di riferimento DIN-ISO 3046 e DIN 6271.
- Condizioni di riferimento DIN-ISO 3046 e DIN 6271:

Pressione aria:	1000 mbar o 100 m S.L.M.
Temperatura aria	25 ℃ o 298 K
Umidità relativa	30 %

- Indicazioni dei volumi in riferimento normale (gas alimentazione, aria comburente, gas di scarico)

Pressione:	1013 mbar
Temperatura:	0℃

Riduzione di potenza per motori sovralimentati
Per installazioni superiori a **500 m** slm e/o temperatura d'aspirazione superiori **30 30 ℃** la riduzione de potenza del motore é da definire in base alle condizioni specifiche del progetto.

Se il valore del numero metanico scende al di sotto del suo valore di riferimento ed il sistema rileva la presenza di autodetonazioni, il regolatore „Engine Management" interviene prima, a pieno carico, modificando opportunamente i tempi di accensione della miscela, poi riducendo la potenza del motore.
Il superamento dei limiti di frequenza e di tensione per i generatori secondo la zona A della IEC 60034-1 comporterà una riduzione della potenza

Condizioni tecniche

L'impianto, in merito tecnica delle vibrazioni, è progettato secondo la ISO 8528-9 e ne rispetta i limiti indicati.

I mezzi d´esercizio e sistemi periferici per l'esercizio dei motori a gas della GE JENBACHER devono soddisfare le prescrizioni contenute nella **IT 1100-0110, IT 1100-0111 e IT 1100-0112.**

7.2 Appendix II: Regolamento Delegato (UE) 2015/2402

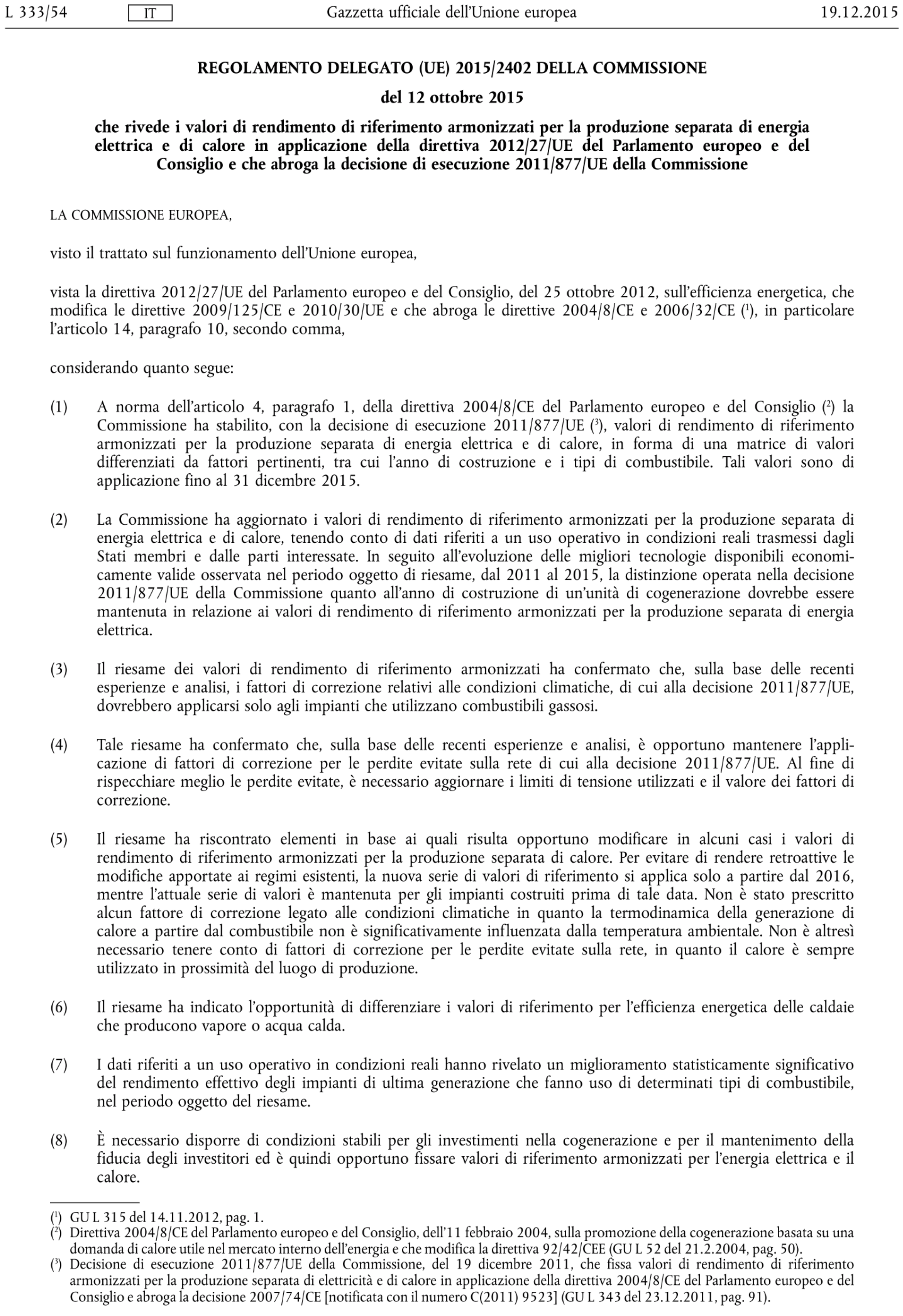

REGOLAMENTO DELEGATO (UE) 2015/2402 DELLA COMMISSIONE

del 12 ottobre 2015

che rivede i valori di rendimento di riferimento armonizzati per la produzione separata di energia elettrica e di calore in applicazione della direttiva 2012/27/UE del Parlamento europeo e del Consiglio e che abroga la decisione di esecuzione 2011/877/UE della Commissione

LA COMMISSIONE EUROPEA,

visto il trattato sul funzionamento dell'Unione europea,

vista la direttiva 2012/27/UE del Parlamento europeo e del Consiglio, del 25 ottobre 2012, sull'efficienza energetica, che modifica le direttive 2009/125/CE e 2010/30/UE e che abroga le direttive 2004/8/CE e 2006/32/CE (1), in particolare l'articolo 14, paragrafo 10, secondo comma,

considerando quanto segue:

(1) A norma dell'articolo 4, paragrafo 1, della direttiva 2004/8/CE del Parlamento europeo e del Consiglio (2) la Commissione ha stabilito, con la decisione di esecuzione 2011/877/UE (3), valori di rendimento di riferimento armonizzati per la produzione separata di energia elettrica e di calore, in forma di una matrice di valori differenziati da fattori pertinenti, tra cui l'anno di costruzione e i tipi di combustibile. Tali valori sono di applicazione fino al 31 dicembre 2015.

(2) La Commissione ha aggiornato i valori di rendimento di riferimento armonizzati per la produzione separata di energia elettrica e di calore, tenendo conto di dati riferiti a un uso operativo in condizioni reali trasmessi dagli Stati membri e dalle parti interessate. In seguito all'evoluzione delle migliori tecnologie disponibili economicamente valide osservata nel periodo oggetto di riesame, dal 2011 al 2015, la distinzione operata nella decisione 2011/877/UE della Commissione quanto all'anno di costruzione di un'unità di cogenerazione dovrebbe essere mantenuta in relazione ai valori di rendimento di riferimento armonizzati per la produzione separata di energia elettrica.

(3) Il riesame dei valori di rendimento di riferimento armonizzati ha confermato che, sulla base delle recenti esperienze e analisi, i fattori di correzione relativi alle condizioni climatiche, di cui alla decisione 2011/877/UE, dovrebbero applicarsi solo agli impianti che utilizzano combustibili gassosi.

(4) Tale riesame ha confermato che, sulla base delle recenti esperienze e analisi, è opportuno mantenere l'applicazione di fattori di correzione per le perdite evitate sulla rete di cui alla decisione 2011/877/UE. Al fine di rispecchiare meglio le perdite evitate, è necessario aggiornare i limiti di tensione utilizzati e il valore dei fattori di correzione.

(5) Il riesame ha riscontrato elementi in base ai quali risulta opportuno modificare in alcuni casi i valori di rendimento di riferimento armonizzati per la produzione separata di calore. Per evitare di rendere retroattive le modifiche apportate ai regimi esistenti, la nuova serie di valori di riferimento si applica solo a partire dal 2016, mentre l'attuale serie di valori è mantenuta per gli impianti costruiti prima di tale data. Non è stato prescritto alcun fattore di correzione legato alle condizioni climatiche in quanto la termodinamica della generazione di calore a partire dal combustibile non è significativamente influenzata dalla temperatura ambientale. Non è altresì necessario tenere conto di fattori di correzione per le perdite evitate sulla rete, in quanto il calore è sempre utilizzato in prossimità del luogo di produzione.

(6) Il riesame ha indicato l'opportunità di differenziare i valori di riferimento per l'efficienza energetica delle caldaie che producono vapore o acqua calda.

(7) I dati riferiti a un uso operativo in condizioni reali hanno rivelato un miglioramento statisticamente significativo del rendimento effettivo degli impianti di ultima generazione che fanno uso di determinati tipi di combustibile, nel periodo oggetto del riesame.

(8) È necessario disporre di condizioni stabili per gli investimenti nella cogenerazione e per il mantenimento della fiducia degli investitori ed è quindi opportuno fissare valori di riferimento armonizzati per l'energia elettrica e il calore.

---

(1) GU L 315 del 14.11.2012, pag. 1.

(2) Direttiva 2004/8/CE del Parlamento europeo e del Consiglio, dell'11 febbraio 2004, sulla promozione della cogenerazione basata su una domanda di calore utile nel mercato interno dell'energia e che modifica la direttiva 92/42/CEE (GU L 52 del 21.2.2004, pag. 50).

(3) Decisione di esecuzione 2011/877/UE della Commissione, del 19 dicembre 2011, che fissa valori di rendimento di riferimento armonizzati per la produzione separata di elettricità e di calore in applicazione della direttiva 2004/8/CE del Parlamento europeo e del Consiglio e abroga la decisione 2007/74/CE [notificata con il numero C(2011) 9523] (GU L 343 del 23.12.2011, pag. 91).

(9) I valori di riferimento per la produzione separata di calore e di energia elettrica di cui alla decisione 2011/877/UE sono di applicazione fino al 31 dicembre 2015 e i nuovi valori di riferimento dovranno essere applicati a decorrere dal 1º gennaio 2016. Per garantire che la nuova serie di valori di riferimento possa iniziare ad essere applicata entro tale data l'attuale regolamento entra in vigore il giorno successivo a quello della pubblicazione.

(10) Gli articoli 14, 22 e 23 della direttiva 2012/27/UE conferiscono alla Commissione il potere di adottare atti delegati per aggiornare i valori di riferimento armonizzati per la produzione separata di energia elettrica e di calore. La delega di potere è conferita alla Commissione per un periodo di cinque anni a decorrere dal 4 dicembre 2012. Al fine di evitare una situazione in cui la delega di potere non sia prorogata oltre il 4 dicembre 2017, i valori di riferimento stabiliti nel presente regolamento continueranno ad essere di applicazione dopo quella data. Se nel frattempo alla Commissione saranno conferiti nuovi poteri delegati, è sua intenzione riesaminare i valori di riferimento stabiliti nel presente regolamento entro quattro anni dopo la sua entrata in vigore.

(11) La direttiva 2012/27/UE mira a promuovere la cogenerazione per risparmiare energia ed è pertanto opportuno incentivare l'ammodernamento delle unità di cogenerazione più vecchie per migliorarne l'efficienza energetica. Per questi motivi e coerentemente con il requisito dei valori di rendimento di riferimento armonizzati definiti sulla base dei principi di cui all'allegato II, paragrafo f), della direttiva 2012/27/UE, i valori di rendimento di riferimento per l'energia elettrica che si applicano alle unità di cogenerazione dovrebbero aumentare a partire dall'undicesimo anno successivo a quello di costruzione,

HA ADOTTATO IL PRESENTE REGOLAMENTO:

Articolo 1

Fissazione dei valori di rendimento di riferimento armonizzati

I valori di rendimento di riferimento armonizzati per la produzione separata di energia elettrica e di calore sono definiti rispettivamente nell'allegato I e nell'allegato II.

Articolo 2

Fattori di correzione dei valori di rendimento di riferimento armonizzati per la produzione separata di energia elettrica

1. Gli Stati membri applicano i fattori di correzione di cui all'allegato III, per adattare i valori di rendimento di riferimento armonizzati fissati nell'allegato I alle condizioni climatiche medie di ciascuno Stato membro.

Se, in base a dati meteorologici ufficiali, la temperatura ambientale annuale presenta scarti di 5 °C o più sul territorio di uno Stato membro, quest'ultimo ha la facoltà, previa notifica alla Commissione, di utilizzare più zone climatiche ai fini del primo comma, quando applica il metodo di cui all'allegato III.

2. Gli Stati membri applicano i fattori di correzione di cui all'allegato IV per adattare i valori di rendimento di riferimento armonizzati fissati nell'allegato I al fine di tenere conto delle perdite evitate sulla rete.

3. Se uno Stato membro applica sia i fattori di correzione di cui all'allegato III, sia quelli di cui all'allegato IV, esso applica l'allegato III prima di applicare l'allegato IV.

Articolo 3

Applicazione dei valori di rendimento di riferimento armonizzati per la produzione separata di energia elettrica

1. Gli Stati membri applicano i valori di rendimento di riferimento armonizzati di cui all'allegato I in relazione all'anno di costruzione dell'unità di cogenerazione. Tali valori di rendimento di riferimento armonizzati si applicano per un periodo di 10 anni a decorrere dall'anno di costruzione dell'unità di cogenerazione.

2. A partire dall'undicesimo anno successivo all'anno di costruzione dell'unità di cogenerazione, gli Stati membri applicano i valori di rendimento di riferimento armonizzati che, a norma del paragrafo 1, si applicano alle unità di cogenerazione di 10 anni di età. Tali valori di rendimento di riferimento si applicano per un anno.

3. Ai fini del presente articolo, l'anno di costruzione di un'unità di cogenerazione è l'anno civile nel corso del quale l'unità inizia a produrre energia elettrica.

Articolo 4

Applicazione dei valori di rendimento di riferimento armonizzati per la produzione separata di calore

1. Gli Stati membri applicano i valori di riferimento armonizzati di cui all'allegato II in relazione all'anno di costruzione dell'unità di cogenerazione.

2. Ai fini del presente articolo, l'anno di costruzione di un'unità di cogenerazione è l'anno civile di costruzione ai fini dell'articolo 3.

Articolo 5

Ammodernamento di un'unità di cogenerazione

Se il costo d'investimento per l'ammodernamento di un'unità di cogenerazione esistente supera il 50 % del costo d'investimento per una nuova unità di cogenerazione analoga, l'anno civile nel corso del quale l'unità di cogenerazione ammodernata inizia a produrre energia elettrica è considerato come l'anno di costruzione dell'unità di cogenerazione ammodernata ai fini degli articoli 3 e 4.

Articolo 6

Miscela di combustibili

Se l'unità di cogenerazione utilizza più tipi di combustibili, i valori di rendimento di riferimento armonizzati per la produzione separata sono applicati in proporzione alla media ponderata dell'apporto energetico dai vari combustibili.

Articolo 7

Abrogazione

La decisione 2011/877/UE è abrogata.

Articolo 8

Entrata in vigore e applicazione

Il presente regolamento entra in vigore il primo giorno successivo alla pubblicazione nella *Gazzetta ufficiale dell'Unione europea*.

Il presente regolamento si applica dal 1° gennaio 2016.

Il presente regolamento è obbligatorio in tutti i suoi elementi e direttamente applicabile in ciascuno degli Stati membri.

Fatto a Bruxelles, il 12 ottobre 2015

Per la Commissione
Il presidente
Jean-Claude JUNCKER

ALLEGATO I

Valori di rendimento di riferimento armonizzati per la produzione separata di energia elettrica

(di cui all'articolo 1)

I valori di rendimento di riferimento armonizzati per la produzione separata di energia elettrica riportati nella tabella sottostante sono basati sul potere termico inferiore e sulle condizioni ISO atmosferiche standard (temperatura ambientale di 15 °C, pressione di 1,013 bar, umidità relativa del 60 %).

Categoria		Tipo di combustibile	Anno di costruzione		
			Antecedente al 2012	2012-2015	Dal 2016
Solidi	S1	Carbon fossile compresa antracite, carbone bituminoso, carbone sub-bituminoso, coke, semicoke, coke di petrolio	44,2	44,2	44,2
	S2	Lignite, mattonelle di lignite, olio di scisto	41,8	41,8	41,8
	S3	Torba, mattonelle di torba	39,0	39,0	39,0
	S4	Biomassa secca fra cui legna e altri tipi di biomassa solida compresi pellet e mattonelle di legno, trucioli di legno essiccati, scarti in legno puliti e asciutti, gusci e noccioli d'oliva e altri noccioli	33,0	33,0	37,0
	S5	Altri tipi di biomassa solida compresi tutti i tipi di legno non inclusi in S4 e liquame nero e marrone.	25,0	25,0	30,0
	S6	Rifiuti urbani e industriali (non rinnovabili) e rifiuti rinnovabili/biodegradabili	25,0	25,0	25,0
Liquidi	L7	Olio combustibile pesante, gasolio, altri prodotti petroliferi	44,2	44,2	44,2
	L8	Bioliquidi compresi biometanolo, bioetanolo, biobutanolo, biodiesel e altri bioliquidi	44,2	44,2	44,2
	L9	Liquidi residui, compresi rifiuti biodegradabili e non rinnovabili (inclusi sego, grasso e trebbie)	25,0	25,0	29,0
Gassosi	G10	Gas naturale, GPL, GNL e biometano	52,5	52,5	53,0
	G11	Gas di raffineria, idrogeno e gas di sintesi	44,2	44,2	44,2
	G12	Biogas da digestione anaerobica, gas da impianti di trattamento di acque reflue e gas di discarica	42,0	42,0	42,0
	G13	Gas di cokeria, gas di altoforno, gas da estrazioni minerarie e altri gas di recupero (escluso il gas di raffineria)	35,0	35,0	35,0
Altri	O14	Calore di scarto (compresi i gas di scarico ad alta temperatura e i prodotti da reazioni chimiche esotermiche)			30,0
	O15	Energia nucleare			33,0
	O16	Energia solare termica			30,0
	O17	Energia geotermica			19,5
	O18	Altri combustibili non menzionati			30,0

ALLEGATO II

Valori di rendimento di riferimento armonizzati per la produzione separata di calore

(di cui all'articolo 1)

I valori di rendimento di riferimento armonizzati per la produzione separata di calore riportati nella tabella sottostante sono basati sul potere termico inferiore e sulle condizioni ISO atmosferiche standard (temperatura ambientale di 15 °C, pressione di 1,013 bar, umidità relativa del 60 %).

Categoria		Tipo di combustibile:	Anno di costruzione					
			Antecedente al 2016			Dal 2016		
			Acqua calda	Vapore (*)	Utilizzo diretto dei gas di scarico (**)	Acqua calda	Vapore (*)	Utilizzo diretto dei gas di scarico (**)
Solidi	S1	Carbon fossile compresa antracite, carbone bituminoso, carbone subbituminoso, coke, semicoke, coke di petrolio	88	83	80	88	83	80
	S2	Lignite, mattonelle di lignite, olio di scisto	86	81	78	86	81	78
	S3	Torba, mattonelle di torba	86	81	78	86	81	78
	S4	Biomassa secca fra cui legna e altri tipi di biomassa solida compresi pellet e mattonelle di legno, trucioli di legno essiccati, scarti in legno puliti e asciutti, gusci e noccioli d'oliva e altri noccioli	86	81	78	86	81	78
	S5	Altri tipi di biomassa solida compresi tutti i tipi di legno non inclusi in S4 e liquame nero e marrone.	80	75	72	80	75	72
	S6	Rifiuti urbani e industriali (non rinnovabili) e rifiuti rinnovabili/biodegradabili	80	75	72	80	75	72
Liquidi	L7	Olio combustibile pesante, gasolio, altri prodotti petroliferi	89	84	81	85	80	77
	L8	Bioliquidi compresi biometanolo, bioetanolo, biobutanolo, biodiesel e altri bioliquidi	89	84	81	85	80	77
	L9	Liquidi residui, compresi rifiuti biodegradabili e non rinnovabili (inclusi sego, grasso e trebbie)	80	75	72	75	70	67
Gassosi	G10	Gas naturale, GPL, GNL e biometano	90	85	82	92	87	84
	G11	Gas di raffineria, idrogeno e gas di sintesi	89	84	81	90	85	82
	G12	Biogas da digestione anaerobica, gas da impianti di trattamento di acque reflue e gas di discarica	70	65	62	80	75	72
	G13	Gas di cokeria, gas di altoforno, gas da estrazioni minerarie e altri gas di recupero (escluso il gas di raffineria)	80	75	72	80	75	72

Categoria		Tipo di combustibile:	Anno di costruzione					
			Antecedente al 2016			Dal 2016		
			Acqua calda	Vapore (*)	Utilizzo diretto dei gas di scarico (**)	Acqua calda	Vapore (*)	Utilizzo diretto dei gas di scarico (**)
Altri	O14	Calore di scarto (compresi i gas di scarico ad alta temperatura e i prodotti da reazioni chimiche esotermiche)	—	—	—	92	87	—
	O15	Energia nucleare	—	—	—	92	87	—
	O16	Energia solare termica	—	—	—	92	87	—
	O17	Energia geotermica	—	—	—	92	87	—
	O18	Altri combustibili non menzionati	—	—	—	92	87	—

(*) Se tali impianti non tengono conto del riflusso della condensa nel calcolo del rendimento della produzione di calore per cogenerazione, i rendimenti per il vapore di cui alla tabella soprastante sono aumentati di 5 punti percentuali.

(**) Occorre utilizzare i valori relativi all'utilizzo diretto dei gas di scarico se la temperatura è pari o superiore a 250 °C.

ALLEGATO III

Fattori di correzione legati alle condizioni climatiche medie e metodo per determinare le zone climatiche in vista dell'applicazione dei valori di rendimento di riferimento armonizzati per la produzione separata di energia elettrica

(di cui all'articolo 2, paragrafo 1)

a) Fattori di correzione legati alle condizioni climatiche medie

La correzione in funzione della temperatura ambientale è basata sulla differenza tra la temperatura media annuale in uno Stato membro e le condizioni ISO atmosferiche standard (15 °C).

La correzione si effettua nel modo seguente:

perdita di rendimento di 0,1 punto percentuale per ogni grado al di sopra dei 15 °C;

guadagno di rendimento di 0,1 punto percentuale per ogni grado al di sotto dei 15 °C.

Esempio:

se la temperatura media annuale in uno Stato membro è di 10 °C, il valore di riferimento delle unità di cogenerazione situate in quello Stato membro deve essere aumentato di 0,5 punti percentuali.

b) La correzione in funzione della temperatura ambientale si applica solo ai combustibili gassosi (G10, G11, G12, G13).

c) Metodo per determinare le zone climatiche

I confini di ogni zona climatica sono costituiti dalle isoterme (in gradi Celsius interi) della temperatura ambientale media annuale, separate da un intervallo minimo di 4 °C. La differenza di temperatura tra le temperature ambientali medie annuali applicate nelle zone climatiche adiacenti sarà di almeno 4 °C.

Esempio:

se, per esempio, la temperatura ambientale media annuale di un determinato Stato membro è di 12 °C in una determinata località e di 6 °C in un'altra località nello stesso Stato membro, quest'ultimo ha la facoltà di definire due zone climatiche separate da un'isoterma di 9 °C:

una prima zona climatica compresa tra le isoterme di 9 °C e 13 °C (4 °C di differenza) avente una temperatura ambiente media annuale di 11 °C e

una seconda zona climatica compresa tra le isoterme di 5 °C e 9 °C avente una temperatura ambiente media annuale di 7 °C.

ALLEGATO IV

Fattori di correzione legati alle perdite evitate sulla rete grazie all'applicazione dei valori di rendimento di riferimento armonizzati per la produzione separata di energia elettrica

(di cui all'articolo 2, paragrafo 2)

Livello di tensione di connessione	Fattore di correzione (all'esterno del sito)	Fattore di correzione (all'interno del sito)
≥ 345kV	1	0,976
≥ 200 — < 345kV	0,972	0,963
≥ 100 — < 200kV	0,963	0,951
≥ 50 — < 100kV	0,952	0,936
≥ 12 — < 50kV	0,935	0,914
≥ 0,45 — < 12kV	0,918	0,891
< 0,45kV	0,888	0,851

Esempio:

Un'unità di cogenerazione di 100 kWel a motore alternativo funzionante a gas naturale produce una corrente elettrica di 380 V. L'85 % di tale corrente è destinata all'autoconsumo e il 15 % della produzione è esportato nella rete. L'impianto è stato costruito nel 2010. La temperatura ambientale annuale è di 15 °C (di conseguenza non è necessaria alcuna correzione climatica).

Dopo la correzione per tenere conto delle perdite sulla rete, il valore di rendimento di riferimento per la produzione separata di energia elettrica in questa unità di cogenerazione (sulla base della media ponderata dei fattori contenuti nel presente allegato) è dato da:

$$\text{Ref E}\eta = 52{,}5\ \% \times (0{,}851 \times 85\ \% + 0{,}888 \times 15\ \%) = 45{,}0\ \%$$

Ringraziamenti

Con questo lavoro si conclude la mia esperienza universitaria durata 5 anni, questo è per me un traguardo importante della mia vita che non avrei mai raggiunto senza l'aiuto e il sostegno di molti.

Per prima cosa vorrei ringraziare la mia famiglia per avermi dato le possibilità economiche per compiere il mio cammino di studi e sostenuto nei momenti più difficili della mia vita.

Vorrei anche ringraziare Mattia, Mattia e Alberto che conosco ormai da una vita e che ritengo i miei amici più cari, i quali mi hanno accompagnato durante tutta la mia esperienza universitaria.

Durante la mia vita universitaria ho conosciuto molte persone con cui ho condiviso momenti importanti della mia vita che sempre porterò con me.

Vorrei quindi ringraziare tutti i coinquilini con cui ho vissuto durante questi 5 anni, in special modo Luca, Lorenzo, Luca, Christian, Giacomo, Lorenzo, Andrea, Michele e Vito, con cui ho condiviso gioie e dolori della vita universitaria e che mi hanno sempre sopportato aiutandomi a crescere come persona, rendendomi un adulto migliore.

Voglio anche ringraziare i miei compagni di università, in special modo Fabio, Andrea, Simone, Daniele, Lorenzo, Federica, Fabrizio, Silvia e Giacomo, i quali mi hanno sempre aiutato nello studio e a prepararmi al meglio per gli esami.

Ringrazio i miei relatori, la prof.ssa Marta Gandiglio e il prof.re Armando Portoraro, i quali sono sempre stati disponibili e pronti nell'aiutarmi durante tutto il lavoro di tesi.

Grazie a tutti.